NANYANG
TECHNOLOGICAL
UNIVERSITY

FEMTOSECOND LASER INTERACTION WITH FUSED SILICA IN SURFACE STRUCTURING

TAN TONG TAT

SCHOOL OF MECHANICAL AND AEROSPACE ENGINEERING

2013

FEMTOSECOND LASER INTERACTION WITH FUSED SILICA IN SURFACE STRUCTURING TAN TONG TAT 2013

FEMTOSECOND LASER INTERACTION WITH FUSED SILICA IN SURFACE STRUCTURING

TAN TONG TAT

School of Mechanical and Aerospace Engineering

A thesis submitted to the Nanyang Technological University
in fulfillment of the requirement for the degree of
Doctor of Philosophy

2013

Abstract

The need for miniaturisation in devices in today's industries has led to a vast array of micromachining processes. Yet, micromachining of glass remains a great challenge due to the extreme brittleness and hardness of the material. With the development of the chirped pulse amplification (CPA) technique in the mid-1980s, powerful femtosecond (10^{-15}s) laser systems are now readily available in the market for carrying out micromachining on various materials.

Femtosecond (fs) lasers have several advantages over their long pulse laser counterparts. First, the high intensity of femtosecond laser pulse will easily triggers the multiphoton absorption process to occur in transparent material enabling bulk modification within the transparent materials. Moreover, the ultrashort pulse duration (~100 fs) of a femtosecond laser enables energy to be dissipated before thermal diffusion occurs (~10 ps), thus collateral damages around the machined area is minimized. These unique properties have opened up new opportunities in using femtosecond lasers for carrying out micromachining and micro fabrication of glass and other transparent materials.

Despite the ongoing work to study femtosecond laser-material interaction, practical use of femtosecond laser for industrial application can be still considered at the development stage as the beam interaction process is not well understood. New physical mechanism and phenomenon can arise when the machining is performed using different materials and conditions. Therefore, in this research, a femtosecond laser was used to carry ablation of transparent material in air using fused silica as a model optical material. The objective of this research is to gain a better understanding on the femtosecond laser irradiation effects on fused silica so that it can be applied to practical micromachining processes. These effects include ripple formation, change in crystal structures and surface morphologies as well as how the laser irradiated machined profiles respond to various laser parameters. Special attention was paid to characterize the laser irradiated morphologies and structures as well as studying phenomenon related to micromachining of fused silica. Major results and new findings are summarized as follows:

Femtosecond laser induced periodic structures on fused silica were systematically studied by irradiating the surface using a wide range of laser processing parameters. It is found that two directional ripples having periods smaller than the laser wavelength can be formed on the surface of fused silica. It is demonstrated that the the origin of the coarse ripple is related to the ultrafast melting and solidification of fused silica and the fine ripple is a result of harmonica wave generation. It is also found that orientation and period of these ripple structures can be controlled experimentally by varying the beam polarization. It is further observed that the influence of the surface defect like scratches exert an even stronger influence on the ripple orientation than the beam polarization. This results in ripple structures changing from polarization-controlled to defect-controlled orientation. Effect of material crystallographic orientation in ripple formation which has never been compared between crystalline and amorphous quartz is found to be independent of the ripple orientation. Instead, it is found that ripple formation can be brought forward and formed earlier on a certain crystallographic plane which is due to the anisotropy properties of the material.

In machining of microholes and channels on fused silica substrate, systematic investigation on the effect of laser processing parameters with regards to the profile and surface morphology was carried out. For experiments on drilling of microholes, beam polarization was observed not to have any significant effect on the profile and machined depth. Two ablation regimes have been identified in the drilling process when ablation was carried out from low to high fluence. The machined depths were compared to the predicted depths and the results matches well with the theory. Material cracking that was rarely reported has been observed when drilling in the high fluence regime. For channel machining, similarly beam polarization was found to have little effect on the machining results. However, it was found that periodic sub-micron gratings (400 nm in width) can be induced within the microchannels along the cutting direction. The submicron gratings were likely to be a result of beam interference. These microchannels and gratings may be used for the manufacture of optical and microfluidic devices. A dependency on the groove depth was observed when ablating with different powers rating and machining speeds. By cutting the same groove with multiple passes, the depths were found to increase linearly up to approximately 10 consecutive passes. Above 10 passes, a decrease in ablation rate was observed until a depth limit was reached.

Study of femtosecond laser irradiation effects was conducted on both transparent and opaque materials having high melting temperature to see study whether or not a femtosecond laser would induce phase changes. Important engineering materials like fused silica, quartz and titanium were investigated using X-ray diffraction (XRD) and transmission electron microscope (TEM). A special technique was used to protect the laser irradiated surfaces in preparing cross-sectional TEM samples. It is to note that the studies conducted on fused silica and quartz was the first direct cross-sectional TEM examination on the silica groove structures after a femtosecond laser beam irradiation. XRD spectra and TEM results revealed that the structures of the fused silica remain amorphous after the femtosecond laser irradiation. For single crystal quartz, TEM observation revealed that micromachining using femtosecond laser induced a thin amorphous layer in the ablation zone. In characterizing the laser irradiated titanium structures, two different results can be observed depending on the working parameters. It was concluded that by increasing the number of pulses, it can lead to the amorphization of the irradiated zones. Preliminary studies on using in-situ TEM heating technique was also performed to study the crystallization process of amorphous titanium structure after femtosecond laser irradiation.

Some of the below findings are new and thus may have great impact on femtosecond laser research. Cracking of glass materials after femtosecond laser machining of fused silica were observed but seldom reported and studied in the literature. In addition, it is widely believed that femtosecond laser ablation is a non-thermal process and thus it does not cause cracking. However, this research has produced convincing evidence to show that cracking can occur in fused silica.

By performing a series design of experiments (DOE) using the concept of full factorial method, the cracking mechanism and conditions for cracking to occur, which has never been studied, has been systematically investigated. Also, the laser processing parameters were studied for process optimization. It was hypothesized that the mechanism for fused silica cracking is a result of stress generated by the recoil pressure and shock waves exceeding the material dynamic strength. Calculation using the Griffith fracture theory based on the crack length proved the hypothesis that the induced stress exceeded the fused silica dynamic strength. Lastly, a crack-free process window together with a development of an empirical formula to predict the crack length based on the applied laser fluences and pulses is proposed for femtosecond laser machining of fused silica. The developed micromachining process has potential application in fabricating optical and microelectronic devices on fused silica material.

Acknowledgements

I would like to express my sincere gratitude to my PhD supervisor, Associate Professor Zhou Wei, and co-supervisor, Dr Zheng Hongyu (Group Manager, Machining Technology Group, SIMTech), for their patience guidance and encouragement throughout the research work.

Besides my advisors, i would also like to extend my sincere thanks to Associate Professor David Lee Butler, Dr Zhu Sha and Dr Huang Zhiqiang for the valuable discussion and help in my PhD work.

My sincere thanks also go to Professor Wang Lumin for offering me the opportunity to carry out an exchange research program in University of Michigan (USA).

I would further like to thank the technicians from Materials Lab A, Metrology Lab, PEN Centre and all the lab mates and friends that has help me in the course of the experimental work.

Lastly, special thanks are given to my wife, parents and siblings for their continuous support and encouragement throughout the entire course of my PhD study.

Contents

Chapter 3 Experimental Procedures 32

List of Abbreviations and Symbols

2D	Two dimensional
AFM	Atomic force microscopy
AWJC	Abrasive water jet cutting
BS	Beam-splitter
CCD	Charge-coupled device
CO2	Carbon dioxide
CPA	Chirped pulse amplification
DIC	Differential interference contrast mode
DOE	Design of experiments
EDS	Energy dispersive spectra
EDX	Energy dispersive X-ray spectroscopy
F1	Neutral density filters
FROG	Frequency-resolved optical gating
fs	Femtosecond
FS	Fast mechanical shutter
FWHM	Full width half max
HAZ	Heat-affected zone

HF	Hydrofluoric acid
HR	High resolution
HWP	Zero order half wave plate
LIBWE	Laser-induced backside wet etching
LIPPS	Laser induced periodic surface structures
M1-M3	Mirror
MEMS	Microelectronics and microelectromechanical systems
MRR	Material removal rate
N.A	Numerical aperture
NPs	Nucleated nanoparticles
OM	Optical microscope
P1	Thin film polarizer
PD1	Photo-detector 1
PD2	Photo-detector 2
PIPS	Precision ion polishing system
ps	Picosecond
PSI	Pounds per square inch
SADP	Selected area diffraction patterns
SEM	Scanning electron microscope

SEW	Surface electromagnetic waves
TEM	Transmission electron microscope
TFT	Thin film transistor
Ti	Titanium
USM	Ultrasonic machining
UV	Ultraviolet
W	Groove width
XRD	X-ray diffractometer
YAG	Yttrium-aluminium-garnet
Z	Stage position
(+)	Beam move above the surface
(-)	Beam move below the surface.
(0)	Stage reference point
a	Long high field axis
b	Short weak field axis
C_p	Specific heat capacity
d	Ablation depth
D	Feature diameter
D_f	Thermal diffusivity

d_p	Ripple period parallel to beam polarization
d_{pe}	Ripple period perpendicular to beam polarization
d_w	Second harmonic wave
E_g	Bandgap
E_{gap}	Excitation energy
E_p	Pulse energy
F_0	Peak fluence
F_a	Absorbed laser fluence
F_{ap}	Applied fluence
F_{th}	Threshold pulse energy
h_m	Melt depth
I_a	Absorbed intensity of the laser beam
l	Heat diffusion depth
M^2	Beam quality factor
m	Number of photons
n	refractive index
N	Number of laser shots
nm	Nanometer
P	Recoil pressure

P_{avr}	Average power
T_a	Average temperature
T_m	Working temperature
μm	Micrometer
μs	Microsecond
ω_o	Beam spot size
ε	Ellipticity
α	Absorption coefficient
ρ	Density
λ	Wavelength
τ	Pulse Width
θ_i	Angle of incidence considered to the surface normal
$h\upsilon$	Photon energy
ξ	Ratio between the thermal and the internal energy
σ_P	Standard deviation of power

List of Figures

List of Tables

Chapter 1 Introduction

1.1 Background

The availability of femtosecond laser or ultrashort pulse laser has opened up a wide range of exciting new possibilities in the area of micromachining and microfabrication on various materials including metals (Pronko *et al.*, 1995; Nikumb *et al.*, 2006), ceramics (Das and Pollock, 2009; Ho *et al.*, 2011), semiconductors (Yokotani *et al.*, 2004; Kam *et al.*, 2011), transparent materials (Ma *et al.*, 2006; Li *et al.*, 2007) and tissues (Alekhin *et al.*, 2010; Ionita and Zamfirescu, 2011) for different industries such as automotive, telecommunication, medical, aerospace and information technology. Comparing to conventional machining techniques, the main advantage of femtosecond laser is that it is able to produce pulse widths equal or shorter than the time scale of lattice vibration. This enables the laser energy to be deposited into the material in the time scale before any thermal diffusion can occur (An *et al.*, 2004), resulting in minimum collateral damages such as a reduction in the heat-affected zone (HAZ) and recast layer within the laser ablated region.

Moreover, by focusing a femtosecond laser beam with high numerical aperture objectives (N.A >1), the laser radiation is confined to a very small focal volume. This can generate sufficient photon density (Mazur *et al.*, 2005) causing localized multiphoton absorption (Kuriyama and Ito, 2003) to occur at the laser wavelength. This allows direct fabrication on wide bandgap materials like fused silica (7.5eV) and sapphire (9eV) that are difficult to be processed using conventional tools. These distinctive advantages achieved by ultrashort laser pulses have stimulated not only interest in understanding the physical mechanisms of short pulse laser ablation but also fabrication of microstructures like waveguides, gratings, holes and grooves in different materials (Crawford *et al.*, 2003; Qiu *et al.*, 2004; Sohn *et al.*, 2004).

Glass especially fused silica has emerged as a major material of interest for the telecommunications industry and it is widely used for fabricating optical devices due to its excellent optical properties. Furthermore, it can be used as an insulator or barrier layer, often in combination with silicon in other photonic devices. A significant amount of research work has been carried out in the past to study femtosecond laser beam interaction with glass. Key areas of research studies include using femtosecond laser for surface (Lenzner *et al*., 1999) and subsurface (He *et al*., 2010; Costa *et al*., 2011) microstructuring, structural modification like refractive index change for waveguide fabrication (Kamata *et al*., 2004; Zoubir *et al*., 2005), surface morphology investigation after femtosecond irradiation (Wu, *et al*., 2002), plasma interaction (Siege *et al*., 2007) and femtosecond laser induced micro (Luo, *et al*., 2002) and nanostructures (Pattathil, *et al*., 2005).

In regard to micromachining of glass, single pulse (Campbell *et al*, 2005) and multiple pulses machining (Yasui *et al*., 2003) with low laser fluence have been carried out. Other studies include drilling of holes using a femtosecond laser oscillator (Cai and Piestun, 2007) or applying a different technique (Yan *et al*., 2001; Zimmer *et al*, 2007) to machine glass. Though the above have highlighted a list of major research studies performed on glass with a femtosecond laser beam, their primary focus was to use a femtoseond laser for micro-structuring and device fabrication. Little is done to study the effect of processing parameters and problems associated to direct machining of glass. An understanding of the laser processing parameters is essential for developing a better control and better use of the microstructures for practical application purposes. This is especially important as the interaction process can be very complex when the material is under intense femtosecond laser pulse irradiation. The interaction between the laser beam and material can become non-linear (Schaffer, 2001, Rayner *et al*., 2005) due to the effect of air (Roso *et al*., 2008) though this non-linear effect may be reduced by machining in inert gas environment.

One phenomenon that is still not well understood is the formation ripples structures after femtosecond laser irradiation. Laser induced periodic surface structures (LIPSS) or ripples have been observed in different kind of materials (Kanemitsu, *et al*., 1984; Anthony and Cline, 1997; Yu *et al*., 1999; Gedvilas *et al*., 2008; Schade *et al*., 2008) for the past few decades. These ripples usually have a periodicity equal or close to the wavelength of the laser radiation. In recent years, LIPSS are attracting increased interest due to its promising potential in micromachining for microelectronics and microelectromechanical systems (MEMS). Potential applications include using the ripples to fabricate gratings and shallow junctions or texturing the surface of magnetic recording media (Hsu *et al*., 2011).

Earlier model assumed that these ripples might be a result of (frozen) acoustic waves where the ripples have a periodicity close to the laser wavelength (Willis and Emmony, 1975). Furthermore, it is observed that the ripples orientation is strongly dependent on the beam polarization and this leads to an evolvement in a ripple model (Emmony *et al*., 1973; Gousheng *et al*., 1982). However, for ripples that are induced by a femtosecond beam, the ripples usually have a period smaller than the laser wavelength. Because of the smaller period and the different ripple's morphology observed, many different explanations have been considered such as self-organization (Gedvilas *et al*., 2008), boson condensation (Van Vechten, 1981; Singh *et al*., 2002) or even Coulomb explosion (Reif *et al*., 2002). For fused silica material, though there were several studies on ripples after laser irradiation (Ihlemann *et al*., 1992; Wager et al., 2006; Bohme *et al*., 2008), however, in-depth characterization and study on the physical phenomena to explain ripple initiation, growth and transitions toward other patterns induced by a femtosecond laser beam is still not fully understood.

Phase transition induced by a femtosecond laser beam is another topic that has been actively discussed and research on. As the thermal diffusion length is proportional to the square root of the pulse duration, the femtosecond laser-induced thermal effect is expected to be negligible (Shirk and Molian, 1998). However in recent years, femtosecond laser-induced crystallization (Pratap *et al*., 2003; Shieh *et al*., 2004; Salihoglu *et al*., 2011) and amorphization (Hirayama and Obara, 2003; Malshe and Deshpande, 2004; Izawa *et al*., 2009; Konishi *et al*., 2010) have been reported in a wide range of materials. Generally, a transition between the crystalline and the amorphous phase following laser irradiation is related to threshold behaviour in the solidification velocity. If solidification proceeds with liquid-solid interface velocities higher than a critical value, irradiation leads to the amorphization of the processed material (Bonse *et al*., 2004). As femtosecond laser can be used for machining optical grating (Zoubir *et al*., 2003), a change in the crystal structural either complete or partial crystallization may affect its optical properties. Thus, an understanding of the material structure after femtosecond laser irradiation is of great importance and studies on whether a femtosecond laser pulse would induce phase change on both amorphous and crystalline glass is rarely investigated.

Lastly, to be able to successfully use femtosecond laser to carry out machining of fused silica for practical industrial applications, the machining process still requires some tuning and understanding of the processing conditions to achieve excellent machining results. This is not an easy task especially considering a large number of processing parameters. Studies have shown that drilling with high laser intensities (10^{15} W/cm^2) can cause some of the advantages of using ultrashort pulses to be lost such as reduction in the strength of the material at high temperature. Also phenomenon like cracking (Kuriyama, and Ito, 2003; Chiwon *et al*., 2009) or melting (Bonse *et al*., 2004) can still occur even though femtosecond laser micromachining is widely considered to be non-thermal and crack free process. As mention earlier, fs-laser has a characteristic time scale far shorter than the thermal diffusion length, generation of liquid phase and heat transfer to the surrounding during machining is expected to be minimum. Absent of liquid phase allow better control of the machining process (Momma *et al*., 1996) with little or no collateral damage. However, based on the above reports, machining with a fs-laser may still induce cracking in material. Till now, no studies have yet been performed to understand the mechanism of femtosecond laser induce cracking and obtaining an optimum window for micromachining of fused silica without crack formation.

1.2 Objectives and Scope

The nature of multiphoton absorption of femtosecond laser enables both surface and subsurface modification of transparent materials. However, femtosecond beam interaction with wide bandgap materials is a complex process especially when the interaction between the laser pulses becomes non-linear. Thus an understanding of the mechanism between the laser and material is needed prior to successfully using femtosecond lasers for any practical applications.

Therefore the primary objective of this research project is to study irradiation effects and phenomenon related to femtosecond laser machining of fused silica. By performing laser ablation experiments over a wide range of experimental parameters, irradiation effects and phenomenon such as ripple formation, cracking, structure change and the laser machined profiles are systematically studied so that a better understanding of the femtosecond laser machining process can be gained and can be put into practical use.

The main scope of this study includes:

(1) Investigating the effects of experimental parameters (fluence, number of pulses, polarization) and the influence of material crystal orientation and on ripple formation.

(2) Performing micromachining of holes and channels in fused silica and investigate the effects of different laser machining parameters (fluence, speed, polarization, cutting orientation, machining pass) on the machining quality, profile, morphology and chemical composition.

(3) Conducting high resolution TEM and in-situ TEM analysis to study femtosecond laser irradiation effects on the structures of some of the technological importance materials like fused silica, quartz and titanium.

(4) Designing experiments to understand phenomenon such as cracking that has never been proven experimentally and proposing an operating window in carry out surface machining of microholes and channels without crack formation.

1.3 Organization of thesis

The thesis is organized as follows:

Chapter 2: Consists of the literature review for this research. First, properties of glass and the current techniques used for machining of glass are reviewed. The limitation of each technique is discussed and the unique characteristics of using femtosecond laser will be highlighted. Following which, the ablation mechanism of long and femtosecond pulse laser are discussed. Lastly, some surface and material phenomena associated with femtosecond laser beam interaction is highlighted.

Chapter 3: Describes the femtosecond laser setup and the various characterization techniques used in this study.

Chapter 4: Reports the formation of ripple structures on fused silica and quartz after femtosecond irradiation. The effects of processing parameters on the ripple morphology, evolution and mechanism of ripple growth were investigated. The influences of surface defects and crystallographic orientations on ripple formation were also discussed.

Chapter 5: This chapter demonstrates the machining capability of femtosecond laser in carryout micromachining of hole and channels on fused silica. A systematic study on the effects of laser processing parameters on surface morphology, width, depth and quality of machining are presented and discussed.

Chapter 6: Reports structural and compositional analysis on femtosecond laser irradiated structures. UV grade fused silica, single crystal quartz and titanium are studied using TEM and the mechanism behind the structure evolution is discussed.

Chapter 7: Design of experiments to investigate the mechanism and conditions for a femtosecond laser beam to induce cracking during surface machining of holes and channels in fused silica.

Chapter 8: Summarizes the experimental results and makes recommendations for future research directions.

Chapter 2 Literature Review

2.1 Introduction

Glass is an important engineering material widely used in many areas such as building, electronics and automotive industries. In its nature form, is consists of almost 100% of crystalline silica in the form of alpha-quartz that is commonly found in sand or rocks. When heated above 573ºC, alpha-quartz undergoes a reversible change to become beta-quartz. Natural quartz is difficult to process because it comes in random shapes and sizes. Also a widespread of impurities can be found in natural quartz which makes it impractical for direct application. In current market, quartz is artificially grown using hydrothermal synthesis process to a specified dimension having controlled crystal orientation, high purity and good uniformly. Because it possesses good optical and piezoelectric properties, quartz is extensively used as wave retardation medium, electronic filters or resonators.

Glass on the contrary is produced by heating the crystalline silica to a high temperature followed by rapidly cooling below its glass transition temperature. By performing rapid cooling, there is insufficient time for a regular crystal lattice to form and this results in glass having amorphous crystal structure. Today, glass properties are altered by adjusting the composition during development so that they can meet the various industry requirements. Generally, glass can be classified into six main types according to their methods of fabrication as well as minor additions and variations in the ingredients used. A summary on the major glasses with their ingredients, properties, and applications are listed in the Table 2.1. For common glass, it consist of 70 ~ 72 weight % of silicon oxide (SiO_2) while ultra-pure glass such as fused silica make up of 99.99 weight % of silicon oxide. Fabrication of fused silica can be either by an electrically heated furnace (electrically fused) or a gas/oxygen-fuelled furnace (flame fused). The key advantage of fused silica over common glass is that it has very low thermal expansion coefficient with excellent optical qualities and exceptional transmittance over a wide spectral range, especially in the ultraviolet**.** Therefore, this material is often used for fabricating high energy laser optics.

In current market, commercial available fused silica and quartz may come in different dimensions in the form of sheets and rods. However, due to the brittle nature of glass, micromachining on glass-based materials using conventional techniques can be very challenging. Advanced micromachining techniques like lithography, water jet cutting or laser cutting are needed. The use of laser, especially femtosecond lasers, has opened up new opportunities in the area of micromachining and microfabrication of glass.

Type of glass	**Ingredient**	**Properties**	**Application**
Fused silica	• Silica (SiO_2) 99.99%	• Low thermal expansion coefficient • Good UV transmission • High corrosion resistance	• Optical fiber • Mask • Lens
Soda-lime-silica glass	• Silica (SiO_2) 72% • Sodium oxide (Na_2O) 14.2% • Magnesia (MgO) 2.5% • Lime (CaO) 10.0% • Alumina (Al_2O_3) 0.6%.	• High thermal expansion • Poor heat resistance • Chemically stable	• Windows • Food containers • Tableware
Sodium borosilicate glass	• Silica (SiO_2) 81% • Boric oxide (B_2O_3) 12% • Soda (Na_2O) 4.5% • Alumina (Al_2O_3) 2.0%	• Low thermal expansion coefficient • Thermal shock resistance • High softening point	• Laboratory glass ware • Flat panel display • Light source
Lead oxide glass	• Silica (SiO_2) 59% • Soda (Na_2O) 2.0% • Lead oxide (PbO) 25% • Potassium oxide (K_2O) 12% • Alumina (Al_2O_3) 0.4% • Zinc oxide (ZnO) 1.5%	• High refractive index • High elasticity • Poor heat resistance	• Food containers • Radiation shield
Aluminosilicate glass	• Silica (SiO_2) 57% • Alumina (Al_2O_3) 16% • Boric oxide (B_2O_3) 4.0% • Barium oxide (BaO) 6.0% • Magnesia (MgO) 7.0% • Lime (CaO)10%	• Chemical resistance • God thermal resistance	• Glass fiber • Halogen bulb glass
Oxide glass	• Alumina (Al_2O_3) 90% • Germanium oxide (GeO_2) 10%.	• Extreme clear	• Fiber optics waveguide

Table 2.1: Type of glasses and its properties.
(http://en.wikipedia.org/wiki/Glass)

2.2 Methods of machining glass

2.2.1 Mechanical scribing and breaking

For centuries, this traditional method has been one of the more commonly used techniques for glass separation. The technique simply involves scribing the surface of the glass using a hard, sharp tool (typically a diamond or carbide wheel) to create a groove on the glass surface. This is followed by using a mechanical snapping force to propagate the crack completely through the glass. In the modern automated factory, the separation of the glass is usually carried out by means of a “chopper bar”. Though this method is the fastest separation technique, however, it has several key drawbacks that include not being able to machine complex shapes and thin substrate.

In fact, it is almost impossible to use mechanical scribing at all when the glass substrate is below 1mm in thickness. This is because mechanical scribing will induce higher stress (Matthew, 2001; Venkatakrishnan and Tan, 2007) in thin substrate as compared to a thick substrate and this results in the formation of micro cracks on the edges. Another reason in particular is that this cutting technique will often require additional grinding, polishing or even cleaning processes so that the uneven cutting edges or debris will not interfere with the subsequent operations and pose a hazard.

2.2.2 Water jet cutting

Water jet cutting is one of the widely used techniques by various industries in a wide range of materials. In this process, highly pressurized water (typically between 20,000 and 60,000 pounds per square inch (PSI)) is forced through a fine orifice. This creates a thin jet of water with very powerful forces travelling at high velocity (close to the speed of sound) which enables machining to take place. However, pure water jet cutting can only cut soft material like thin wood and is not effective for cutting hard materials like glass or metals. This is because the water jet tends to entrain into the atmospheric air causing the cutting efficiency to be greatly reduced. Very often, abrasive water jet cutting (AWJC) is used to machine harder materials instead.

By adding abrasive particles such as garnets or glass beads into the water, machining efficiency can be greatly improved. The mechanism of material removal by AWJC is similar to a grinding wheel which the particles chip out small pieces of material upon impact. In AWJC cutting of ductile materials, the material removal is mainly by low angle impact by the abrasive particles, leading to ploughing and micro cutting (Engels, 1978). Further at higher angle of impact, the material removal involves plastic failure of the material at the site of impact, which was studied initially by Bitter (1953). Hashish (1989) unified such models and applied it under AWJC at a later stage. In the case of cutting of brittle materials, other than the above two models, material would be removed due to crack initiation and propagation because of brittle failure of the material.

The key benefit of the water jet machining is its ability to cut material without changing their intrinsic properties as there is no heat-affected zone (Yang *et al.*, 2008). However, the disadvantages are high initial cost, frequent maintenance and replacement of the nozzle due to erosion. Moreover, this technique cannot machine submicron features as the feature size in water jet cutting is proportional to the diameter of the jet stream in which the water droplets or abrasives are confined (Liu, 2010). Therefore, the key challenge for the water jet technology is to reduce the diameter of the jet stream. Till now the smallest features machined with commercial water jet cutters are generally larger than 200 μm.

2.2.3 Ultrasonic machining

Ultrasonic machining is a process in which abrasive slurry is used to perform material removal from the workpiece. Quite similar to abrasive water jet machining, the slurry consists of tiny granular particles having grain size and hardness equal or greater than the hardness of the workpiece. Materials like silicon carbide and boron carbide are usually used because of their high hardness. Material removal is achieved by directing the slurry between the workpiece and a vibrating tool so as to allow the abrasive particles to hit against the workpiece surface causing cracks and finally material removal from the work piece.

A schematic on ultrasonic machining (USM) principle with major elements are shown in Figure 2.1 (Nath *et al*., 2012). The advantage of this process is basically non-thermal thus leaving the chemical and physical properties of the workpiece unchanged (Deng and Lee, 2002). Furthermore, this technique is suitable for machining brittle material like glass and ceramics as the cut provides reduced stress and a lower tendency of fractures. A limitless number of feature shapes including odd-shaped thru-holes and cavities of varying depths having high quality and consistency features can be fabricated on glass using this technique. However, the disadvantage of ultrasonic machining is that this process has low material removal rate (MRR) and the machining time highly depends upon the viscosity of the slurry fluid and frequency at which the tool is vibrating. Also the slurry may wear the wall of the machined hole as it passes back towards the surface. This limits the accuracy particularly for milling of small holes.

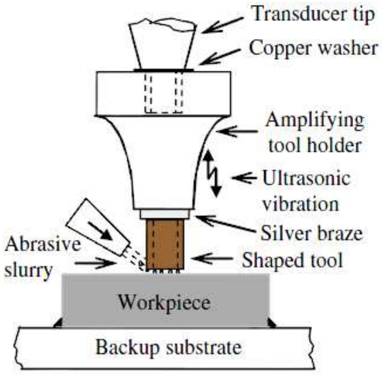

Figure 2.1: Schematic illustration of ultrasonic machining (USM) principle with major elements (Nath *et al*., 2012).

2.2.4 Photolithography

The use of photolithography technique offers another solution for processing of glass. This method was borrowed from the semiconductor industry where mask lithography is used to pattern the surface of silicon wafers for printed circuit boards. Similarly, in glass processing using photolithography technique, a light sensitive photochemical or photoresist is applied onto the glass substrate. The desired pattern is then transferred onto the photoresist by exposing ultraviolet (UV) light through the mask. Usually regions that are exposed by UV light will be hardened while non-exposed region will be washed away after developing the photoresist. The final pattern is then transferred to the glass substrate by either wet or dry etching process.

In wet etching of glass, common chemical agent use is hydrofluoric acid (HF) while dry etching uses reactive-ion etching which combines both plasma and sputter etching processes. The plasma systems are used to ionize reactive gases and the ions are accelerated to bombard the glass surface. Chemical such as Fluoroform + Oxygen gas (CHF3 + O2) or Tetrafluoromethane + Hydrogen gas (CF4 + H2) are employed in dry etching process.

The key advantage of photolithography technique is that it offers very high resolution (Nano scale) especially with the introduction of immersion lithography (Rothschild *et al*., 2005). However, cost is the main concern as commercial photolithography systems are very costly and to fabricate the required mask sets further adds to the capital cost. Moreover, this technique has been well optimized to handle standard silicon wafers but not on glass. Thus there might be difficulties and limitations when used for direct patterning of glass especially glass is an isotropic material and the etching can be non-directional (Malek *et al*., 2007) especially with wet etching process. This results in structures with curved sidewalls and having relatively low aspect ratios to be produced. Furthermore, material removal rate (MRR) is rather slow. For example, wet etching rate ranges from 10-1000 nm/min while dry etching is approximately 20 nm/min. These restrictions limit the use of photolithography for precision patterning of glass material.

2.2.5 Long pulse laser machining

The use of laser has proven to be another fast and effective ablation technique for processing of glass. This technique can correct many of the deficiencies associated with other techniques. First, laser ablation is a non-contact process that can completely eliminate the problem of additional cleaning step induced from mechanical methods. Second, laser machining is one step cutting process that does not require complex set-up as compared to the lithography technique. The laser beam can be easily focused to the micro scale using a simple lens and mirror setup to facilitate the micromachining or micropatterning of glass surface**.**

The idea of using laser to machine glass was first originate by Lambert and his group in 1976 where they employed two separate laser beam to machine glass. The first beam usually produced using a YAG laser (Yttrium-Aluminium-Garnet Laser) or a diode laser is used to melt a 0.2 mm deep groove-crack, while a second laser beam is used to generate thermal stress at the crack tip to make the material separate controllably. This method is an extension of the laser cutting of controlled fracture and the laser scribing method, previously proposed by Garibotti (1963) and Lumley (1969). In Garibotti's method, a laser is used to scribe the substrate along the desired separation line. The scribed materials are then immersed in an ultrasonic cell and broken along the scribed lines by ultrasonic energy. Alternatively, the scribed substrate is broken along the scribed line by applying a mechanical force induced from the cracking roller. This fracture technique however is less controllable. Lumley's method on the contrary is much simpler and has great potential in machining brittle material. In his invention, a single beam is use to generate mechanical stress and this causes the material to separate along the path of the laser beam. This separation technique is similar to a crack extension and the fracture growth is controllable. Dicing of brittle materials such as alumina ceramic substrate and glass has been successfully demonstrated by Lumley using the carbon dioxide (CO_2) laser.

	Mechanical Cutting	**Water Jet Cutting**	**Ultrasonic Machining**	**Lithography**	**Laser Cutting**
Capabilities	• Minimum Feature Size: >1 mm	• Minimum Feature Size: 300 µm • Aspect Ratio: 30:1	• Minimum Feature Size: 200 µm • Aspect Ratio: 25:1	• Minimum Feature Size: 0.1 µm • Aspect Ratio: 3:1(glass)	• Minimum Feature Size: 1-50 µm • Aspect Ratio: 10-20:1
Advantages	• Inexpensive • Minimum setup needed.	• Can cut almost all material • No heat affected zone	• High aspect ratios • Able to drill straight sidewalls and produce very fine features	• Highly precision • Minimum human intervention once setup done. • Able to print complex shapes	• Extreme versatile. • Able to machine complex shapes. • Can cut almost all material • No mask, tooling or tool wear
Disadvantages	• Poor accuracy • Tool wear • Require post cleaning process	• Slow process • Higher cost due to abrasive material use. • Taper profile when machine thick parts	• Slow process • Large capital investment cost • Difficult to machine asymmetrical patterns	• Large capital investment cost • Undercut problem when using wet etching. • Multi step process	• Large capital investment cost • High power consumption • Difficult to create blind holes
Capital Investment	$10k to $20k	$60k to over $300k	$60k to over $300k	$200k to over $1M	$200k to over $1M

Table 2.2: List of machining techniques and its capabilities (http//:www.memsjournel.com).

Table 2.2 shows a summary of the various machining techniques as compared to laser micromachining. From the table, it can be observed that though the investment cost for a laser system is higher than that of a mechanical system, generally it is cheaper when compared to conventional lithography system. The overall investment cost of a laser cutting system in the long run is still cheaper when compared to mechanical processing techniques that require additional grinding or cleaning (Finlay and Frank, 2009). Most importantly, laser cutting makes it easier to produce curved cuts in glass. The demand for curved cuts is increasing, especially in mobile phones, where many manufacturers would like to replace plastic covers with glass to increase scratch resistance and this generally requires small radius rounded edges, and sometimes even cut-outs.

In today industry, high power pulse lasers such as carbon dioxide (CO_2) laser operating at a wavelength of 10.6 μm are widely used for cutting of glass. These CO_2 laser can generate very high power ranging from 50W to 500W. By irradiating the glass surface, tensile stress is generated with CO_2 laser heating. This is followed by injecting a cold jet of air at the irradiated region causing cracking along the direction of cutting to break the material (Hermanns, 2000). Because of the high power output, these lasers can direct machine glass having a thickness of several millimetres at very high federate with micro-scale precision. However machining with a CO_2 laser is essentially a thermal process and can induce undesirable side effects such as cracking (Rolo *et al.*, 2005). Figure 2.2 shows the possible damages on the surface of material when machining using a long pulse laser.

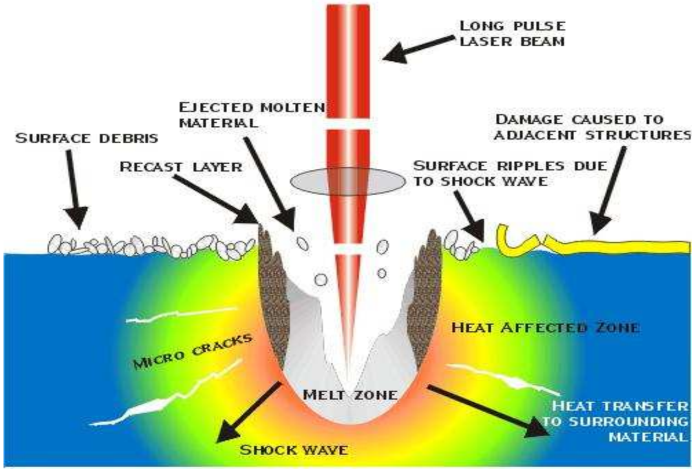

Figure 2.2: Long-pulse laser-matter interactions. It highlights the numerous physical phenomena that are present when machining with a long laser pulse. (http://www.cmxr.com)

2.2.6 Femtosecond laser machining

Femtosecond lasers, also known as ultrafast or ultrashort pulse lasers emit a pulse width in a time scale of femtosecond (10^{-15} s). In some literature, it also refers to pulses less than 10 ps (Craig, 1998). In order for a laser system to generate ultrashort pulses, three essential elements are required. First, a gain medium must be present in a laser system. This medium is usually made of an ion doped crystal or glass having a wide emission bandwidth. Moreover, to generate short pulses, the gain medium must be broad in frequency and must be able to produce these frequencies. The second mechanism is used to compensate for the dispersion in the laser cavity. This is because the group velocity in the optics (and even in air) inside the laser cavity is frequency dependent, and the initial short pulses tend to spread in time because different frequency components travel at different velocity. Typically a prism pair is used to compensate for this dispersion in the laser cavity, though recent advances in mirror coating technology allow the dispersion in the laser cavity to be taken care of in the optics themselves (Xu *et al*., 1996).

The last mechanism is needed to make the laser run in a pulsed, as opposed to a continuous wave mode. Essentially, all the different frequency components supported by the laser cavity (in terms of gain and dispersion compensation) must add constructively to produce a pulse, a process known as mode-locking (Ippen, 1994). For long pulse laser, mode-locking can be achieved by inserting an active modulator into the laser cavity that makes the gain in the laser cavity exceed the loss for only a short time, ensuring that the laser produce a pulse. However, no active modulator can switch fast enough to produce a femtosecond pulse, thus the gain (or loss) of the cavity must be modulated in some other ways.

In Ti:sapphire lasers, this modulation is accomplished by so called Kerr-lens mechanism (Christov *et al*., 1995). Briefly, weak self-focusing of the pulse in the gain crystal reduces the transverse size of the beam so that there is a better overlapped optically pumped gain region. It is thus energetically favorable for the laser to run pulsed as opposed to continuous wave (indeed, in a well-aligned Ti:Sapphire laser the average power will go up when the laser is mode-locked). Typically, a Ti:Sapphire laser oscillator will produce an output of 20 fs, 5 nJ, 800 nm pulses at a repetition rate of about 90 MHz. However, for many applications, higher laser density is desirable which requires amplification of the laser energy. This amplification of femtosecond laser pulses requires care, however, as the laser energy grows, the non-linear optical effects occur in the amplification chain, degrading the pulse. In extreme cases, non-linear absorption of laser energy by the optics in the amplification chain could cause permanent damage.

In order to avoid this non-linear effect and still pump more energy into the pulse, Mourou and co-workers devised a clever strategy of chirped-pulse amplification (CPA) (Strickland and Mourou, 1985). The CPA scheme works as follows (see Figure 2.3). Ultrashort light pulses are generated at low pulse energy through the use of an ultrashort-pulse mode-locked laser ‘‘oscillator.’’ This mode-locked laser typically generates light pulses at a high repetition rate ($\approx 10^8$ Hz) with pulse energies in the range of 10^{-9} J, and with pulse durations in the range of 10^{-12}–10^{-14} s.

These femtosecond pulses are then chirped using a dispersive delay line consisting of either an optical fiber or a diffraction-grating arrangement. The pulse is stretched from a duration under 100 fs to typically ~100 ps, decreasing its peak power by approximately three orders of magnitude. One or more stages of laser amplification are used to increase the energy of the pulse by six to nine orders of magnitude to achieve a sufficient fluence to efficiently extract energy from the laser amplifiers. This amplification typically requires a total of between 4 and 50 passes through an amplification medium, with a gain of between 2 and 100 per pass. After optical amplification, when the pulse is very energetic, a second grating pair is then used to ‘‘recompress’’ the pulse back to femtosecond duration using an optical pulse compression technique (Treacy, 1969; Fork *et al.*, 1984). To achieve this recompression back to near the original input pulse duration, proper optical design of the amplifier system is required.

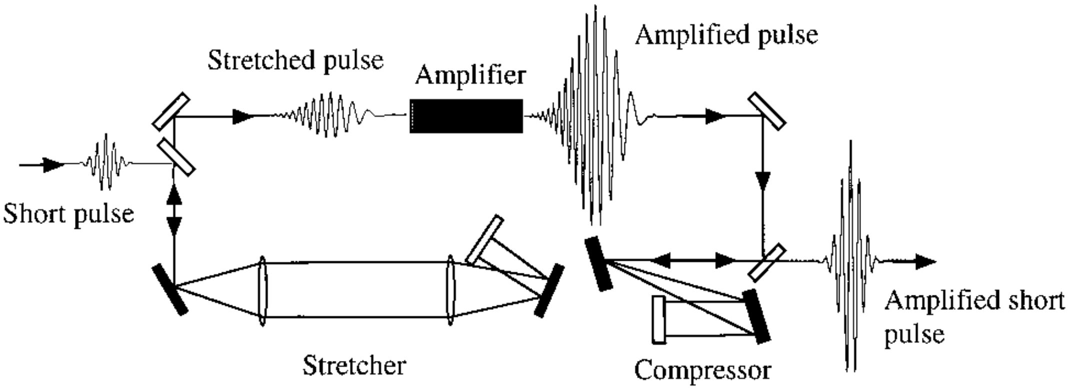

Figure 2.3: Schematic diagram of an amplifier system based on chirped-pulse amplification.

The development of femtosecond laser or (fs-laser) may offer an alternative solution for processing of glass. Despite the fact that the cost of femtosecond laser system is generally much higher as compared to conventional long pulse laser system. However, in the recent years, reduction in the cost and complexity of the femtosecond laser system has generated interest in using ultrashort pulse laser for micromachining and micro-fabrication applications. The advantage of femtosecond laser is that it has a pulse width shorter than or equal to the time scale of lattice vibration. As a result, the energy deposited into the material is far shorter than thermal phonon diffusion process. This means that femtosecond laser-induced thermal effect is considered to be negligible (Liu *et al*., 1997; Bank *et al*., 1998).

An illustration on ultrafast pulse laser-matter interaction as compared to long pulse laser is shown in Figure 2.4. Moreover, femtosecond laser can also generate very high peak power intensity resulting in non-linear multi-photon absorption to occur in glass. This can result in an increase in the refractive index at the focal point inside the glass, which is potentially effective to produce structures in nano-scale (Theppakuttai and Chen, 2003). This unique property allows processing of materials like glass (Ferna *et al*., 2011), ceramic (Wang *et al*., 2010) and explosive (Roeske *et al*., 2003) cannot be achieved in using conventional long pulse laser. Though femtosecond laser has many advantages over long pulse laser but when compared to high power CO_2 laser in term of high volume manufacturing, femtosecond laser has lower machining rate. Moreover it cannot direct cut thick glass having a thickness greater than 200µm in one single pass.

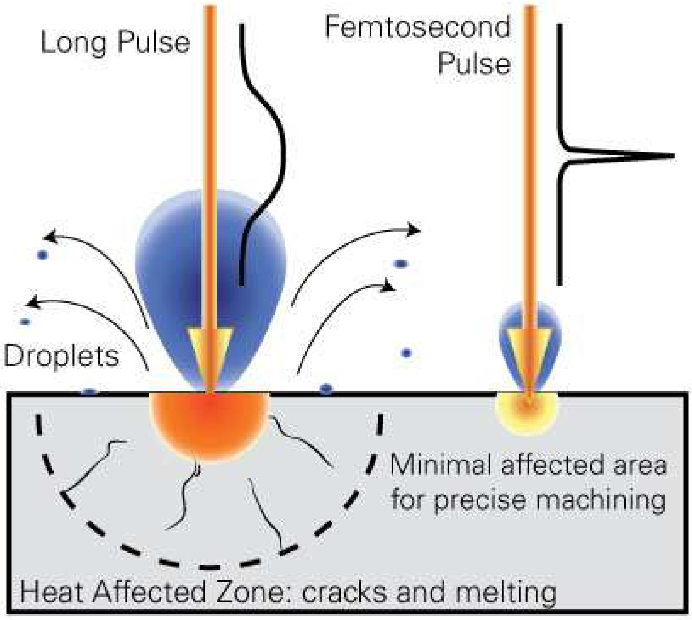

Figure 2.4: Ultrafast pulse laser-matter interaction (https://www.imra.com).

2.3 Ablation mechanism between long and femtosecond pulses lasers

Understanding the physical process in laser material interaction is important as it allow one to understand the capabilities and limitations of laser machining processes. Below describe the ablation mechanism between a long and ultrashort pulse laser.

2.3.1 Long pulse laser ablation

Lasers with pulse duration longer than a few tens of picoseconds (ps) are often classified as long pulse lasers. For long pulse laser material interaction, the laser energy is basically transferred from the laser-excited electrons to the material lattice by thermal diffusion process. Damage occurs when the temperature at the laser irradiated region become relatively high to cause melting or even fracture (Stuart *et al.*, 1996). A schematic showing long pulse laser ablation is shown in Figure 2.5.

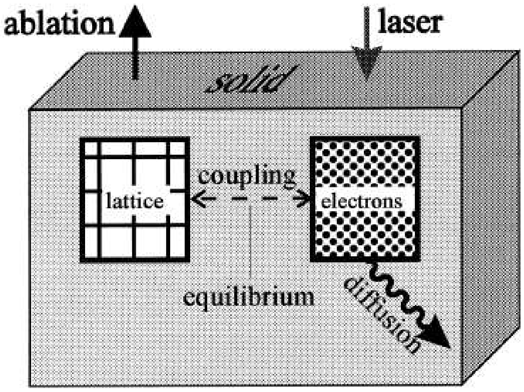

Figure 2.5: Schematic diagram showing long pulse laser ablation (Chichkov *et al*., 1996).

In long pulse laser interaction, free electrons gain kinetic energy by the absorption of photon energy through a series of inverse Bremsstrahlung process (Gamaly *et al*., 2002). Once the free electron gain sufficient kinetic energy, a portion of the energy is transferred to a bound electron by collisions to overcome the ionization potential to form two free electrons (Wong *et al*., 2003). This process is called impact ionization (Quere *et al*., 2001). Consequently, this results in more free electrons absorbing the photon energy to produce more free electrons from the bounded electrons. This results in a series of impact ionization process which is called avalanche ionization (Pronko *et al*., 1998) as shown in Figure 2.6.

Avalanche ionization strongly depends on the free electron density and is sometimes assumed to be linearly proportional to the laser intensity (Stuart *et al*., 1996). The reason for avalanche ionization is very efficient in long pulse ablation is due to availability for the exponential growth of the electron density. For long pulse laser ablation of wide bandgap materials, typical laser energy is below 10^{12} W/cm^2 and avalanche ionization is responsible for the ablation.

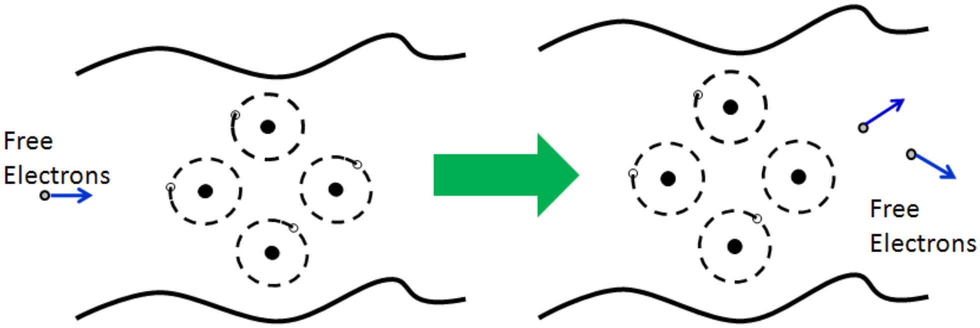

Figure 2.6: Schematic diagram showing impact ionization; avalanche ionization consist of a series of impact ionizations (Jiang and Tsai, 2011).

2.3.2 Short pulse laser ablation

Energy transfer during femtosecond laser ablation can be separated into two different stages: (1) the absorption of photon energy by electrons and (2) redistribution of the absorbed energy to the surrounding lattice leading to material removal (Ladieu *et al.*, 2002; Jiang and Tsai, 2011). The absorption of photon energy can be further categorized into either linear or non-linear. In the linear photon absorption, the process basically obeys the Beer-Lambert Law (Jiang and Tsai, 2011) which states that the absorption of a specific wavelength transmitted through a material is a function of material path length and is independent of incident intensity.

However, ablation in the femtosecond regime results in non-linear absorption rather than linear absorption for all materials. Avalanche ionization multi-photon ionization and/or tunnel ionization are major competing mechanisms for free electron generation. For a femtosecond laser, the laser intensity is typically greater than 10^{13} W/cm^2. Therefore multi-photon ionization (Guy *et al.*, 1993) becomes significantly stronger as compared to avalanche ionization for material ablation.

Multi-photon absorption occurs due to the simultaneous absorption of multiple photons by an electron in the valence band. The number of photons *m* required to bridge the bandgap must satisfy $mh\upsilon > E_g$, where E_g is the bandgap, and $h\upsilon$ is the photon energy. A schematic of a multiphoton ionization process is shown in Figure 2.7.

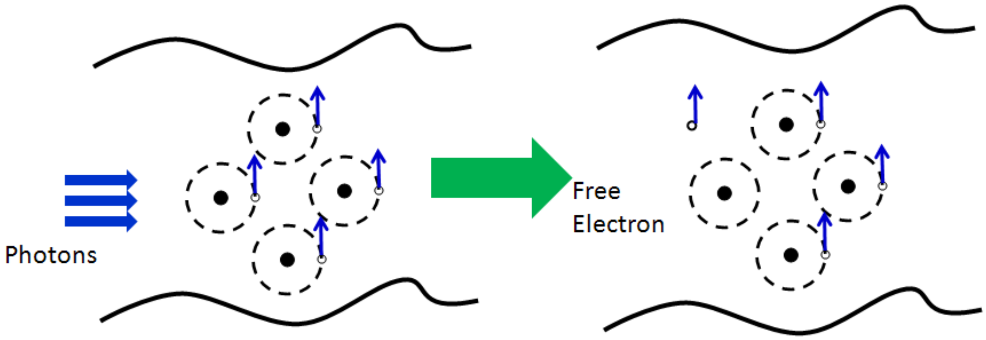

Figure 2.7: A schematic of a multiphoton ionization process (Jiang and Tsai, 2011).

Since the laser energy absorbed by the photons is usually greater than the ionization potential (Liu *et al*., 1997), a bound electron can be freed from the valence band after absorbing the energy from several photons. Thus seed electrons are not required to start the ionization process in wide bandgap materials. Moreover, the presence of defects and impurities play a negligible role due to high the high field ionization and impact ionization process (Jasapara *et al*., 2001). Thus, for laser intensities greater than 10^{15} W/cm^2, tunnel ionization is to be considered as well (Stuart *et al*., 1996).

For femtosecond ablation of wide bandgap materials, both multi-photon ionization and tunnel ionization makeup of the photo-ionization process. Absorption of the energy occurs on a time scale much shorter as compared to the time scale for energy transfer to the lattice, this result in the decoupling of the absorption and lattice heating processes as shown in Figure 2.8 (Stuart *et al*., 1996). Furthermore, material damage induced by ultrashort pulse laser is far more regular and confined as compared with longer pulse laser (Glezer *et al*., 1996) and the larger statistical variation for long pulses is not present for short pulses (Morou, 1997). This is because lesser energy is required to produce optical breakdown within the material by short pulse laser. This leads to a more precise ablation or bulk material modification. This deterministic breakdown and damage near threshold and controllable material alteration make femtosecond lasers an ideal tool for micromachining (Liu *et al*., 1997).

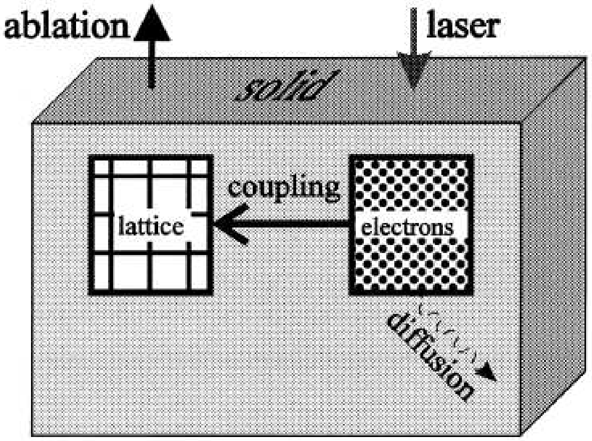

Figure 2.8: A schematic of short pulse ablation (Chichkov *et al*., 1996).

2.4 Femtosecond laser induced phenomenon and structure changes

Laser interaction with matter can lead to various permanent surface micro/nano structures in different material systems. The interaction of femtosecond laser pulse with material surface has attracted much interest among researchers because of its capabilities of unique surface modification and efficient material ablation. A literature review on the past work performed on femtosecond laser machining of glass and also laser-induced related phenomenon like both surface morphological and structure changes is reviewed in the following section.

2.4.1 Laser machining of glass

The use of laser to process glass has been an area of intensive research due to its technological importance. Much of the earlier work performed on glass using long pulse laser like, CO_2 laser to study the ablation behaviour between the laser beam and glass (Kestenbaum *et al*., 1990; Dyer *et al*., 1997). The development of femtosecond laser has stimulated research interest in the application of femtosecond laser for both surface and subsurface machining of transparent materials (Lenzner *et al*., 1999; He *et al*., 2010; Costa *et al*., 2011). Initially, the research on femtosecond laser on glass was mainly focused on studying ablation threshold (Kuger *et al*., 1997; Ashkenasi *et al*., 1999) and surface morphology (Schaffer *et al*., 2001; Kawahara *et al*., 2002)

With the rapid advancement in femtosecond laser technology, the use of femtosecond laser as potential tool for material processing has been demonstrated by many groups (Yuan *et al*., 2005; Zheng *et al*., 2006; White *et al*., 2008; Bellourd *et al*., 2010). Now, femtosecond laser technology has entered the industrial market, there is a need for systematic analysis and characterizing the laser ablated structure machined by femtosecond laser. In practical application, such as drilling or scribbling, one must understand the processing parameters so that the desired results can be achieved. For example, it has been reported that using shorter wavelength would improve the drilling rate due to better absorption in metal (Tunna *et la*., 2006). In another report, using different laser wavelength can affect the ablated profile (Witte *et al*., 2007). Other laser parameters include pulse energy, polarization, pulse duration, federate and repetition rate. The work performed here is an extension of the experimental work performed by a few groups (Yasui *et al*., 2003; Campbell *et al*, 2005) on single and multi-pulse machining of glass. No detailed study on the effects of processing parameters has been carried out especially on beam polarization effect in machining.

2.4.2 Laser induced ripple formation

Ever since Birnbaum (1965) first reported the formation of periodic structures on the surface of germanium substrate using a ruby laser, laser induced periodic surface structures (LIPSS) have been intensively studied over a wide range of materials ranging from metals (Regelskis *et al.*, 2007; Kim *et al.*, 2008), semiconductors (Serna *et al.*, 1994; Tan and Venkatakrishnan, 2006) and dielectric materials (Peng *et al.*, 2003; Liu *et al.*, 2011). In most cases, the ripples are found to have an orientation perpendicular to the laser polarisation with a periodicity close to the wavelength of the laser radiation.

Moreover, these ripples were found to have a period smaller or bigger than the laser wavelength if the radiation was performed at an inclination to the surface normal. Early model assumed that the ripples might be a result of frozen acoustic surface waves (Willis and Emmony, 1975).Very often, however, ripples having a periodicity at the order of the wavelength were observed. Furthermore, the ripples orientation strongly depends on the polarization of the incident laser light. This evolves into a model explaining the ripples are a result of interference between the incident laser radiation and scattered or excited surface waves (Emmony *et al.*, 1973; Gousheng *et al.*, 1982). For more than ten over years, this interference theory was able to successfully predict the periodicity of the ripples which is highly dependent on the laser wavelength and the angle of incidence.

Recently, these ripples have also shown to find potential application in micromachining MEMS structures (Brugger *et al.*, 2000; Chen *et al.*, 2002). Applications such as fabricating of gratings, shallow junctions of metal-oxide-silicon transistors, liquid-crystal display to texturing of magnetic recording media (Hsu *et al.*, 2011). Also, these ripples have shown to improve the adhesion of surface (Vajpayee *et al.*, 2011). A large diversity of patterns at the modified surface region was revealed with the use of femtosecond laser irradiation. These include periodic structures with many bifurcations

(Reif *et al*., 2002; Varlamova *et al*., 2007), uniformly distributed nanodots (Tomita *et al*., 2009; Yang *et al*., 2011) or even conical structures (Zhao *et al*., 2003; Nayak *et al*., 2010). Very often, ripples with spacing smaller than the laser wavelength was observed after femtosecond laser irradiation and using the interference theory could no longer account for the formation of these subwavelength ripples. Instead various mechanisms have been proposed to explain the observation of these ripples. These include interaction between incident light and excited surface plasmon (Bonse *et al*., 2009; Huang *et al*., 2009), self-organization (Varlamova *et al*., 2007; Weizman *et al*., 2008), second harmonic generation (Bonse *et al*., 2005; Dufft *et al*., 2009) and Coulomb explosion (Dong and Molian, 2004).

For ripple induced on fused silica after laser irradiation, some preliminary studies have been carried out. Ihlemann *et al* (1992) carried out ablation of fused silica using both nanosecond and femtosecond Excimer laser. They reported that the ripples maybe due to melting and resolidification or even perhaps recrystallization process. In another study, Wager *et al* (2006) observed subwavelength ripples when scanning perpendicular to polarization. A preliminary explanation proposed by them is the interaction of incident wave with the surface electromagnetic waves (SEW). They also suggested that the ripples might be due to higher harmonic generation. Bohme *et al* (2008) carried out laser-induced backside wet etching (LIBWE) of fused silica using a sub-picosecond UV laser and observed subwavelength ripples as well. However, as the laser irradiation was performed at the solid/liquid interface, they proposed that these ripple maybe defect-mediated. Despite the fact that the mechanism of the femtoseond laser-induced ripple formation is still under keen discussion, there are also other factors that can affect ripple formation. One such factor is the effect of surface roughness.

Yang *et al* (2010) reported that the ripple periodicity tends to decrease with larger surface roughness but increase with higher laser fluence. For the increased roughness, the change in ripple periodicity becomes more sensitive to the incident laser fluence. Tomita *et al* (2007) also carried out femtosecond irradiation of single crystal 4*H*-SiC wafer and observed that the fine ripples were remarkably reduced on the surface roughened by intentional rubbing, while the threshold for the formation of the coarse ripple were not affected. They suggest that the formation of fine ripples may be explained by non-uniform free electron density due to the initial surface roughness. Though the above experiments and theories on laser-induced ripples have been studied, however, in-depth characterization and study on the physical phenomena to explain ripple initiation, growth and transitions toward other patterns induced by a femtosecond laser beam on fused silica is still not fully understood.Therefore, further research is still needed in understanding ripple formation.

2.4.3 Laser induced recrystallization and amorphization

In addition to the laser induced periodic structures formation, laser irradiation effects on materials have been studied extensively in the past due to its great technological importance. For example, the use of long pulsed laser such as Excimer laser can be used to induce crystallization in amorphous thin film for thin-film transistor (TFT) application (Staudt *et al.*, 1998). By irradiating the film with the long pulse laser, energy is basically transferred from the laser-excited electrons to the material lattice by thermal diffusion process. Once sufficient energy is employed, melting of the material occurs. Once the pulse is over, nucleation and solidification of the material took place leading to the resultant microstructures.

Another irradiation effect is the transformation of crystalline to amorphous phase after laser irradiation. Generally, the transition between crystalline and the amorphous phase is highly dependent on the solidification velocity. If the velocity of the solidification front is greater than a critical value, amorphization of the laser-irradiated structure can occur (Cerny *et al.*, 1999). Femtosecond laser is well known to be a non-thermal process since the laser pulse wide is shorter than the electron-phonon energy relaxation time. Energy is deposited into the material before thermal diffusion occurs. However, in recent years, femtosecond laser-induced amorphization (Rodenas *et al*., 2006; Budiman *et al*., 2010; Konishi *et al*., 2010) and crystallization (Shiek *et al*., 2004; Valette *et al*., 2005) have been reported for a wide range of materials. As femtosecond laser can be used to make optical gratings (He *et al*., 2009) and waveguides (Ams *et al*., 2010) in glass, a change in the material crystal structure can alter the optical properties. Thus characterizing the irradiated structure is important for device fabrication.

2.4.4 Laser induced cracking

Cracking is a common phenomenon especially when carrying out machining of brittle material like glass. Laser machining of glass has always been very challenging due to the transmissive nature of glass in the visible region. The use of a nanosecond laser in machining glass usually requires the use of high pulse energies since linear absorption is not efficient. However, this would often lead to thermal induced damages such as chipping and micro-cracking (Lan *et al*., 2003). Carbon dioxide lasers are often used to machine glass since glass has better absorption in the far infrared range (Lane, 1990). However, the long pulse durations (μs) of the CO_2 laser can result in crack formation (Ozkan and Migliore, 2003).

Femtosecond laser machining has proven to be an effective tool for carrying out micromachining of glass and other transparent materials without any crack formation. However, in recent years, material cracking induced by a femtosecond laser beam has been reported (Lai *et al*., 2007; Qiu *et al*., 2008; Cheng *et al*., 2010). Though some preliminarily investigations have been carried out (Seydoux *al*., 2010), the cracking mechanism and conditions for cracks to form is still not well understood and this warrants further studies.

2.5 Summary

Various techniques on machining of glass have been review in this chapter. The use of a femtosecond laser has shown to be a promising tool for carrying out micromachining of glass as compared to long pulse lasers. Though many studies have been carried out to study femtosecond laser beam interaction with various materials, femtosecond laser beam interaction process with glass is still very complex and the laser irradiation can induce various phenomenon such as cracking, ripples and structure change which till now is still not very clear and need to be investigated.

Chapter 3 Experimental Procedures

3.1 Introduction

This chapter describes the femtosecond laser system, laser ablation set-up, sample preparation techniques and the different diagnostic tools used to characterize the laser irradiated sample.

3.2 Laser system and ablation set-up

3.2.1 Femtosecond laser system

The laser system used was based on a regenerative Ti:Sapphire amplifier using chirped pulse amplification technique (Clark-MXR, CPA 2001) to provide high-intensity fs laser pulses. A schematic of the laser ablation set-up is shown in Figure 3.1 while photographs of the femtosecond laser system with optical setup are shown in Figure 3.2. The output beam from the CPA system was directed onto the mechanical stage using 3 highly reflective mirrors (M1-M3). A beam-splitter (BS) was used to divert a portion of the output beam to a photo-detector (PD1), which monitors the beam quality during the laser experiments. A second photo-detector (PD2) was placed just before the objective lens for measuring pulse energy used in ablation experiments. Various pulse energies for the machining experiments were obtained by adjusting using a zero order half wave plate (HWP) and a thin film polarizer (P1). The maximum pulse energy output from the femtosecond laser system is 0.8mJ. However for ablation threshold studies which require much lower beam energies, different neutral density filters (F1) with different attenuation values were used.

The pulse duration of the output beam from amplifier was 150 fs with nominal wavelength at 775 nm. The repetition rate was set at 1 kHz and the beam profile emitted from the regenerative amplifier was approximately Gaussian with a M^2 factor <1.2 base on the specification from vendor. The linearly P-polarized laser beam was focused on the sample at normal incidence by a fused silica focusing lens having a focal length of 25mm. Circular and elliptical polarized light was obtained using a half and quarter-wave plate. The focused beam spot size was estimated to be 7 μm at $1/e^2$. The number of pulses delivered to the sample was achieved via adjusting the open time of a fast mechanical shutter (FS) synchronized with the laser operation at 1 kHz. A summary on the laser specification provided by Clark-MXR, Inc have been listed in table 3.1.

Maximum Pulse energy	0.8 mJ at repetition rates = 1 kHz.
Pulsewidth (FWHM)	<150 fs
Wavelength	775 nm
Transverse mode	TEM_{00}
Repetition Rate	User adjustable up to 1 kHz
Polarization	Linear, horizontal
Energy stability	<1% rms all versions
Prepulse extinction ratio	>500:1 all versions
Postpulse extinction ratio	>100:1 all versions
M^2 factor	< 1.2
Beam Diameter (FWHM)	4-6mm
Beam divergence	<100 microradians

Table 3.1: Performance parameters of a CPA-2001 system.

The substrate is mounted on an x-y-z variable speed motor driven stage with a step resolution of 0.1 µm. A CCD camera arrangement was aligned through the dielectric mirror (M3) which has high reflector at a laser wavelength but transparent in the visible region, was used to monitor the sample alignment and the machining process during the course of the experiments. All experiments were performed in ambient conditions.

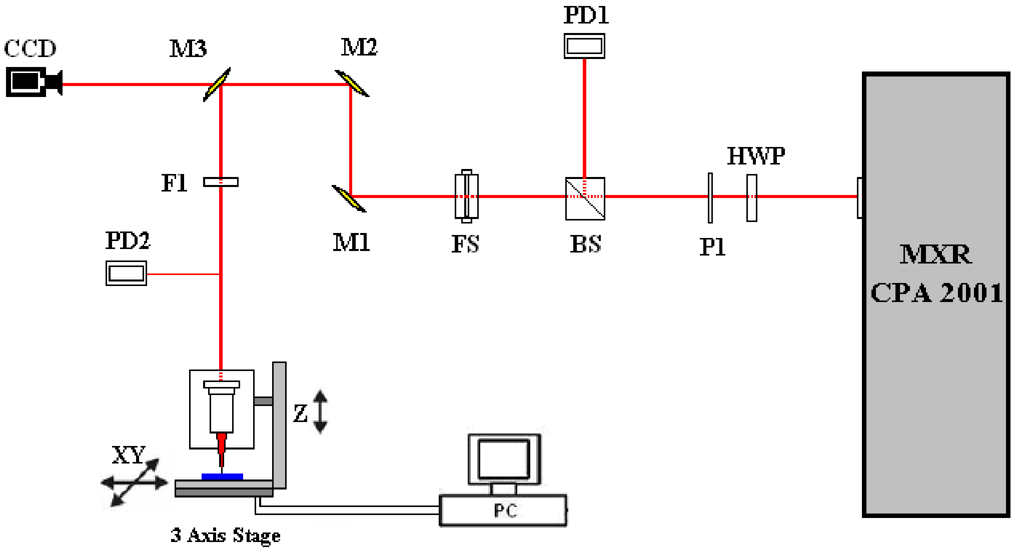

Figure 3.1: Schematic of set-up for femtosecond laser processing of materials.

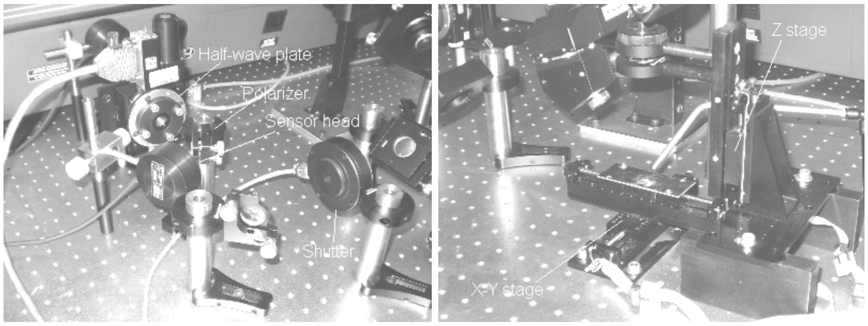

Figure 3.2: (a) Photographs of femtosecond laser (CPA2001) with optical components and (b) showing machining stage with lens.

3.2.2 Single and multiple pulse ablation experiments

In experiments dealing with single and multiple pulse ablations, it was necessary to select a known number of pulses from the 1 kHz pulse train. The number of pulses delivered to the sample was achieved via adjusting the open time of a fast mechanical shutter synchronized with the laser operation at 1 kHz. In this research study, the laser pulses used ranged from 1 to 100000 pulses.

3.2.3 Groove cutting experiments

In the experiments involving groove cutting the individual pulse energy measurements were not required. Instead, the average power was measured with the power meter prior to the experiments. Three basic types of experiments were routinely performed involving characterization of the groove depth as a function of the pulse energy, the feed rate and the number of consecutive passes over the same area (multiple pass cutting). The sequence of these experiments was as follows: After one of the routines was initiated, a groove of specified length was cut by translating the sample relative to the stationary beam in both x and y axis at a specified feed rate (10 μm/s to 500 μm/s). The sample was then moved to a new position with a new set of parameters and the process was repeated until a specified number of grooves were cut. A summary of the parameters is described in Table 3.2.

Description	**Parameters**
Scribing Orientation	X or Y
Power (mW)	15,25,50,100,250 and 500
Polarization	P-Polarized or C-Polarized
Feed-rate (μm/s)	10,50,100,250 and 500
No of Cutting Passes	1,2,4,8,10,25,50 and 100

Table 3.2: Parameters used for groove scribing.

3.3 Laser diagnostic tool and alignment

3.3.1 Beam profile measurement

Characterizing the laser beam profile prior to the ablation study is of great importance to ensure the stability of the laser system in term out beam energy distribution. The spatial profile of the beam from CPA 2001 was characterized using a CCD-based laser beam profiler (SPIRICON, LBA-PC Series). The beam quality factor (M^2) for the laser system is approximately 1.5. Under most of the experimental conditions the beam profile and the far field profile after the microscope objective closely followed a Gaussian intensity distribution as shown in Figure 3.3.

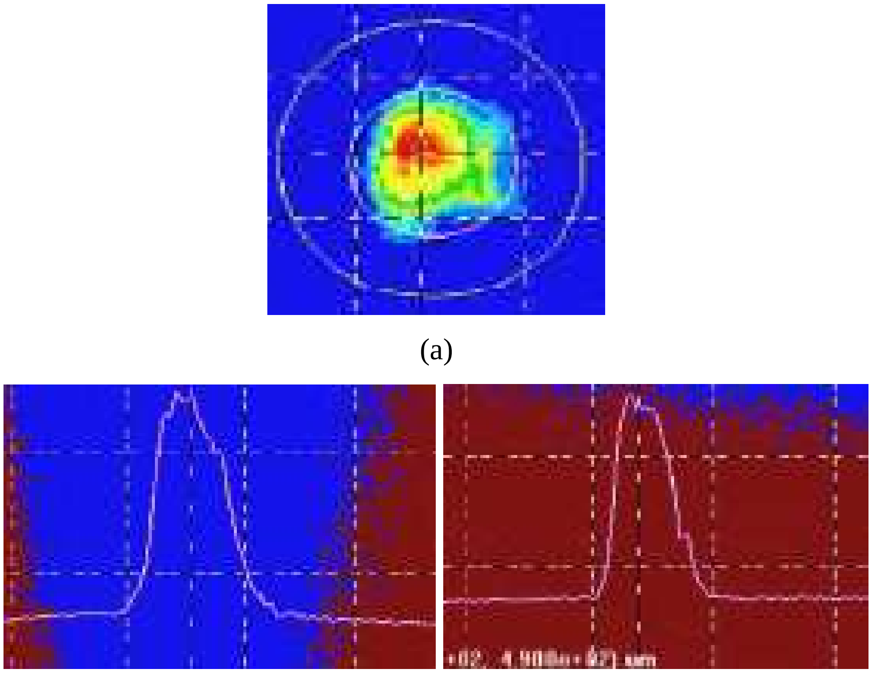

(a)

(b) (c)

Figure 3.3: (a) Typical beam profile of the CPA2001 beam (775 nm wavelength) taken with a CCD beam profiler. The curve in figures (b) and (c) represents a Gaussian fit to the intensity distribution along the horizontal and the vertical direction.

3.3.2 Pulse width measurement

Important information about the temporal behavior of the phase of the pulsed field may be obtained by spectrally analyzing the second-harmonic or sum frequency signal produced by the two pulses as a function of delay time. This technique was first introduced by Trebino and Kane (1993) and is called FROG (frequency-resolved optical gating). A typical SH-FROG trace and the retrieved pulse shape are shown in Figure 3.4 with FWHM of 210 fs,

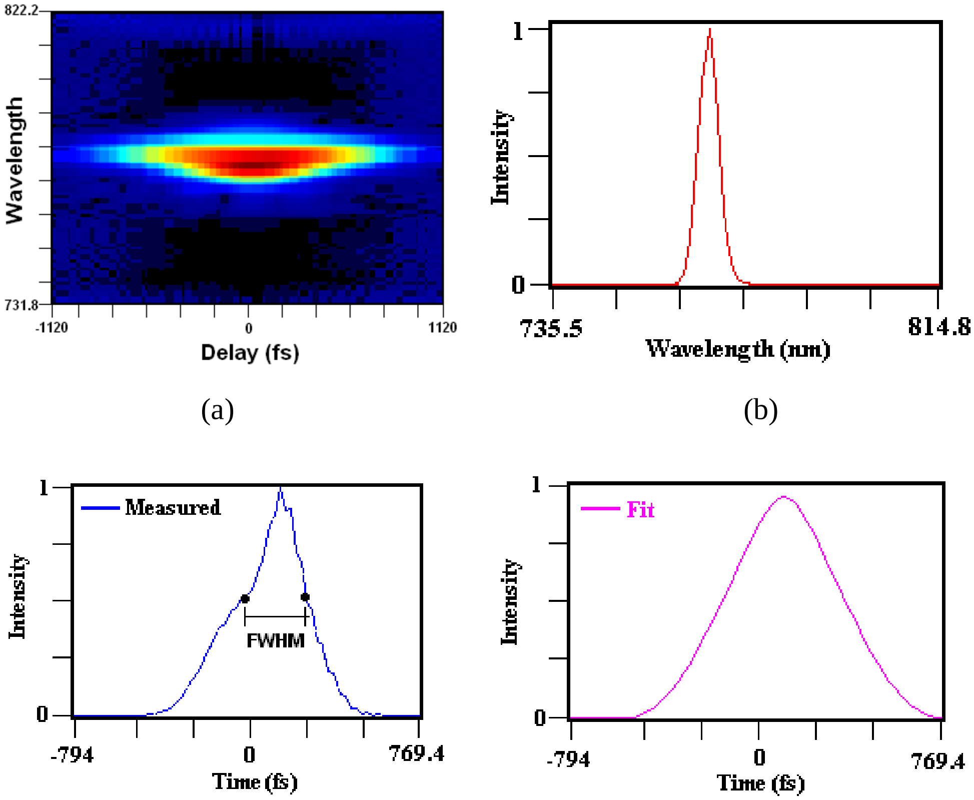

(a) (b)

(c) (d)

Figure 3.4: (a) SHG-FROG trace for a train of pulses from the 775nm Ti: Sapphire femtosecond laser. (b) Spectrum derived for the pulse who FROG trace is shown in Figure 3.4 (a). (c) Measure intensity whose SHG FROG trace shown in Figure 3.4 (a). (d) Fitted intensity whose SHG FROG trace shown in Figure 3.4 (a).

3.3.3 Spectrum measurement

Spectral measurement in the visible wavelength range was performed using a spectrometer E201 LSA03A (IST). A typical spectrum from the CPA 2001 is shown in Figure 3.5. It can be observed that the measured wavelength of the laser system is approximately centered at 775 nm which is close to the specification specified by the manufacturer.

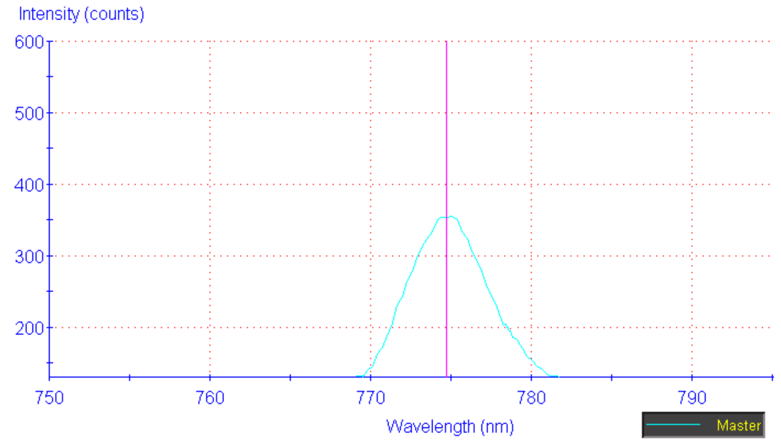

Figure 3.5: Spectrum from the CPA2001 femtosecond laser at 150 fs output.

3.3.4 Power measurement

Accurate power measurements were very important since the goal of many investigations was to determine the ablation thresholds and characterizing the dependence of various machining parameters with respect to the laser pulse energy or fluence. The power measurement was carried out using a dual channel energy meter (Ultima LabMaster, Coherent) and an absorbing detector head (LM-3, Coherent) with an accuracy of ±2% and resolution 0.01W base on specification from Coherent. All power (pulse energies) measurements were always made just before the microscope objective to account for all throughput losses during the beam delivery to the lens. Typically, energy loss through mirror is approximately 3 percent of the output power.

Before the start of every experiment, the required beam energy was adjusted by inserting different neutral density filters with different attenuation values. Following which, the pulse energy was measured and monitored using a computer based strip chart program for a period of 10 minutes and the average power (P_{avr}) and the standard deviation (σ_P) were calculated. To further account for power fluctuations or drifts, during the course of experiments, the secondary output power from the beam splitter (Refer to earlier Figure 3.2) was monitored on the other channel of the power meter. Any differences in the secondary output power would indicate an energy drift which occurs but in the course of most experiments, no significant energy drift was observed.

3.3.5 Spot size measurement

Determination of the laser fluence is essential for characterization of the ablation process and the accuracy of fluence determination largely depends on the measurements of the spot size on the sample surface. For a Gaussian beam, the peak fluence is given by (Trans *et al*., 2005):

$$F_o = \frac{2.E_p}{\pi \omega_0^2} \qquad (3.1)$$

where, E_p is the pulse energy and ω_o is the spot size, i.e., beam radius measured at $1/e^2$ of the intensity profile.

Several methods have be used for carrying out spot size measurement like using a CCD profiler (Roundy,1999) knife edge technique (Firester *et al*., 1977; Bilger, and Habib, 1985) or measuring the laser spot size of tightly focused beams and analysis of the lateral dimensions of the ablation craters (Lui, 1982). The last method has been widely adapted by many groups in studying laser ablation and micromachining as it also allows one to determine the modification threshold of the target material.

Using this technique, a set of single pulse ablation craters were produced on the sample with decreasing pulse energy. The crater diameters (D) were measured as a function of the pulse energy F_o, then F_{th} and ω_o were determined by fitting the data to Equation. (3.2) where the diameter (*D*) of the ablation crater is related to the energy of the incident pulse by (Bonse *et al*., 2001; Borowiec and Haugen, 2004):

$$D^2 = 2\omega_0{}^2 In\left(\frac{F_0}{F_{th}}\right) \qquad (3.2)$$

F_{th} is the threshold pulse energy, that is the minimum pulse energy required to produce permanent material modification. With the obtained fit parameters the threshold fluence was calculated with Equation. (3.1).

A typical set of experimental data is shown in (Figure. 3.6), obtained for fused silica irradiated by 150 fs, 775 nm pulses, focused with a 25mm focal length lens. The solid line represents the fit to Equation. (3.2). In this experiment, the least square fit yielded a spot size of 10.56 µm. To verify the consistency of the measured spot size and polarization effect, another set of single pulse ablation experiment was carried out using various laser polarizations as shown in Figure 3.7. For this set of experiments, the least square fit yielded a spot size of 11.2 µm and comparing the two sets of measurement data, the error difference is less than 10% indicating a good consistency in the results.

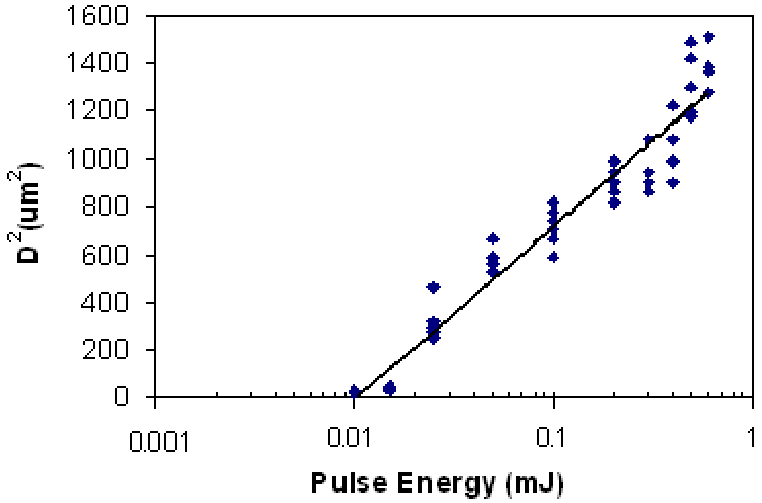

Figure 3.6: Spot size measurements of beam focused on the sample surface by a 25mm focal length lens.

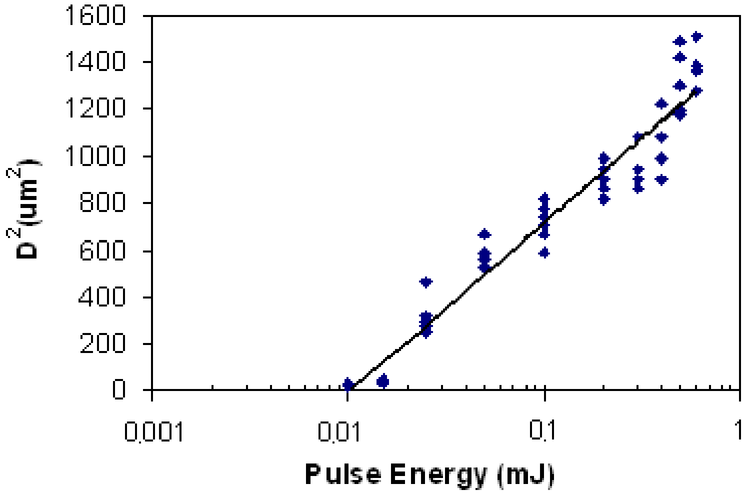

Figure 3.7: Spot size measurements of beam focused on the sample surface by a 25mm focal length lens using various polarizations.

3.4 Sample and sample preparation techniques

UV grade fused silica having a dimension of 10mm by 10mm with thickness of 1 mm was used throughout the experiment. This material has thermal coefficient of expansion of 0.55–0:57 x 10^{-6} ºC^{-6} which makes it an ideal candidate for high repetition rate laser processing. For crystalline quartz (100) and (111), it also has similar dimension as the fused silica substrate.

3.4.1 Preparation of metallographic samples

Prior to the laser ablation experiments, all samples having a dimension of (10mm x 10mm x 1mm) were pre-cleaned in an ultrasonic bath containing acetone to remove any grease or surface contaminants on the surface. The samples were dried using nitrogen gas.

3.4.2 Preparation of cross-sectional SEM samples

Preparing cross-sectional samples of the laser machined grooves and holes require great attention and skill as the laser machined grooves and holes tend to fracture during the sectioning and grinding process. To reduce the fracturing tendency, a special technique was applied. First a glass substrate was preheated to a temperature of 70 °C on a hot plate. Next, a small portion of wax was applied on the heated substrate surface followed by placing the laser-machined sample on the surface. More wax was further applied on the sample surface (see Figure 3.8) until the entire sample surface was covered in wax. The sample was then left to cool in air for the wax to solidify. Once the sample was firmly held in place, it was then sectioned using a diamond saw. The cut sample was then ground with silicon carbide paper progressively from a grits of 1000 to 4000. Careful cleaning of the samples was performed between each step to prevent cross contamination of coarse abrasive particles in the finer steps. To avoid the formation of directional grinding, these operations were performed with a rotation of the specimen by 90° after each step to eliminate scratches formed in the previous step.

After the fine grinding step, the surface was progressively polished using diamond particle suspension solutions with sizes from 6 µm, 3 µm and 1 µm at a constant rotating speed of 250 revolutions per minute. Polishing lubricants were applied constantly to prevent embedding of diamond particles into the sample surface. Visual inspections were also frequently carried out under an optical microscope to ensure that the final surfaces were free from scratches and embedded particles from previous polishing process. The samples were cleaned in an ultrasonic bath containing acetone to dissolve the wax and also to remove any grease or surface contaminates on the surface.

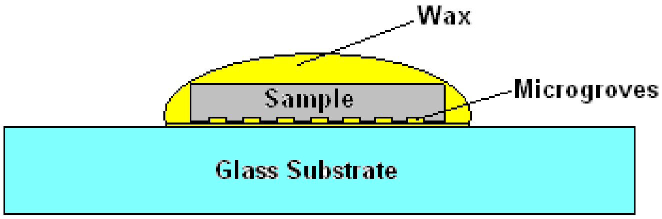

Figure 3.8: Cross-sectional view of the laser machined sample covered in wax on the glass substrate.

3.4.3 Preparation of plane view & cross-sectional TEM samples

Great effort was made to prepare samples in order to carry out TEM observation of the laser-irradiated materials. In this research study, two types of TEM samples were prepared, namely, plane view and cross sectional samples. The sample preparation techniques are described in greater detail as follows:

Plane view samples were prepared by cutting laser-irradiated region to a dimension around 2 mm x 2 mm using a diamond saw. The sample was ground using diamond abrasive papers from grit of 30 µm progressive down to 0.5 µm using an in-house built tripod jig fixture. Constant monitoring of the sample thickness was carried out under an optical microscope operating in transmission mode between each grinding steps. The ground sample was thinned to perforation by an Ar-miller from the substrate side towards the laser-irradiated surfaces using a Gatan Precision Ion Polishing System (PIPS 691) operating at 5 keV. The thinning parameters used were as follows: rotation speed was at 3.5 rpm and milling angle was set at 7º and 4º respectively. In order to reduce the ion-induced rippling effect, specimen rotation and shocking were adopted in the thinning process (Carter, 1997; Mongeot *et al*., 2000).

Cross-sectional TEM specimens were prepared either by using FIB or a special technique that was able to protect the top layer of the laser-irradiated surface. The samples were cut into slices using a diamond saw and subsequently glued face to face using M-bond 610 adhesive joining the laser irradiated surface as shown in Figure 3.9. These sandwiches were then ground and introduced onto the TEM copper tube and then thinned down as for the plane views.

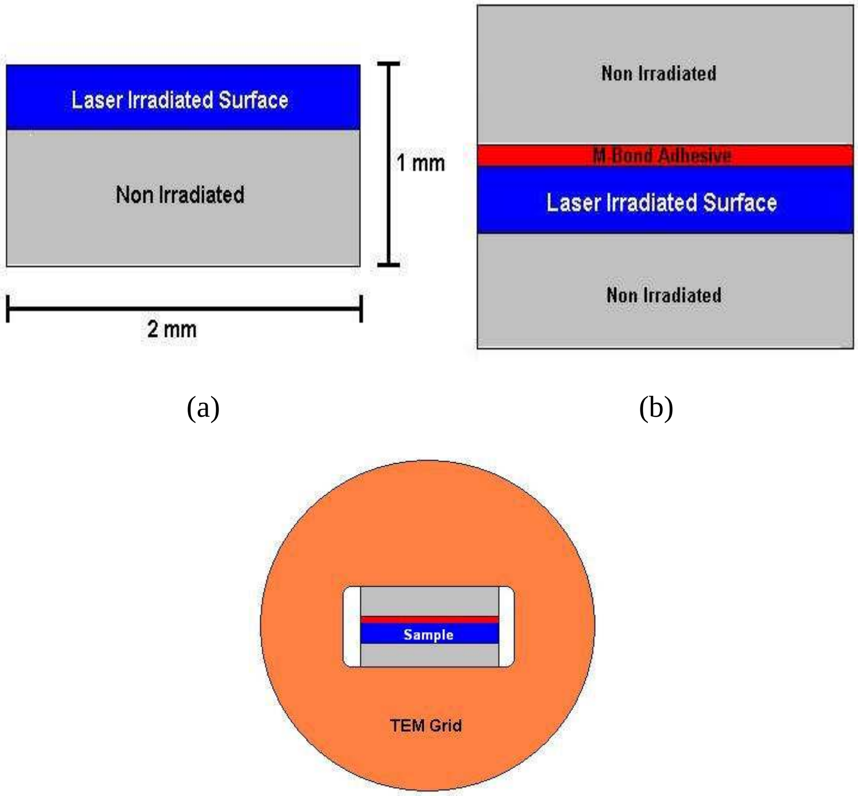

(a) (b)

(c)

Figure 3.9: Steps in preparation of cross-sectional TEM sample. (a) Cross-sectional slice of microchannels sectioned with diamond saw; (b) Two slices of microchannels glued face to face to protect irradiated surfaces; and (c) Transfer of sample onto TEM grid after grinding.

3.5 Characterization techniques

3.5.1 Optical microscope (OM)

Optical microscope (OM) was first used to carry out preliminary assessment of the material surface after femtosecond irradiation. All the optical measurements were performed using an Axioplan 2 (Zeiss) microscope, which operates in the differential interference contrast mode (DIC). Optical images of the laser-ablated surfaces were captured with a digital camera using various magnification objective lenses (5× to 50×). Image Pro Plus software was used for image processing and carrying out quantitative measurement of the laser ablated surfaces in terms of length and area. Using the OM is a convenient and easy tool to capture the surface morphology and it is especially sensitive to changes in surface reflectivity induced by laser irradiation. However, the resolution of the OM is relatively low, approximately 0.5 μm and since most of the ablation features were less than 20 μm, SEM was the primary measurement instrument.

3.5.2 Scanning electron microscope (SEM)

In this project, the scanning electron microscope (SEM) was used as the primary tool for characterizing the surface morphology, lateral dimensions of ablated features and the depth of the grooves viewed in cross-section. The SEM images present in this thesis are mostly captured using JEOL LV5600 SEM and LEICA S360 (Cambridge, UK) SEM. All the SEM systems are equipped with Energy Dispersive X-ray Analysis (EDX) for carrying out fast detection of the chemical compositions of materials. A thin layer of gold was sputtered on the laser irradiated sample to prevent charging of the glass sample. However, sputtering the sample surface with gold was performed after completing the chemical composition analysis. This is to ensure that the accuracy of the EDX results so that the original chemical composition was not altered. The beam energy can be in the range of 5-20 keV, but in most cases it was kept constant at 20keV for both imaging and chemical composition detection purposes

3.5.3 Transmission electron microscopy (TEM)

JEOL 2012F and JEOL JEM-2012 transmission electron microscope operating at 200 kV were used to study material damage and structure change induced by femtosecond laser beam irradiation. Both TEMs were also equipped with EDX facilities (energy dispersive X-ray analytical system) for carrying out chemical analysis. Selected area diffraction technique was used to determine the crystallographic structures of the regions investigated. Preparation of the TEM samples has been described in detail in Section 3.5.3.

3.5.4 Atomic force microscopy (AFM)

A multimode AFM (Digital Nanoscope III) operating in tapping mode was used to characterize the three dimensional topography of laser irradiated surface. Due to its high lateral and vertical accuracy, the AFM is well suited for characterizing very shallow features and allows measurement of small crater depths and volumes. Furthermore, measurement can be directly performed in air rather than vacuum and it does not require the sample surface to be conductive. This greatly improves the operational convenience; however, several disadvantages of AFM include low dynamic range, typically less than 2 μm, and a scanning area limited to 150 x 150 μm^2. If the sample has large topology variation, the tip would not be able to measure and the image will be distorted due to noise.

3.5.5 Talyscan stylus profiler

A stylus profiler (Taylor Hobson Precision Talyscan 150) was used to characterize the laser machined grooves profiles. The stylus profiler has two modes of operation, which are contact, and non-contact mode.

In contact mode, a sharp diamond tip with a diameter of 5 μm is in contact with the surface. The height difference during scanning causes deflection to the tip and is picked up by an inductive transducer. A change in the electrical inductance due to the movement of the stylus was converted to height information with the help a signal processor. Measurements carried out in contact mode are often very damaging, as it will cause scratches on the material surfaces.

In non-contact scanning mode, a laser beam was used. The non-contact scanning was carried out using a pulse laser operating at a wavelength of 670 nm. The beam was focus onto the surface to a diameter of 100 μm. The stylus operating in non-contact mode made used of laser triangulation principle to determine the surface topology. During scanning, the beam is projected on to the target and a portion of the beam is reflected through focusing optics onto a detector. As the target moves, the laser beam proportionally moves on the detector. A change in the detector signal is used to determine the height data with the aid of a signal processor. For both contact and non contact measurements, the samples sit on a high precision x-y motorized stage and the lateral resolution for contact scanning is 0.06μm while non-contact scanning is 1μm. Vertical accuracy resolution for laser gauge measurement on diffusing surfaces with homogeneous properties is 1μm.

3.5.6 X-ray diffractometer (XRD)

X-ray diffraction patterns for the non-laser irradiated and femtosecond laser irradiated surfaces were obtained using a XRD (Philips Model PW1830). A copper target was used for producing a X-ray source having a wavelength of λ=1.5404 Å (Cu Kα1). All the samples were scanned at a speed of 0.02 °/s. with the scanned angle from 10° to 120°.

Chapter 4 Ripple Formation upon Femtosecond Laser Irradiation of Fused Silica

4.1 Introduction

Ripple formation after femtosecond laser irradiation has been observed over a wide range of materials and the possible mechanisms have been reviewed in Chapter 2. Though the literature have provided some in-depth understanding on the mechanism on ripples formation on various materials using both long and short pulse lasers, ripple induced on fused silica after femtosecond laser irradiation is still not well understood even though there are already some preliminary ripple studies performed on fused silica material during the course of my PhD research. For example, Ihlemann *et al* (1992) carried out ablation of fused silica and they reported that the ripples maybe due to melting and resolidification or even perhaps recrystallization process. Wager *et al* (2006) observed subwavelength ripples when scanning perpendicular to polarization and they explained the ripple formation in term of the interaction of incident wave with the surface electromagnetic waves (SEW). Bohme *et al* (2008) performed laser-induced backside wet etching (LIBWE) of fused and since the laser irradiation was performed at the solid/liquid interface, they proposed that these ripple maybe defect-mediated. Gottmann *et al*., 2009 proposed a different reason on the ripple formation which was a result of interference.

This chapter reports a detailed study on the formation of periodic structures on fused silica after femtosecond laser irradiation. By employing a wide range of laser parameters such as varying the laser fluence, number of pulses, beam polarization orientation and material crystallographic orientation, the growth and evolution of the ripples on fused silica is studied using SEM and AFM techniques. Two directional ripples were observed after femtosecond laser irradiation. The ripple mechanism is discussed based on the framework of the conventional theory and in terms of irradiated surface morphology. Calculation on the melt depth tallies with the depth of the coarse ripples measured using AFM. It is proposed that the coarse ripple is likely a result of freezing capillary waves while fine ripples are induced by the harmonic wave generation during femtosecond laser irradiation. The influence of the beam polarization, crystallographic orientation and surface defects in the ripple orientation is also discussed.

4.2 Ablation threshold determination

Determining the ablation threshold of a material is important prior to any laser machining studies as it enables the end user to know the minimum amount of fluence required to ablate the material of interest as well as to control the machining process effectively. In this study, the threshold fluence can be obtained using the following equations. For a Gaussian shape beam, the change in the feature diameter can be related to the laser fluence by the following relationship (Qi *et al*., 2010):

$$D^2 = 2\omega_0{}^2 In\left(\frac{F_0}{F_{th}}\right) \qquad (4.1)$$

where, D is the feature diameter, ω_0 is the l/e^2 beam radius, F_0 is the fluence at the centre of the focused beam, and F_{th} this the threshold fluence for creating the feature. F_0 is related to the laser pulse energy by:

$$F_o = \frac{2.E_p}{\pi\omega_0^2} \qquad (4.2)$$

where, E_p is the laser pulse energy. From equations (1) and (2), ω_0 and F_{th} can be determined from the slope and intercept of the logarithmic dependence of D^2 on E_p. In this experiment, the feature diameter (D) is obtained by measuring the laser-ablated profile using the optical microscope. The maximum threshold fluence can be obtained by extrapolating D^2=0. The threshold represents the lowest level of material modification detectable using the optical microscopy which is 3.5 J/cm^2. The result for single pulse laser ablation of fused silica is shown in Figure 4.1.

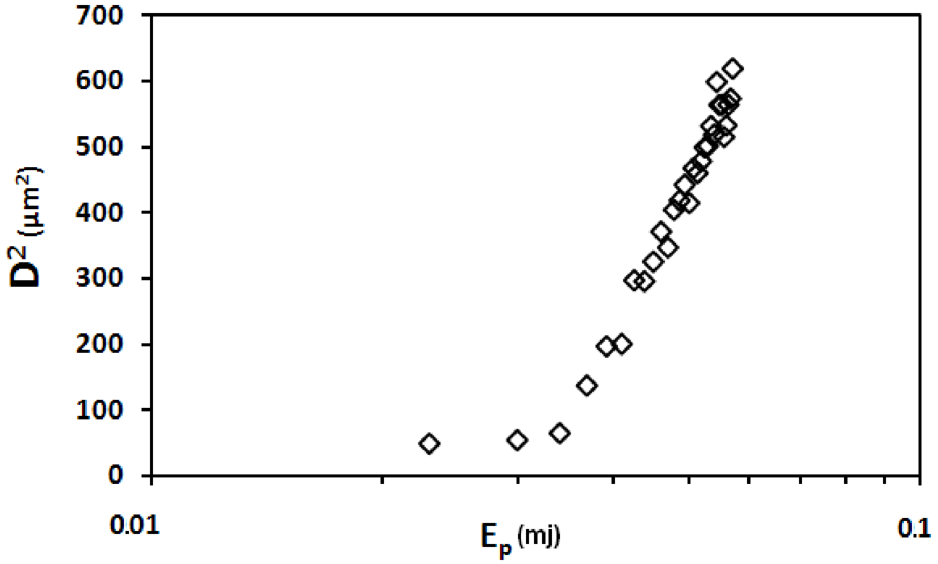

Figure 4.1: Squared diameter (D^2) of the ablated area versus the applied pulse energy (E_p) on femtosecond laser ablation of fused silica by single laser pulse irradiation.

4.3 Effect of laser fluence and pulses in ripple formation

4.3.1 Low fluence regime with increasing laser pulses

To study the evolution of ripples, the fused silica substrate was first irradiated using a low fluence of 4.7 J/cm^2 which is slight above the ablation threshold of 3.5 J/cm^2. In this study, low fluence regime refers to laser fluence close to the threshold value while high fluence regime refers to using a fluence ten times the threshold value. The evolvement of the ripples with the increasing number of laser pulses in the low fluence regime is shown in Figure 4.2. From Figure 4.2(a) and (b), no ripples can be observed on the surface after irradiating with one or two laser pulses. This indicates that a feedback mechanism is likely to be involved in the formation of surface patterns when carrying out single-pulse ablation (Bonse *et al.*, 2002). However, after irradiating with 4 consecutive laser pulses, fine ripples having an orientation perpendicular to laser polarization were formed on the fused silica surface (See Figure 4.2 (c)).

By further increasing the number of irradiated pulses to 8 and 10 laser pulses, the ripples become broader and more regular (See Figure 4.2(d) and (e)) but these ripples tend to become rougher when more pulses were applied. It is also observed that the width and the height of the ripples decrease monotonically from the center to the edge, which is consistent with the Gaussian distribution of the focused laser energy. Judging from the SEM results, the fine ripples evolved from an initial period of 100nm to a final period of 320nm.

After 13 laser shots, the center of the irradiated spot broke open and a second ripple structure was observed to superimpose onto the original fine ripples as shown in Figure 4.2(f). This second structure, also known as coarse ripple in this chapter is observed to have a larger period as compared to the fine ripples. The orientation of the coarse ripple is opposite of the fine ripples which is parallel to the beam polarization. Based on the SEM images, the coarse ripples have a period of approximately 580 nm. It should be noted that ripples parallel to polarization are seldom observed, however, this does not imply that our results are necessarily contradictory to others as ripples parallel to laser polarization have been previously observed and reported (Sung *et al*., 2001; Qian *et al*., 2005; Han *et al*., 2011).

By further increasing the number of consecutive laser pulses to 17 shots (See Figure 4.2(g)), it is observed that the region of the coarse ripples gets larger but at the edges of the laser irradiated spot the primary fine ripple structure can still be observed. Slight traces of melting can be observed within the ablated crater. This melting could be a result of a liquid layer that has undergone phase explosion due to superheating by the high intensity beam (Bonse *et al*., 2002). Figures 4.2(f) and 4.1(g) clearly show evidence for a rapid expulsion of liquid droplets that was cooled almost instantly and solidified.

Upon irradiating with 20 consecutive pulses, the primary ripples disappeared completely leaving behind only the coarse ripples at the bottom of the ablated crater as shown in Figure 4.2 (h). Massive ablation leading to rapid deepening of the ablated crater is observed when the applied laser pulses (> 40 pulses). At the bottom of the crater the regular ripple structures can be still observed until the total pulses reaches 70 pulses.

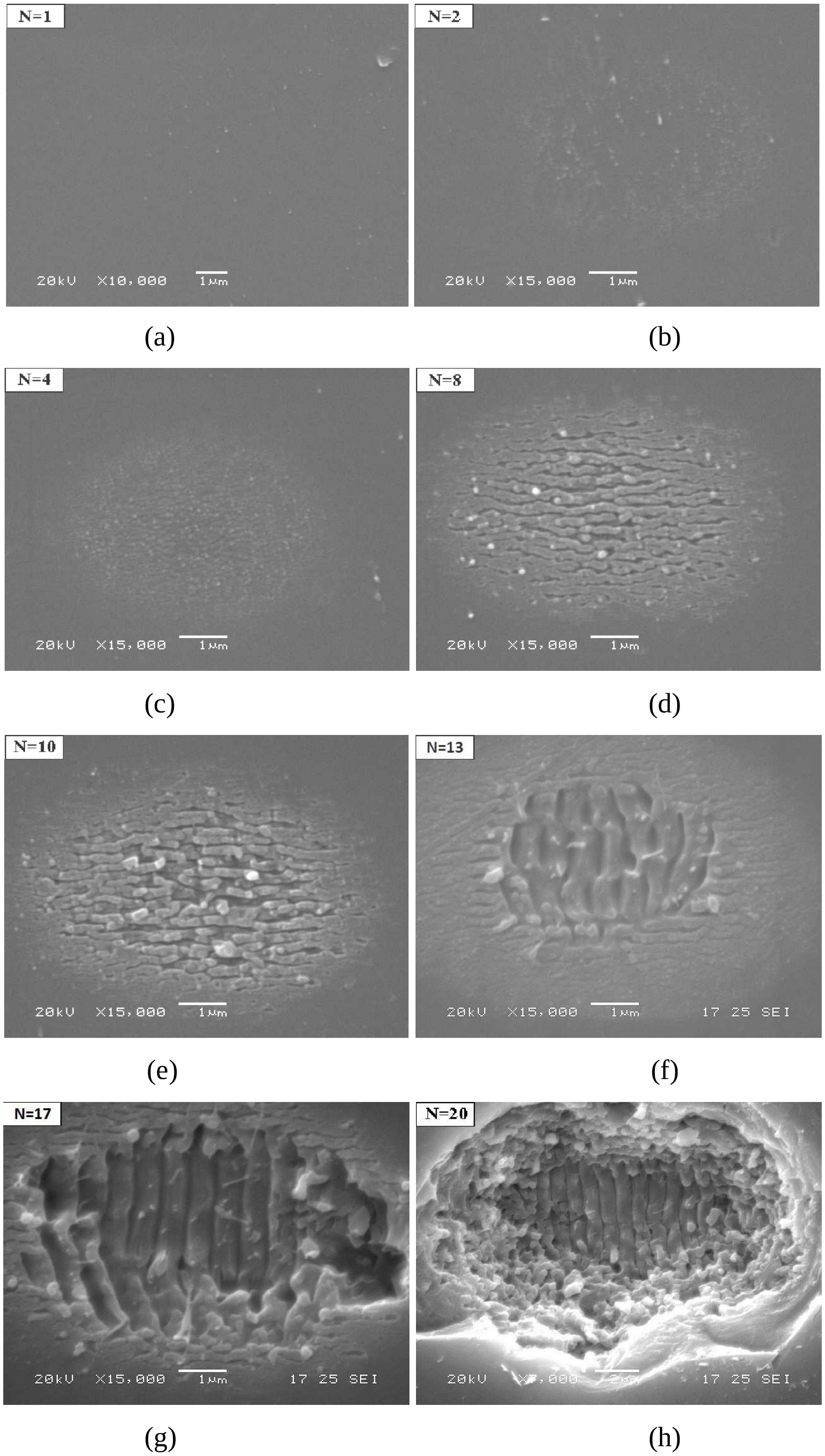

(a) (b)

(c) (d)

(e) (f)

(g) (h)

Figure 4.2: SEM images of fused silica surface after irradiation at 4.7 J/cm^2 for pulse number of (a) 1, (b) 2, (c) 4, (d) 8 (e) 10, (f) 13, (g) 17 and (h) 20.

AFM was used to characterize the period and depth of the ripples. The 2D AFM surface morphology and cross sectional profile of the ripples after 4 and 15 laser pulses are shown in Figure 4.3 and Figure 4.4 respectively. From the AFM cross-sectional profile in Figure 4.3 (c), the fine ripple after 4 consecutive pulses has a period of 120nm and the measured depth is 40nm. It is interesting to note that the topology of fine ripples when observed at high AFM magnification resemble many short linear strings arrays having a length of approximately 500nm (See Figure 4.3(b) and (d) on an enlarged view of 4.3 (a)). These arrays seem to be made up of many nanospheres arranged in an orderly manner.

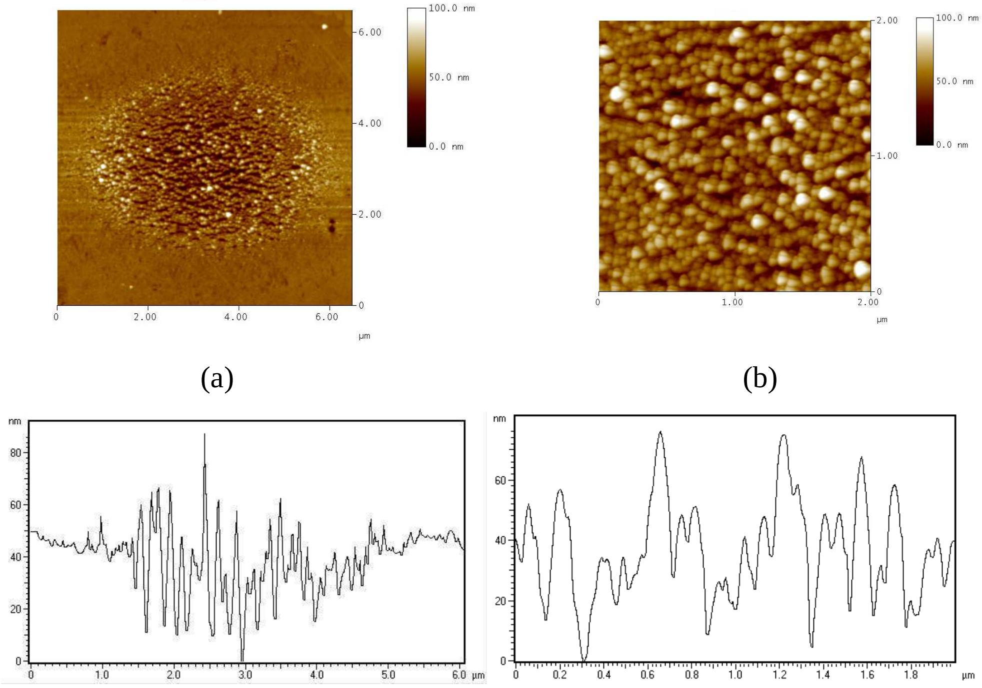

(a) (b)

(c) (d)

Figure 4.3: AFM images of fused silica surface after irradiating with 4 laser pulses using a fluence of 4.7 J/cm^2. (a) Overview of surface morphology at low AFM magnification (b) Close-up AFM profile of the ripples. (c) Cross-sectional profile of the ablated crater and (d) Cross-sectional profile of the ripples.

For ripples irradiated with 15 laser pulses, AFM results in Figure 4.4 shows that the fine ripples have a depth and period of 100nm and 340 nm respectively. It is observed that both the modulation depth and ripple period increases with an increase in the pulse number. For the coarse ripple, it has a larger period and depth as compared to the fine ripples. AFM results show that the coarse ripple period is approximately 550nm with a depth of 300 nm. The increase in the ablation depth is due to the increase total cumulative pulses applied.

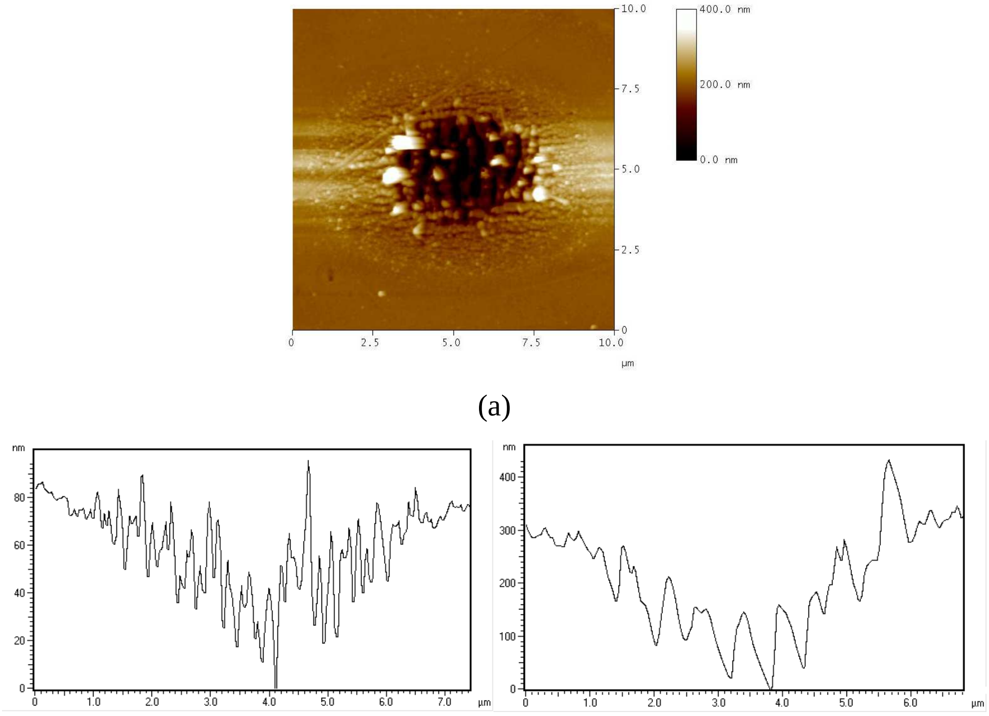

(a)

(c)

(d)

Figure 4.4: AFM images of fused silica surface after irradiating with 15 laser pulses using a fluence of 4.7 J/cm^2. (a) Overview of surface morphology at low AFM magnification (c) Cross-sectional profile of the fine ripple and (d) Cross-sectional profile of the ripples.

4.3.2 Intermediate fluence regime with increasing laser pulses

By irradiating with a laser fluence (15.9 J/cm^2) which corresponds to three times higher than that of the first applied fluence, it is observed from Figure 4.5 (a) and (b) that ripples have already formed on the surface after irradiating with only 1 and 2 laser pulses. A close-up examination at higher SEM magnification (See Figure 4.5(e)) shows that these ripples have orientations both parallel and perpendicular polarization. Comparing to the earlier results in the low fluence regime, ripples with only two orientations can be observed at higher pulses. This shows that by irradiating with higher laser fluence brings forward the formation of two directions ripple. It should be noted that the two direction ripples can only be observed in a certain fluence and pulse conditions based on our experimental results.

By irradiating with 4 or 8 consecutive pulses in this intermediate fluence regime (Figure 4.5(c) and (d)), no ripples can be observed within or along the peripheral of the laser ablated crater except sign of material chipping. Some chaotic structures can also be observed within the laser ablated crater. This strongly suggests that ablating the fused silica surface at higher fluence do not favour ripple formation. Instead it promotes surface defects formation like chipping or even cracking when higher laser fluence is used.

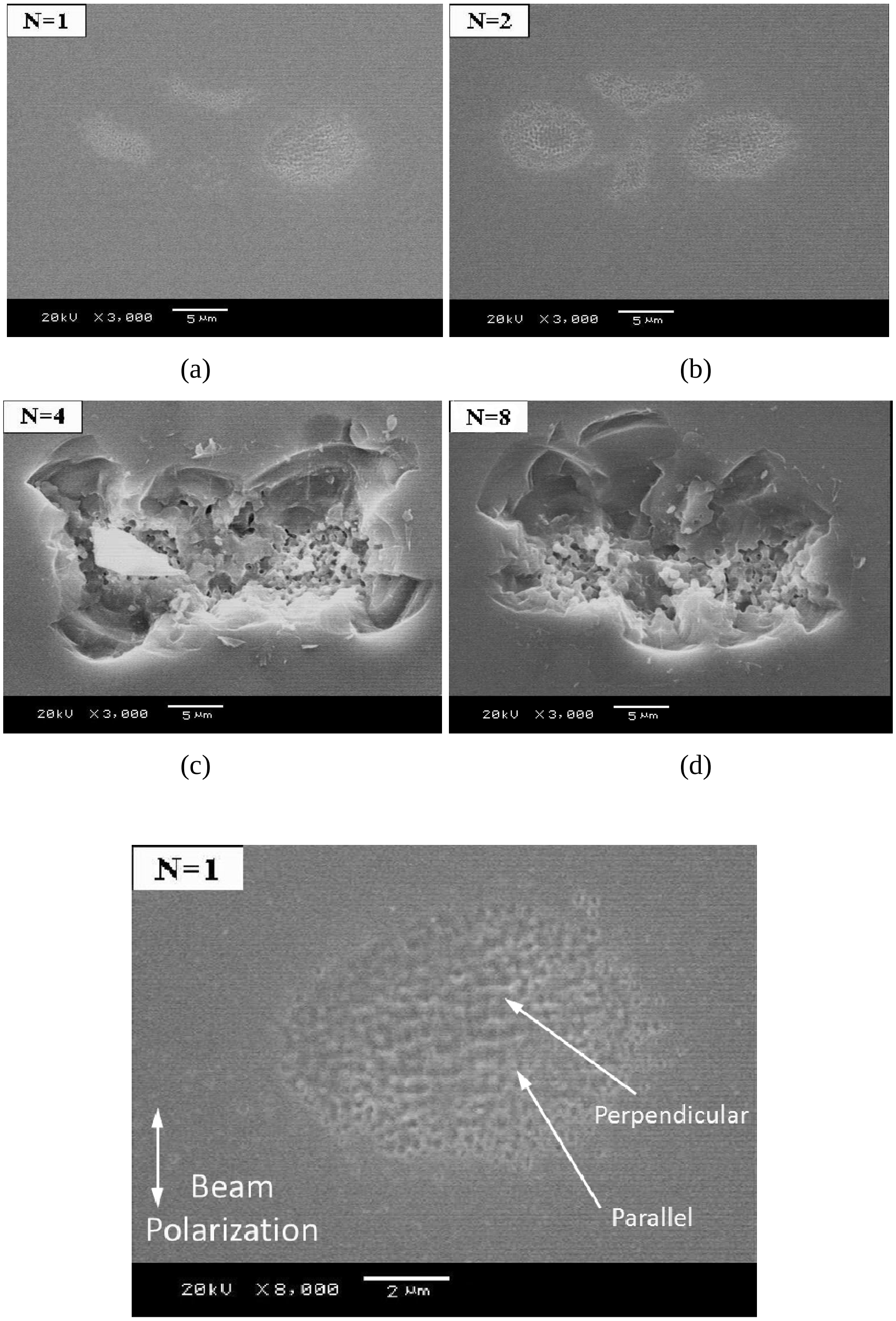

(a) (b)

(c) (d)

(e)

Figure 4.5: SEM images of fused silica surface after irradiation at 15.9 J/cm^2 for pulse number of (a) 1, (b) 2, (c) 4, (d) 8 and (e) Close-up image of surface irradiated with 1 pulse having ripples in 2 orientations.

4.3.3 High fluence regime with increasing laser pulses

Results of fused silica irradiated at even higher fluence of 31.3 J/cm^2 are presented Figure 4.6. As expected, ripples could only be observed for the first few pulses when irradiating the surface at even higher fluence (See Figure 4.6 (a) and (b)). By taking a closer examination of the fused silica surface irradiated with 2 pulses (See Figure 4.6 (e), it is surprising to see that the surface consists of both ripples as well as nano-voids. Slight traces of melting can also be observed which is indicated by the strands of white lines in the SEM image. The formation of the nano-voids is a result of the inhomogeneous nucleation of the bubble in the melted fused silica layer after slight ablation by phase explosion (Bonse *et al*., 2002). It is known from the earlier results that by irradiating with even higher fluences would lead to massive ablation and defects formation. As shown in Figure 4.6 (c), cracking was observed with a dramatic increase in the ablated depth when 4 or more consecutive pulses were applied.

Similarly, no periodic ripples could be observed within the crater except for a chaotic structure which was observed earlier that resembled highly disorientated ripples. Judging from the feature size which is close to the laser wavelength, these chaotic structures may be the result of beam interference due to multiple reflections from the side-walls and bottom surface. This is because fused silica is transparent to the 775 nm beam during the laser processing and by irradiating with higher laser intensity; it will lead to stronger beam reflection (Han *et al*., 2009).

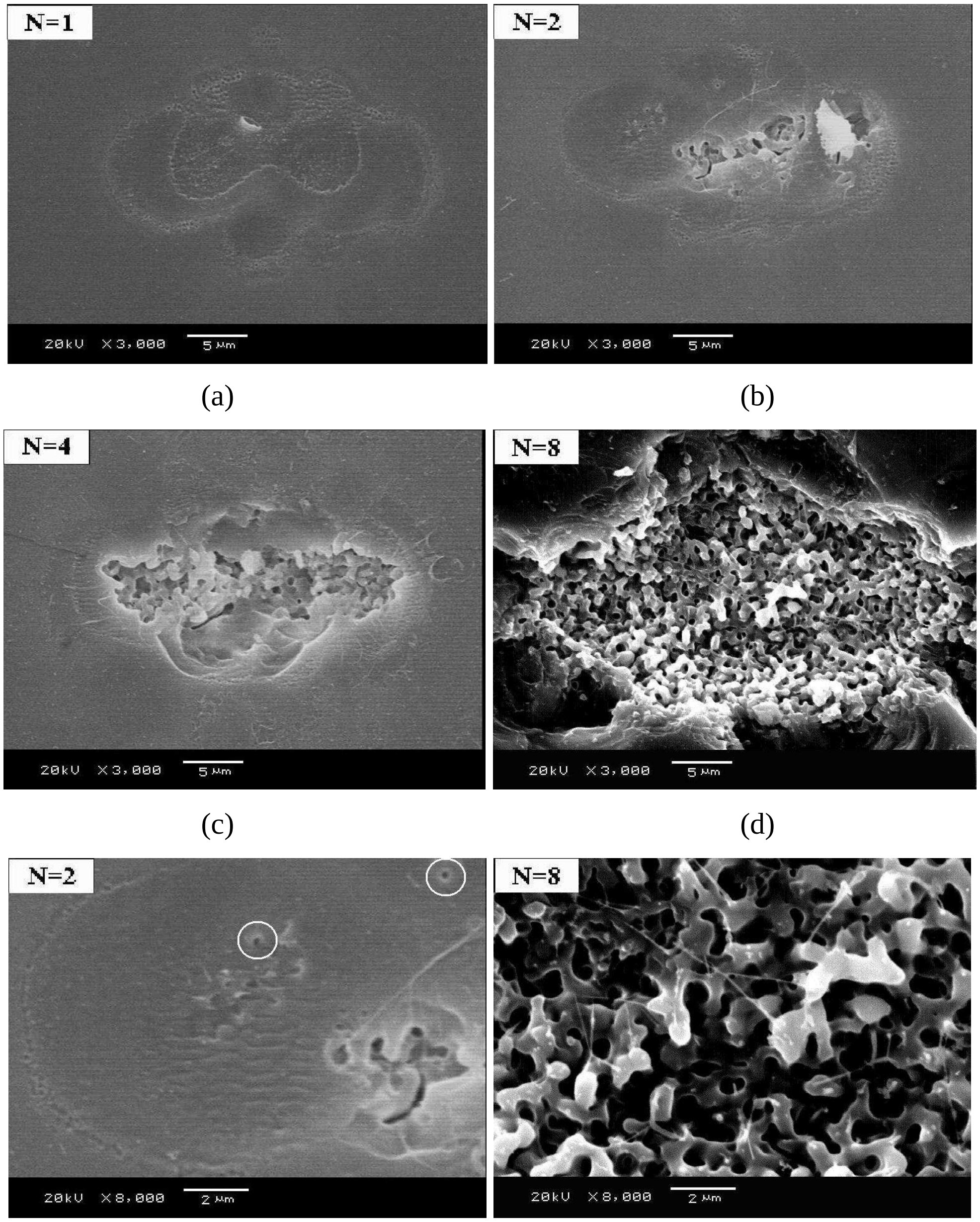

(a) (b)

(c) (d)

(e) (f)

Figure 4.6: SEM images of fused silica surface after irradiation at 31.3 J/cm^2 for pulse number of (a) 1, (b) 2, (c) 4, (d) 8, (e) Close-up image of surface irradiated with 2 pulses having ripples and nano voids and (f) Close-up image of surface irradiated with 8 pulses.

4.3.4 Discussion on ripple formation

Next, the mechanism for ripple formation on fused silica will be discussed based on the earlier experimental results obtained. For solid surfaces subjected to multiple linear polarized laser pulses irradiation, it is widely accepted by many that ripple formation is a result of interference between the incident laser radiation and scattered or excited surface waves (Emmony *et al*., 1973). Very often, two distinct types of ripples have been observed after laser irradiations which are the low and high spatial frequency ripples (Couillard *et al*., 2007). For low spatial frequency ripples or (coarse ripple), they are generally observed to have a period close to the irradiation wavelength and with an orientation perpendicular to the laser polarization. The ripple period using the interference model can be described as:

$$d_p = \frac{\lambda}{1 \pm \sin\theta_i} \tag{4.3}$$

Where λ=laser wavelength; (θ_i) refers to angle of incidence considered to the surface normal (Costache *et al*., 2003). A third pattern, (rarely observed mainly induced by p-polarized beam, was described to be orientated parallel to the beam polarization having a period of:

$$d_p = \frac{\lambda}{Cos\theta_i} \tag{4.4}$$

In contrast, the high spatial frequency ripples (fine ripples) have a period significantly smaller than the laser wavelength and their origin is still under much discussion in the literature. Since the classical interference theory can be used to describe most of the ripple phenomenon, this theory cannot be ignored and need to be considered.

By comparing our results with the literature, irradiating the fused silica at normal incident would produce both low and spatial frequency ripples and indeed the fused silica results tallies with those reported by others. However, when comparing the ripple period against the interference model, both the fine and coarse ripples cannot be described by the simplified classical model as the ripples period are significantly smaller than the wavelength of the laser radiation used. To satisfy the interference criteria, the ripple period has to be somewhere closer to the laser wavelength.

Since, the classical interference theory cannot be used to explain the subwavelength ripples on fused silica, another theory needs to be considered. Self-organization is another popular theory that is widely used to explain sub wavelength ripples formation after femtosecond laser processing of transparent dielectrics (Reif *et al*., 2008; Schade *et al*., 2010). It is to note that the formation of these sub-wavelength ripples is well known to occur only by femtosecond laser irradiation (Tomita *et al*., 2007).

For ripples induced by self organization, they have several particularly strong distinct indications. One of which is the obvious presence of bifurcations along the ripples while another indication for ripple structure arise from self-organization is that the ripple structure will rise above the initial surface, whereas the valleys in between appears depressed (Schade *et al*., 2010). Based on the above two features and comparing against the SEM and AFM results, none of the above features can be observed. It is very likely that ripples arising from self-organization are highly material dependent as different ripple morphology varies on different materials when irritated using the same laser parameters (Wagner and Gottmann, 2007).

A study by Levchenko et al (2011) reported that two key factors are needed for self-organizing behavior of the nanoarrays which are nucleation and the growth kinetics. They reported that surface diffusion was the main physical process responsible for self-organization in nanoarrays. They also reported that the probability of nucleation depends mainly on the density of adsorbed atoms (adatoms) on the surface, whereas the growth kinetics of nucleated nanoparticles (NPs) depends mainly on the material flux to the (NPs). To control the self-organization in nanoarrays, proper adsorbed atoms /adradical density and electric field patterns should be created by sophisticated tailoring of the process parameters. Meanwhile, other driving forces such as the surface free energy and surface diffusion due to a chemical potential gradient can play a leading role in specific cases.

In femtosecond irradiation of fused silica, since glass has good glass former ability in nature, it is very difficult to initiate nucleation especially for ultrapure material like fused silica which makeup of only single component such as silicon dioxide (SiO_2). Furthermore, femtosecond laser ultrashort pulse width does not favor nucleation process. For nucleation and recrystallization process, thermodynamic driving forces must be present. Thus the theory of self-organization is unlikely to be the reason for the subwavelength ripple observed in fused silica as compared to other glass containing impurities (Serfret *et al.* 2005).

Since the both the classical and self-organization theory could not be used to explain the ripple observed and it seems hard to carry out direct measurement to determine the exact physical mechanisms and dynamics that occurs during the ablation process as the material properties would keep changing during the irradiation process. However, to some extent, we can make use of the surface morphology characteristics after irradiating with different laser parameters to deduce the ultrafast process of ripple formation in fused silica. One key observation is the splashed like effect together with the fine droplets and strands of nano- thread like structures that grow outwards and on top of the coarse ripples (See Figure 4.2(g) and 4.10(b)). These images suggest that during the femtosecond ablation process, the centre region undergoes material melting and resolidification and the formation of the coarse ripples is very likely to relate to the melted material dynamics. Phase explosion may even occur due to superheating by the high intensity beam (Bonse et al., 2002)

Base on the above observations, the following mechanism is proposed for the formation of fused silica ripples after femtosecond laser irradiation. For the coarse ripples, it is likely to be resulting from the freezing interference capillary waves due to surface plasma at the air-liquid interface. The following explanation supports the coarse ripple formation mechanism. During ultrafast laser ablation of dielectric material, the interaction between the femtosecond laser beam and the material often involves a number of different processes which includes, non-linear absorption, plasma generation, shock propagation, melting propagation and resolidification (Brodeur and Chin, 1998). However, during energy deposition into dielectric material, not all energy is used for the ablation.

Ladieu, et al. (2002) reported that that about 8% of the laser energy was thermalized and transmitted to the undamaged part of the quartz using a 100 fs pulse during plasma expansion. In another report, Perry et al., (1999) shows that a large portion of the energy is reflected back to the sample. At a laser irradiance of 10^{12} W/mm^2, they calculated the reflectance of a fused silica surface to be around 70%. This result in the formation of a transient shallow molten zone below the plasma (Yakar *et al*., 2003) and if the melt lifetime is long enough, the forces acting on the fluid can drive molten material from the center to the edges of the crater. Numerical stimulations (Aggoune *et al*., 2010) performed on aluminum irradiated with 100-ps laser pulses have shown that for the few microseconds after irradiation; about 70% of the absorbed energy is used by the expanding plasma to move the ambient gas. Another 20% of the absorbed energy is lost in radiation and only 10% of it remains in the target as thermal energy.

To estimate the thickness and the lifetime of the molten layer, an analysis is performed on the absorption of the laser energy and its dissipation using a one-dimensional heat conduction calculation base on the above assumption from the numerical stimulation. Here it is assumed that less than 3% of the incident laser energy (i.e., 10% of the absorbed energy) is available to heat the undamaged material. Therefore, at an incident laser fuence of 4.7 J/cm^2, less than 0.001 J/cm^2 goes into heating of the material. Because glass does not have a latent heat of melting, all of this energy goes into melting (Yakar *et al*., 2003).

The average melt depth (h_m) can be calculated using

$$h_m \approx \frac{F_a}{T_m \rho c_p} \tag{4.5}$$

where F_a = 0.001 J/cm^2 is the portion of the absorbed laser fluence that goes into heating, ρ = 2.23×10^3 kg/m^3 (Doremus, 1994) is the density, C_p = 1250 J/kgK (McLellan and Shand, 1984) is the specific heat at an average temperature of T = 900K, and T_m = 1500K (Doremus, 1994) is the working point of glass, defined as the temperature at which the glass can be easily formed and sealed. This calculation yields a molten layer of thickness $h_m \approx 250$nm at the irradiated surface below the expanding plasma. This value tally with the depth of the crater measured using AFM which is shown in Figure 4.4(d). Also, the lifetime of the molten region is calculated using one dimensional heat equation, given that the heat diffusion depth is approximately given by

$$l \approx \sqrt{Dt} \tag{4.6}$$

where $D = \dfrac{k}{\rho C}$ is the thermal diffusivity. Using an average temperature around 900 K and D = 1.6x 10^{-6}m^2/s (McLellan and Shand, 1984), we estimate that the 250nm thick layer remains molten for about a time $h_m^2 / D \approx 0.04$ µs after which resolidification begins. During the melt lifetime, capillary waves are generated. Upon ultrafast solidification the excitation of capillary waves at the liquid-air interface freeze to become the coarse ripple. This mechanism described by Young e al. (1984) may provide a plausible explanation to the femtosecond laser induced periodical surface structures observed on femtosecond irradiated fused silica. Young studied LIPSS with a nanosecond laser and characterized the development of LIPSS into four regimes based on the irradiation fluence. At the lowest fluence, regime A, the material melts locally and forms periodic concave meniscus and after irradiation, these meniscuses resolidify, leaving steady-state morphology on the material surface.

Furthermore, when dielectric materials are subjected to intense femtosecond laser pulse irradiation, the plasma interaction also facilitates harmonic wave's generation during dielectric breakdown (Von *et al*., 1995; Carr *et al*., 2005). A second harmonic wave is given by (Wang *et al*., 2005):

$$d_w = \frac{\lambda}{2n} \tag{4.7}$$

Where (λ =775 nm, the fundamental laser wavelength; n =1.45 for 775nm light, the refractive index of fused silica. By substituting in the laser wavelength and refractive index, this gives a value of 267nm. The result is somehow close to the fine ripples period (~300nm) obtained and this may give a good indication that the fine ripples is likely to be a result of harmonic waves.

4.4 Effect of laser polarization

In order to reveal the dependence of the ripples on laser polarization, the linear polarized femtosecond laser beam was transformed into circular or elliptical polarization by means of a rotatable half and quarter wave plate. In this experiment, by rotating the optical axis of the quarter wave, different ellipticity (ε) can be achieved to gives the different laser polarization state. The E-field ellipticity is given as:

$$\varepsilon = \frac{(a-b)}{a} \qquad (4.8)$$

where, a is the long (high field) axis and b the short (weak field) axis of the laser electric field ellipse (Reif *et al*., 2008).

Figure 4.7 shows the SEM images of the laser irradiated surface using various polarizations. The angle of rotation is indicated on the upper right corners of the SEM micrographs. It is evident from the SEM images that the orientation of the ripples is always perpendicular to the long axis, a, of the polarization ellipse. By comparing the ripples irradiated with different polarization having different ellipticity such as a p-polarized beam (ε=1), elliptical beam (ε =0.5) and circularly polarized beam (ε=0), no significant difference can be observed in term of the ripple period except the orientation. This result indicates that the ripple period is not dependent on the laser polarization. Close up AFM images of the ripples are shown in Figure 4.8.

From the AFM results, no significant difference can be observed in terms of the ripple depth and period after irradiating with different laser polarization. The average ripple depths measured after irradiating with 4 laser pulses ranges from 40nm to 50nm while the average period ranges from 150 to 200nm respectively. For circularly polarized beam (ε=0), it is interesting to see that these ripple structures could still be observed as irradiating with a circular polarized beam would often produce dots instead of ripples. However, this again does not mean that our results are different from others as ripples or pillars have been observed after irradiation is carried out using a circular polarized beam as well. Also the ripple morphology can be highly dependent on the material and the gas environment.

Varlamova et al. (2008) reported the formations of orderly dots array when irradiating with a circular polarized beam. However, it is to note that these nano-dots array are actually ripples arranged in a well-defined line. In another report by Nayak et al. (2010), they also observed the formation of ripples on the surface of silicon after irradiating with a circular polarized femtosecond laser beam. The ripples could evolve to form pillars if the laser irradiation is carried out under reactive gases environment.
For example, the presence of an ambient gas can affect the laser ablation, plume dynamics and surface structure formation (Geohegan, 1994; Zhigilei, 2003; Henley *et al*., 2005). In the presence of different gas pressure and composition, the thermal conductivity can be affected. Also, the presence of a gas confines the plasma plume and can lead to shockwave formation. This directly returns the material back to the surface in the form of re-deposition.

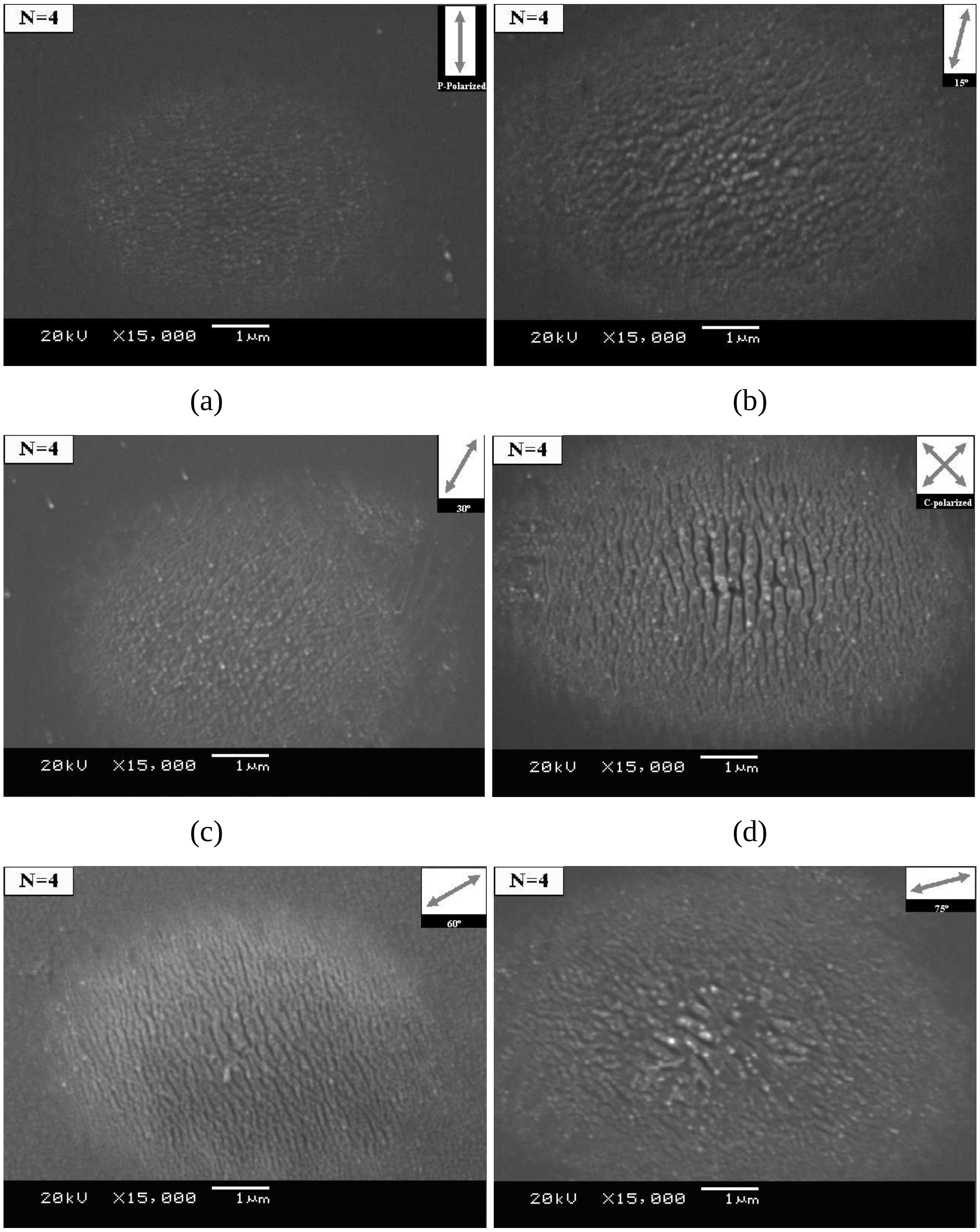

(a) (b)

(c) (d)

(e) (f)

Figure 4.7: SEM images of fused silica surface after irradiation at 4.7 J/cm^2 with 4 pulses using various polarization angle (a) P-polarized - 0º, (b) Elliptical polarized - 15º, (c) Elliptical polarized - 35º, (d) Circular polarized - 45º,(e) Elliptical polarized - 60ºand (f) Elliptical polarized - 75º.

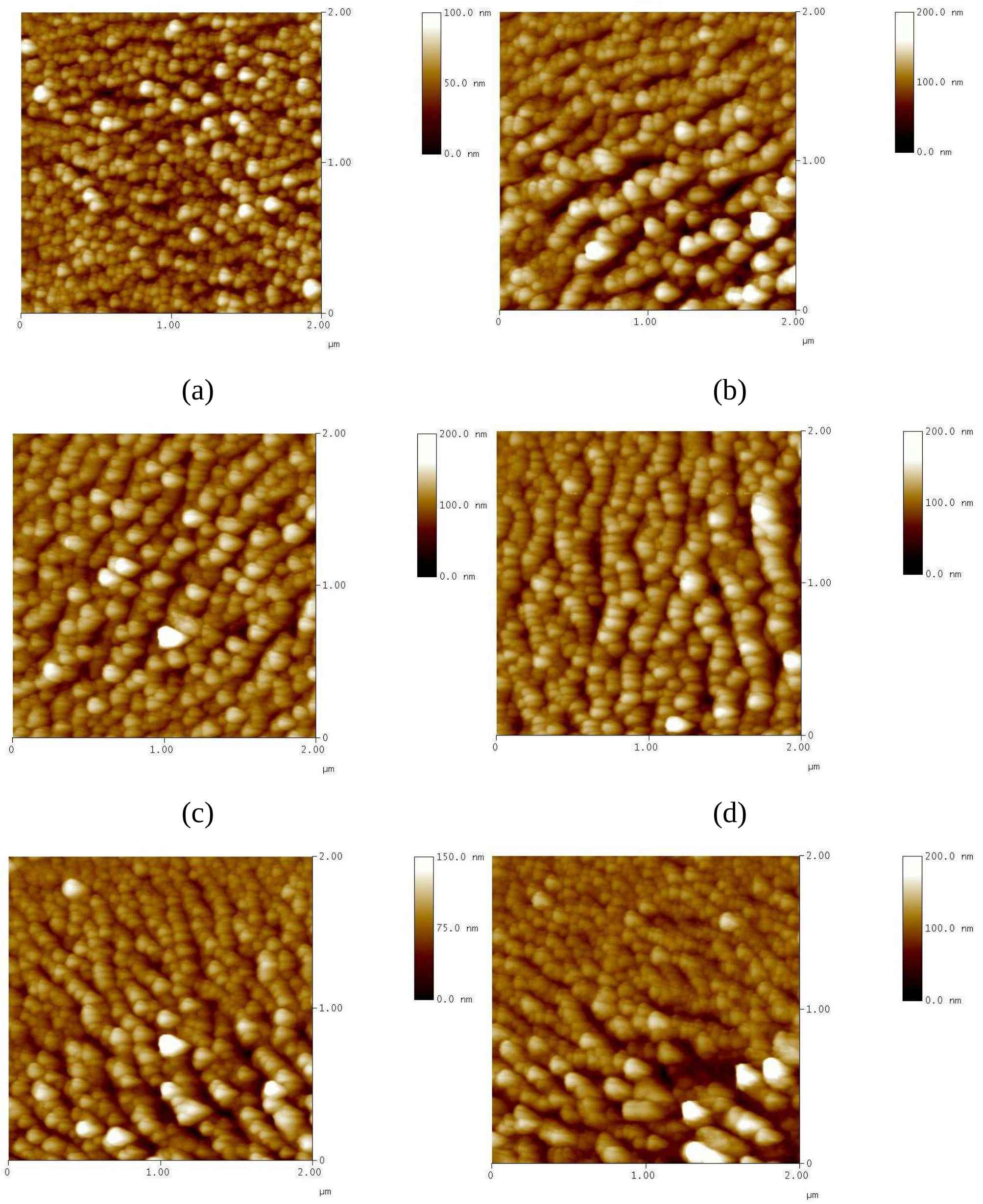

(a) (b)

(c) (d)

(e) (f)

Figure 4.8: AFM images of fused silica surface after irradiation at 4.7 J/cm^2 with 4 pulses using various polarization angles (a) P-polarized - 0º, (b) Elliptical polarized - 15º, (c) Elliptical polarized - 35º, (d) Circular polarized - 45º,(e) Elliptical polarized - 60º and (f) Elliptical polarized - 75º.

4.5 Effect of surface defect in ripple formation

As demonstrated, the ripple orientation is highly dependent on the laser polarization. Here we demonstrate another important parameter that has significant influence on the ripple orientation. It has been known from some previous studies (Costache *et al*., 2003; Theppakuttai and Chen, 2004) that macroscopic surface defects can have an important influence on ripple orientation.

Shown in Figure 4.9(a) and (b) are two SEM images having pre-existing defects like scratches on the fused silica surface. Especially in Figure 4.9(b), it clearly shows that the ripple is formed along the same orientation of a scratch with an angle of 30°. It can be observed that the surface scratches not only act as seed for ripple formation but also intensified the ripples where as compared to locations that is smooth. This obviously indicates that the influence of surface defects on the ripple orientation is significantly stronger than that of the polarization. Though the roughness of the scratch is unknown, the effect of surface scratch having different surface roughness in ripple formation can be further explored in future work.

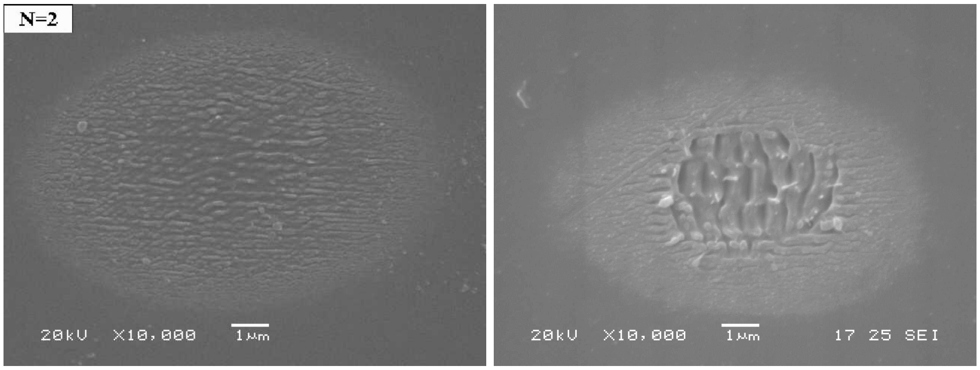

(a) (b)

Figure 4.9: SEM images of fs laser irradiated surface showing ripple orientation high dependent on the scratch line orientation. The laser fluence was 4.7 J/cm^2, (a) 2 pulses and (b) 10 pulses.

4.6 Effect of crystallographic orientation in ripple formation

It has been reported that the material crystal orientation may influence the ripple orientation when subjected to laser irradiation. For example, Blamires and Totterdell (1983) reported that laser irradiation of cadmium telluride with different crystallographic orientations would produce ripples with different orientations. In another report however, Borowiec and Haugen (2003) report that ripples orientation is independent of crystallographic orientation. Thus it seems that the ripple orientation might be highly material dependent. We also conducted preliminary experiments on the crystal orientation dependence of ripple formation on commercial available cultured quartz (100) and quartz (111). The quartz samples were irradiated using a fluence of 4.7 J/cm^2 similar to the laser fluence use in the earlier fused silica experiment in the low fluence regime. Figure 4.10 and Figure 4.11 shows selected SEM images of the two quartz samples irradiated for different numbers of pulses.

Within the set of parameters investigated, it is observed that the ripple orientation was found to be independent of the crystal orientation relative to the polarization of the incident beam. However, one interesting observation is that the 2D ripples tend to form earlier in quartz (100) when few pulses are used as compared to quartz (111). This may be related to the anisotropy properties of quartz such as having different optical and thermal properties when cut in different crystal axis. Wachtman (1969) reported that the thermal conductivity for single crystal quartz is higher (~10Wm^{-1}K^{-1}) when the cutting orientation is parallel to the optical axis as compared to cutting perpendicular to the optical axis (~6Wm^{-1}K^{-1}). Also maximum birefringence occurs when the light passes perpendicular to the optical axis. For the two quartz samples, quartz (100) cutting orientation is perpendicular to the optical axis (c-axis) while quartz (111) is cut at 54.7 degree with respect to the (100) plane. The thermal conductivity for quartz (100) and quartz (111) are 6.1Wm^{-1}K^{-1} and 8.5 Wm^{-1}K^{-1} respectively. Lower thermal conductivity favors cumulative effect (Schille, 2010). Thus, a considerable temperature rise around the irradiated area enhances the laser beam absorption and this results in lowered ablation threshold and higher ablation rate. That why ripple form earlier on quartz (100) than quartz (111). This result is consistent with the data observed on fused silica having even lower thermal conductivity value of 1.38 Wm^{-1}K^{-1}.

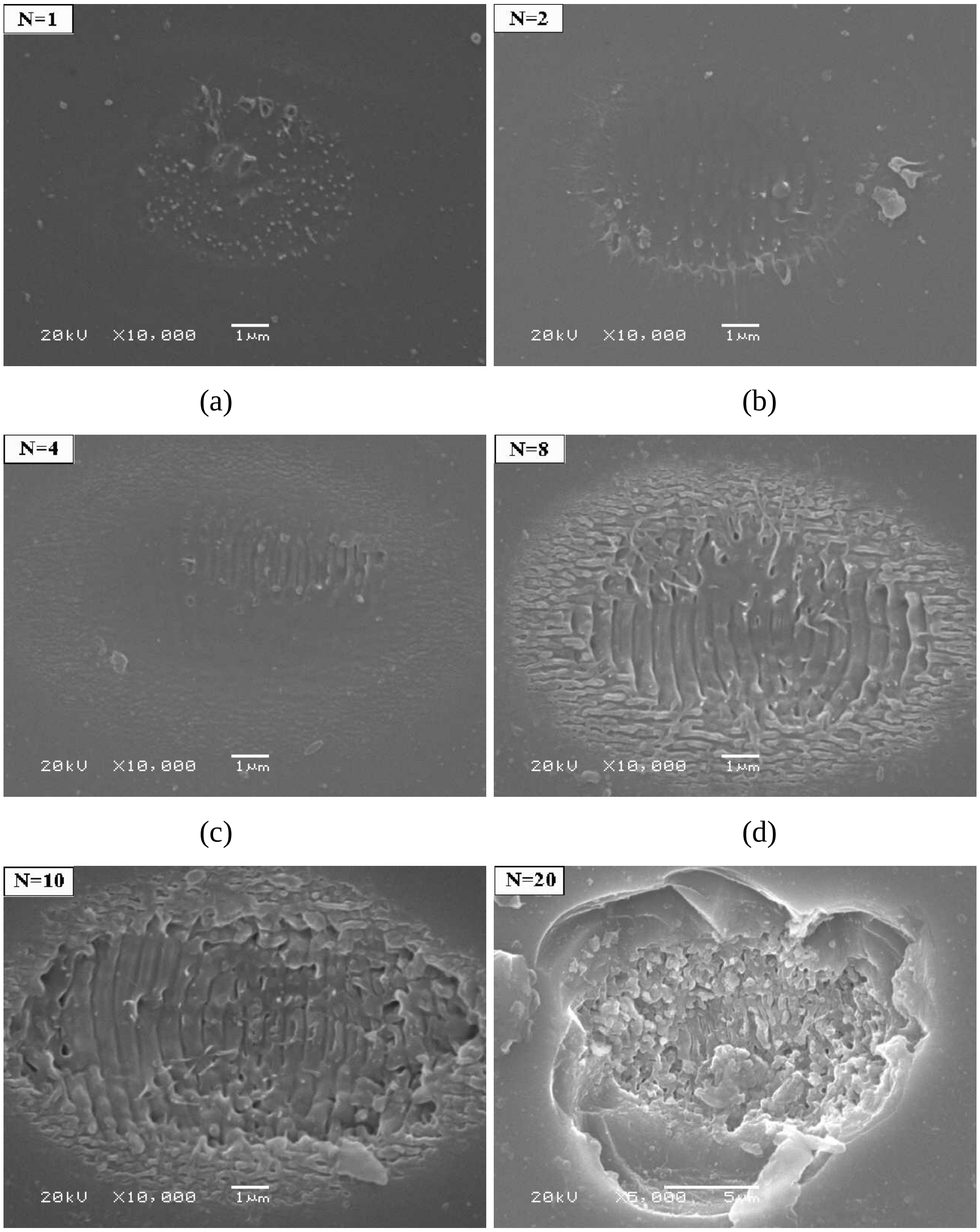

(a) (b)

(c) (d)

(e) (f)

Figure 4.10: Scanning electron microscope images showing LIPSS at various sites on Quartz (100). The number of laser shots (*N*) is shown in each image. The laser fluence 4.7 J/cm^2.

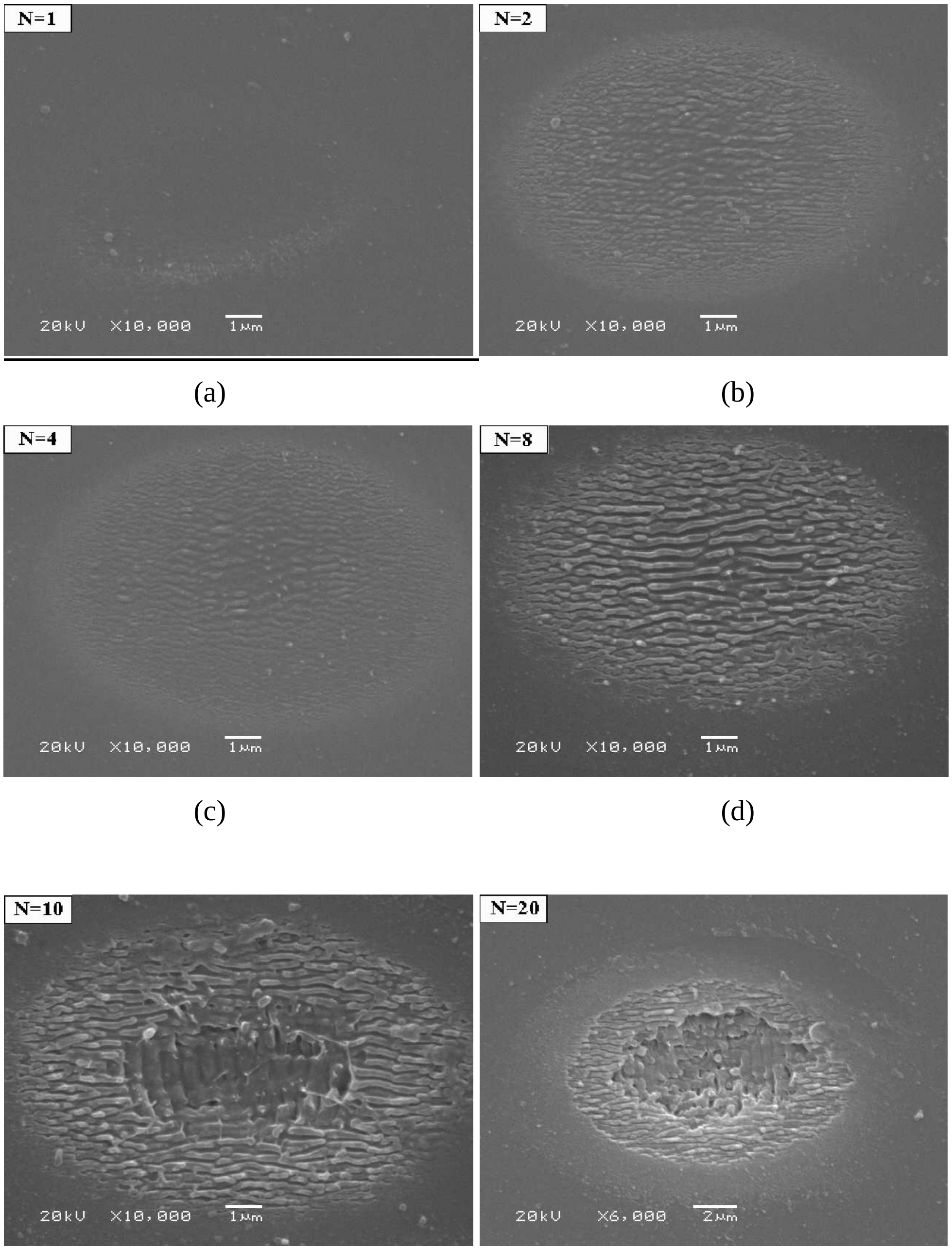

(a) (b)

(c) (d)

(e) (f)

Figure 4.11: Scanning electron microscope images showing LIPSS at various sites on Quartz (111). The number of laser shots (*N)* is shown in each image. The laser fluence is 4.7 J/cm^2.

4.7 Summary

Formation of subwavelength ripples was observed on fused silica after irradiating with a femtosecond laser beam. By varying the laser parameters such as using different fluence, pulses and polarization to irradiate the fused silica surface, ripple evolution and mechanism was systematically studied. It was shown that two directional ripples could only developed under certain irradiations conditions. Moreover these ripples were observed to be highly dependent on the beam polarization orientation but the presence of surface defects was found to have even greater influence on the ripple orientation as compared to the laser polarization. Finally no dependency in the ripple orientation was observed when comparing crystalline quartz having different crystallographic orientation to fused silica. However, it is found that the materials having lower thermal conductivity would enhance the laser beam absorption, resulting in ripples to form earlier.

Chapter 5 Femtosecond Laser Micromachining of Fused Silica

5.1 Introduction

Machining of transparent materials using femtosecond lasers has become one of the most popular subjects as femtosecond laser pulses have shown to have distinct advantages against long pulse laser. However, for practical applications, femtosecond laser processing of materials still requires some tuning and an understanding of the processing conditions to achieve optimal machining results. This is not an easy task especially when working with transparent materials as the process can be complicated due to the nonlinear effects in the air which can cause distortion to the beam profile. This chapter investigates the use of a stationary and a moving femtosecond laser beam to carry out micromachining of holes and channels in UV grade fused silica. A systematic study on the influence of laser processing parameters on surface morphology, width, depth and quality of machining are presented and discussed.

5.2 Femtosecond laser drilling of fused silica

5.2.1 Best focus determination

It is well known that the focal position of the beam will directly affect the beam spot size as well as the amount of power delivered to the surface (Duan *et al*., 2001). Moving the focus position from the surface of the material somewhere above it will result in a larger entrance diameter, smaller exit diameter and a poor roundness of the exit. In the opposite direction the opening at the exit will be larger, while the entrance will develop a taper profile. This behavior is due to the beam propagation and is a function of the Rayleigh length (Witte *et la*., 2007). In both cases, since off focus position will induce a larger beam diameter, the total fluence delivered to the machine surface will be smaller as compared to a beam at focus having a smaller beam spot size when the same amount of power is used. Therefore, it is very important to find the optimum focus position before any the laser ablation experiment takes place as incorrect focal position would greatly reduce the drilling and machining efficiency due to reduction in the power distribution at off focus position. By adjusting the stage height at a step of 20 µm, a series of grooves were machined on the fused silica substrate using a fixed laser power of 25 mW. The machining speed was kept constant at 50 µm/sec.

Figure. 5.1 illustrates a through focus plot of the laser machined groove width with respect to the various stage positions. Here a positive value (+) defines as the beam move above the surface, while a negative value (-) indicate the beam move below the surface. (0) is defined as the stage reference point. It can be clearly observed from Figure 5.1 is that as the laser beam tends to approach the optimum focal position; the groove width tends to get smaller until a minimum cut width is achieved. Moving away from the focal position would results in a gradual increase in the groove width. For this case, the optimum focal position is around -0.05 µm.

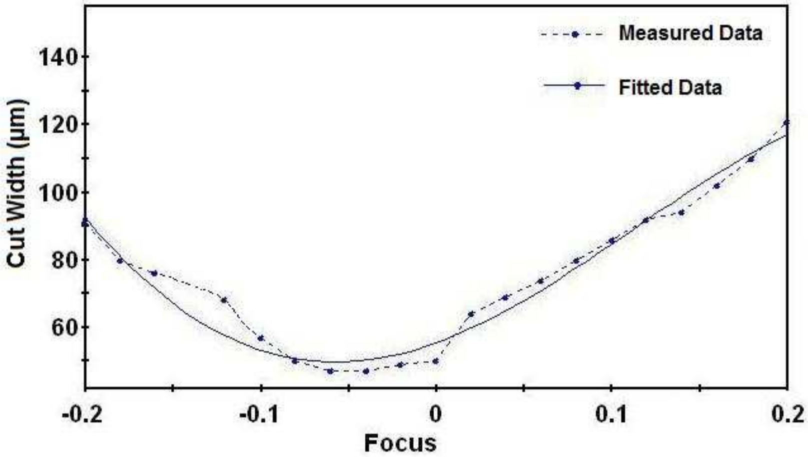

Figure 5.1: Plot of through focus as a function of cut width.

5.2.2 Effect of laser polarization in drilling

It has been reported that the influence in laser polarization can affect the profile (Nolte *et al*., 1999; Venkatakrishnan *et al*., 2002) as well as the cutting efficiency (Niziev and Nesterov, 1999). To study the polarization effect, a series of blind holes were machined using a P-polarized and circular polarized beam. Figure 5.2 shows two optical micrographs on the hole machined on fused silica using a p-polarized and a circular polarized beam. The laser fluence is approximately 5 J/cm^2. It can be seen from the micrographs that the shape of machined hole is independence on the polarization of the femtosecond laser beam. No cracking except slight chipping around the circumference of the ablated crater is observed. By examining the crater at higher SEM magnification (See Figure 5.3), two difference types of surface morphologies was observed at the bottom of the crater.

For a p-polarized beam, it is observed that periodic structures have an orientation parallel to the laser polarization while circular polarized beam have an orientation perpendicular to the laser polarization. To further investigate whether polarization has any effect on drilled depth, a series of holes were drilled with increasing number of pulses using a p-polarized and circular polarized beam. The drilling depth was measured using a white light optical imaging profiler (Sensofar PLu 2300). Figure 5.4 shows the mean depth profile obtained for a p-polarized and c-polarized beam (See Appendix A for raw data). As observed from the graph, no significant difference in term of the drilled depth when drilling with different laser polarizations.

Tao et al. 2011 performed a modeling on fs-laser beam propagation in micro holes. They reported that drilling microholes having a diameter larger than the incoming beam diameter will not have significant effect on the profile regardless of beam polarization. However, when the incoming diameter is obviously smaller than the laser beam intensity profile, the cross section inside the hole will be different from the incoming beam at the hole entrance. For a circularly polarized beam, the profile inside the hole will still be axis-symmetric but with higher peak intensity at the beam center, and the intensity drops faster as it goes away from the center. For a linearly polarized incoming beam, the laser intensity inside the microhole will have an elliptical profile.

Similar observation was observed by Venkatakrishnan et al (2002) using femtosecond laser to ablated sub-micron holes on thin metal film. In our experiment, since the drilled diameter is larger than the incoming spot size thus no polarization effect is observed.

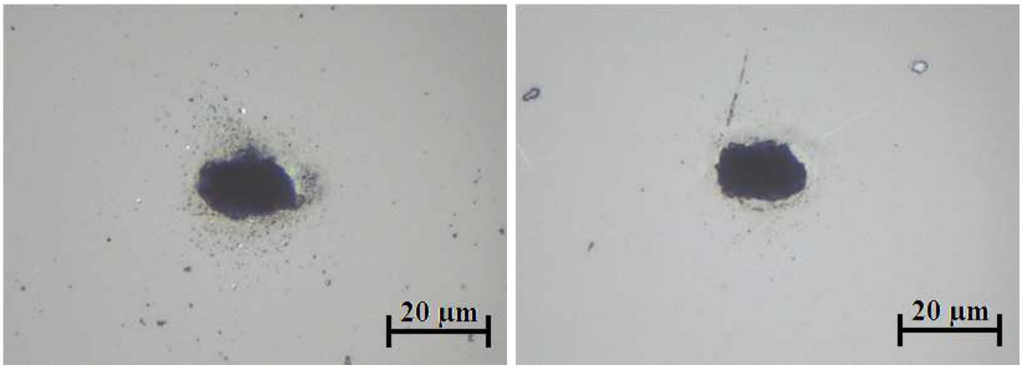

Figure 5.2: Optical micrographs of blind holes drilled using (a) P-polarized and (b) Circular Polarized beam. The applied fluence is 5 J/cm^2.

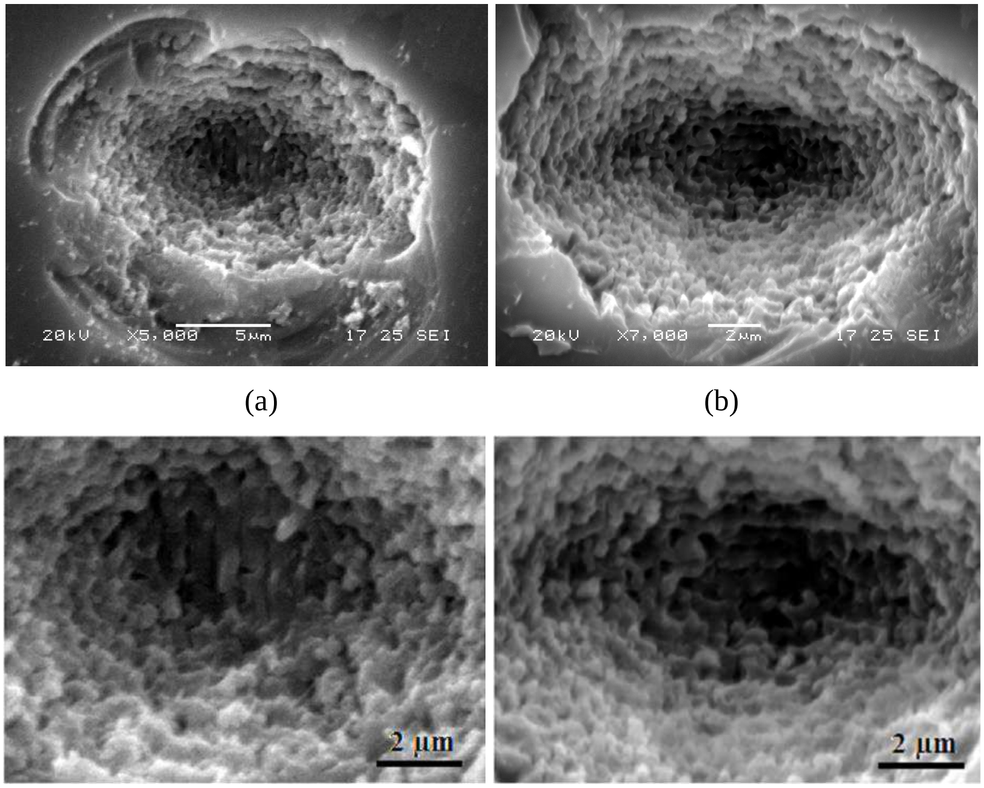

(a) (b)

(c) (d)

Figure 5.3: SEM images of blind holes drilled using (a) P-polarized and (b) Circular Polarized beam. A morphology of the hole showing ripples (c) parallel and (d) perpendicular to beam polarization. The applied fluence is 5 J/cm^2

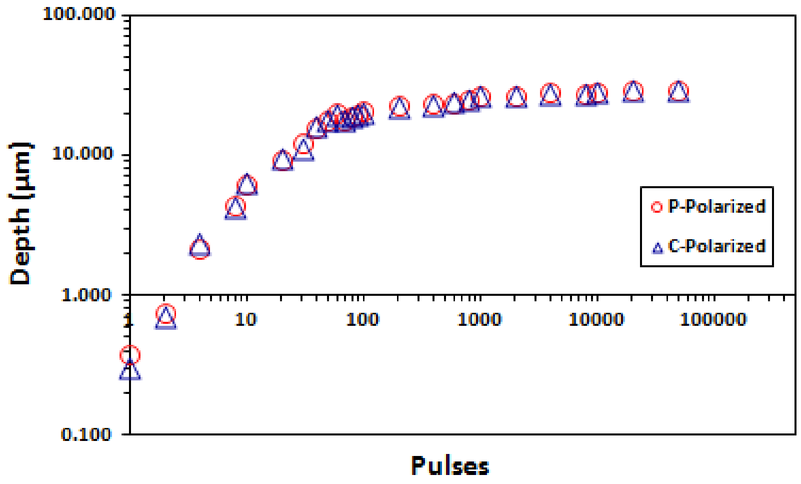

Figure 5.4: Femtosecond laser drilling depth as a function of the number of pulses at different polarization.

5.2.3 Effect of laser fluence and pulses in drilling

Experiments on varying the fluence and number of pulses were carried out to understand how the material responds in terms of the laser irradiated surface morphology as well as the depth information. By first keeping other process parameters constant, a series of holes were drilled with different laser fluences using a polarized beam of 200 pulses. The ablation depth is then compared with the predicted the ablation depth using Beer’s law with constant optical properties. The predict ablation depth as a function of applied fluence can be calculated using (Jiang and Tsai, 2006)

$$d = \left(\frac{1}{\alpha}\right) In \frac{F_a}{F_{th}} \tag{5.1}$$

Where α is the absorption coefficient of the fused silica, which is estimated to be 4 x 10^4 cm^{-1} (Hiroaki and Saulius, 2006). Figure 5.5 shows surface morphologies of fused silica irradiated at different fluence level while Figure 5.6 shows a comparison between the calculated ablated depths versus the machined depths. From Figure 5.6, it is observed that the depth calculated matches well with the machined depth at low fluence. However, with increasing fluence, there is a deviation from the calculated and measured depth value. This deviation is a result of change in the absorption coefficient of the material as the absorption coefficient changes significantly with time and the laser intensity during the femtosecond laser irradiation (Adreev *et al*., 2003). In equation 5.1, the mean absorption coefficient is used for the calculation, thus resulting in the measured. Also from the SEM image and depth profile using low fluences, it is observed that the diameter of the hole is smaller and the machined depth is shallow. This is because the ablated material will easily cool down and cannot escape through the small opening. As expected, when increasing laser fluence, ablated depth increases as well due to higher energy supplied leading to deeper carter. It is further observed that at very high fluence ranges, the ablation rate is reduced. The reduction in machining efficiency at high fluence is attributed to plasma shielding effect (Vadillo *et al*., 1999).

One significant effect observed when drilling at high fluence is the formation of surface cracks around laser drilled holes. Material cracking when machined with a femtosecond laser is quite surprising as femtoseond laser machining is well known to be a non-thermal machining process that produces little or no collateral damage (Banks *et al*., 1998; Ionita and Zamfirescu, 2010 & 2011). In this study, cracking is observed when carrying out drilling of holes in fused silica at higher fluence and the cracking becomes more severe with increasing fluence. It is known that femtosecond laser machining of transparent material in air can generate plasma (Vanagas *et al*., 2004; Hanada *et al*., 2004) and the intensity of the plasma emission increases as a function of the laser fluence (Demos *et al*., 2001). Therefore the most probable cause for this damage is the laser induced breakdown and plasma which is also recognized by other authors (Vanagas *et al*., 1999; Yoshida *et al*., 2006).

At lower fluences, although plasma is formed, the energy deposited is not sufficient to cause cracking of the material. However, in the event of higher fluence like in this case using a fluence ranging from 63.6 J/cm^2 to 127.3 J/cm^2 at 200 shots, the material is heated to even higher temperature and the energy deposited can be large enough to create a shockwave that is sufficient to cause mechanical failure of the surrounding material (Bernath *et al*., 2006). A detailed study and analysis on the mechanism on femtosecond laser induce cracking and how fused silica can be safely machined without cracking will be reported in the chapter 7.

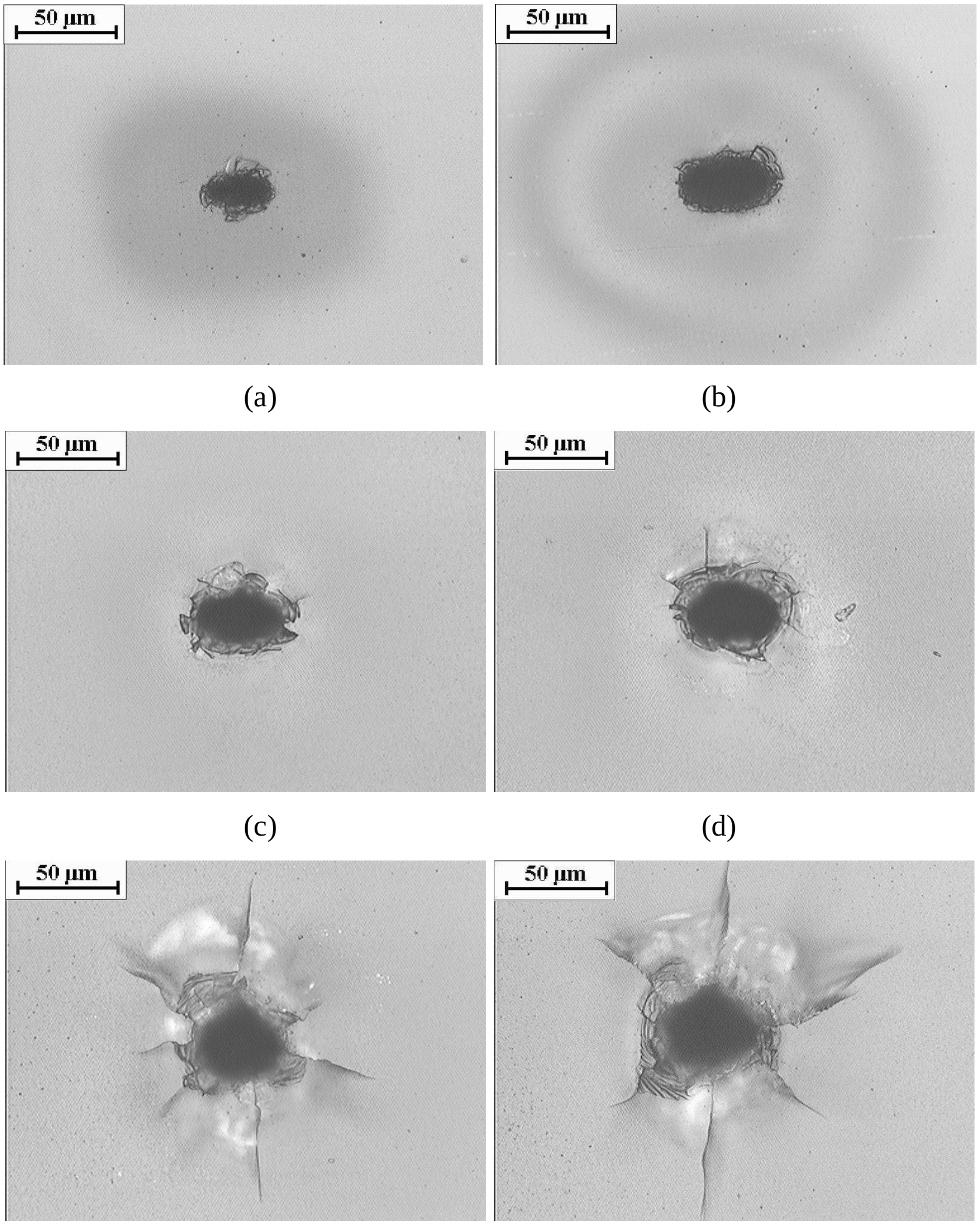

(a) (b)

(c) (d)

(e) (f)

Figure: 5.5. Optical micrographs of holes drilled using 200 pulses. The laser fluence used is (a) 7.96 J/cm^2, (b) 15.9 J/cm^2 (c) 31.8 J/cm^2 (d) 63.65 J/cm^2, (e) 95.48 J/cm^2 and (f) 127.3 J/cm^2.

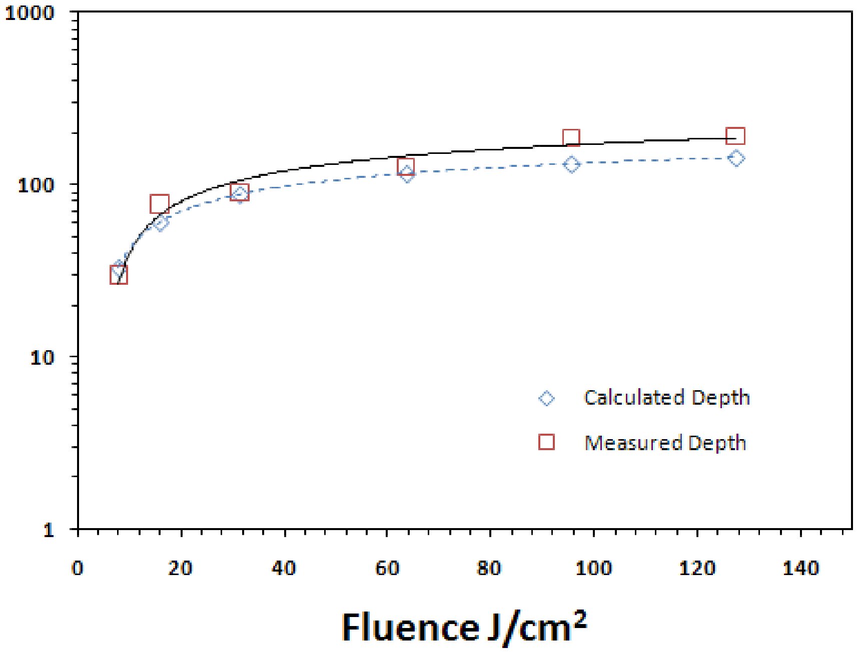

Figure 5.6: Femtosecond laser drilling depth as a function of fluence at 200 pulses.

Next a series of holes were machined by varying both the laser fluence and pulses. The objective is to examine the irradiation effect on the ablated depth when varying both parameters. Figure 5.7 shows the measured depth at different fluence and pulses. From this figure, two regimes can be identified when drilling fused silica in air with progressive laser pulses. In the first regime, there is a steep increase in the ablation rate until the drilling enters into the second regime (Pulses >100) where the ablation begins to slow down. This curve pointed out a linear dependence of the applied pulses at the beginning of the ablation process; subsequently, as the hole is becomes deeper, the increasing rate diminishes. Similar behaviors were found for all the laser fluences used. This decrease in ablation rate at the roll over point can be explained using the observations made by Shah et al., (2004). By performing in-situ monitoring of the plasma distribution within the crater, they observed at the roll of point, the laser plasma within the ablated crater become non uniform and the ablating tip is much narrower. The plasma cools before it can complete escape from the hole. This results in the decrease in ablation rate.

By doubling the laser fluence, it is observed that the drilling depth will nominally increase. However, it is interesting to observe that when the machining is carried in the high fluence range, the ablated depth seems to be independent of the applied fluence. This phenomenon is a result of plasma shielding effect. By irradiating the sample with highly intense femtosecond laser beam, electrons from the fused silica surface are easily excited causing nonlinear multi-photon absorption and subsequent avalanche ionization to take place. Dense plasma is then formed and the laser energy is transferred to the lattice (An *et al.*, 2004). Moreover, the ablation occurred close to the surface also leading to the avalanche ionization of ambient air due to the intense femtosecond beam. As a result the ejected material was blocked by the plasma from air ionization resulting in the saturation of the holes depth even when higher fluence is used.

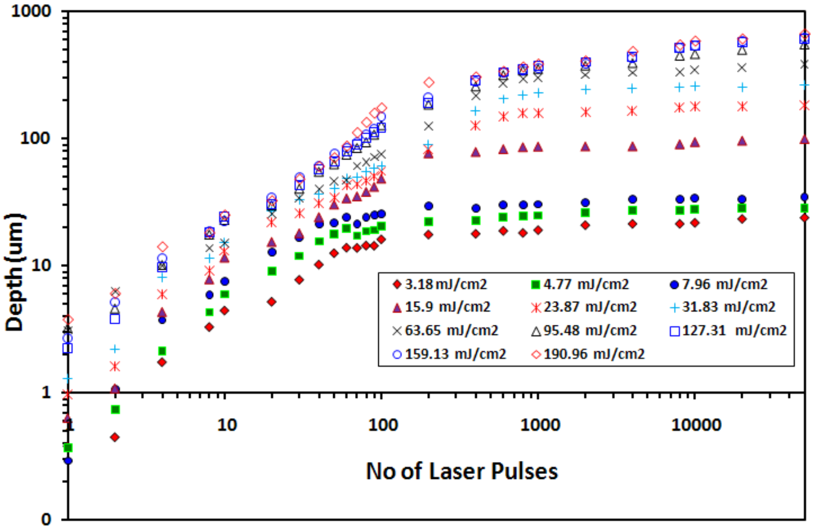

Figure 5.7: Fs laser ablation curve showing the drilled depth for fused silica at various fluence level.

5.3 Machining of microgrooves in fused silica

5.3.1 Effect of laser polarization

In surface machining, studies have shown that for long pulse laser, maximum efficiency is achieved when the cutting direction is parallel to the oscillation plane of the electric field vector (Olsen, 1982; Niziev and Nesterov, 1999). However, the beam polarization effect on fs-laser machining is not clearly understood. It has been reported that the laser beam polarization does not influence the cutting speed in the linear cutting of silicon wafer (Ostendorf *et al*., 2003). In the same report, it was reported that the beam polarization did have a major influence on the exit surface quality of the cuts. Best results were achieved when cutting vertically to the polarization direction (linearly-polarized beam) (Ostendorf *et al*., 2003). In another report, circularly-polarized laser beam was preferred for uniform cutting of silicon wafers (Tnshoff *et al*., 2001). It was also reported that ripple-like structures were formed upon fs-laser irradiation on various materials. The orientation of the ripples was influenced by the laser beam polarization. Ripples were oriented to be perpendicular to the beam polarization for TiN and silicon (Hoche *et al*., 2003; Bonse *et al*., 2000 & 2002), whereas to be parallel to the beam polarization for polyimide (Baudach *et al*., 1999 & 2001). From the literature, it appears that the beam polarization effect on fs-laser machining varied depending on the substrate materials to be processed. To our knowledge, the beam polarization effect on fs-laser machining of fused silica has not been reported.

Figure 5.8 shows optical micrograph of the microchannels successfully machined on fused silica with a femtosecond laser using both p-polarized and circular polarized beam. No difference in terms of the groove profile was observed when cutting using a p-polarized and circular polarized. The average fluence was calculated to be 9 J/cm^2 based on the cut width of 20 µm. After the laser irradiation, a significant amount of material redeposition was observed on the surface of the micro channels. However, after cleaning with diluted HF acid bath for 10 s, the redeposition was removed, as shown Figure 5.9. This demonstrates the effectiveness of acid cleaning after fs laser machining.

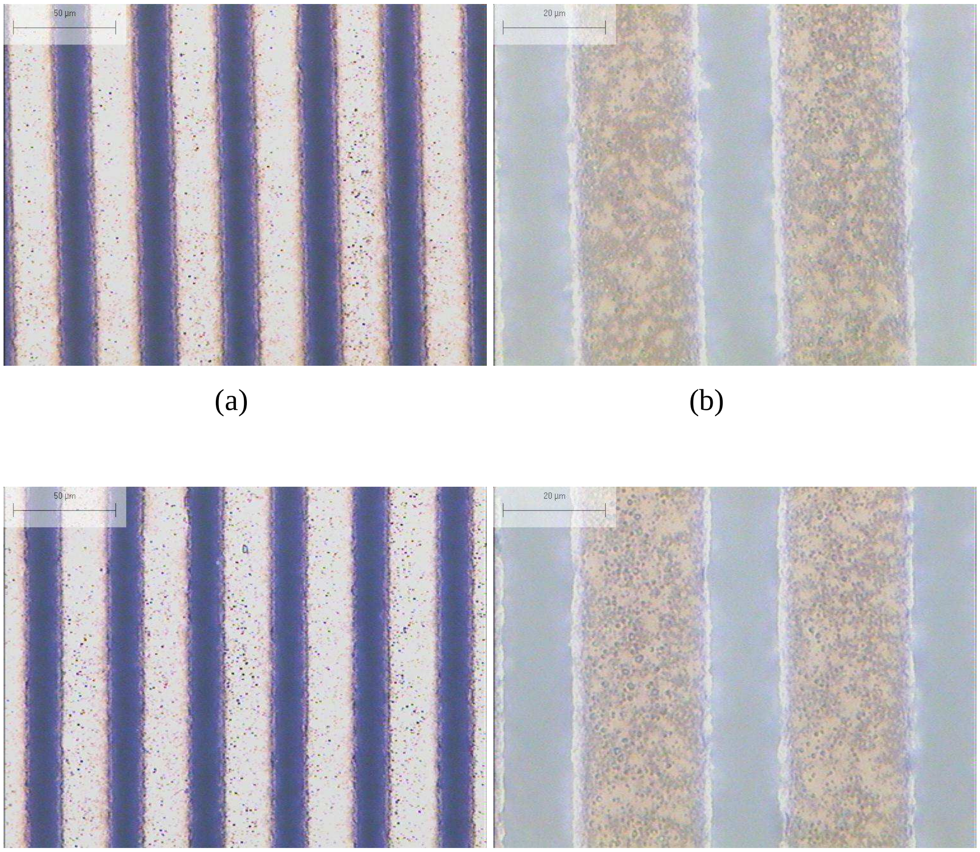

(a) (b)

(c) (d)

Figure 5.8: Optical micrographs of fs-laser machined microchannels with cutting direction parallel to p-polarization (y-direction), (a) P-polarized, (b) Close up of image in (a), (c) Circular polarized, (d) Close up of image in (c). Average fluence: 9 J/cm^2, sample moving speed: 50 µm/s.

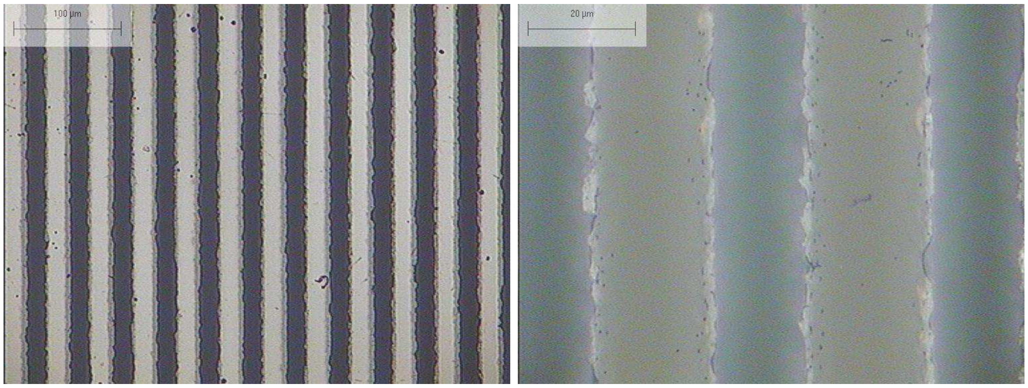

(a) (b)

Figure 5.9: Optical graphs of fs-laser machined microchannels with cutting direction parallel to p-polarization (y-direction) after HF acid cleaning, (a) P-polarized, (b) Close up of image. Average fluence: 9 J/cm^2, sample moving speed: 50 µm/s.

To study the effect of cutting orientation, grooves were machined at different orientations. Figure 5.10(a) and (b) shows optical micrographs of microchannels machined using the p-polarized beam, where Figure 5.10(a) shows cutting in the direction parallel to polarization (y-direction) and Figure 5.10(b) shows cutting in the direction perpendicular (x-direction) to polarization, respectively. It was observed that the microgrooves were straight with consistent cut width for both cutting directions. No difference in cut width was observed for cutting in the different directions.

The same microchannels were also analyzed with SEM showing the detailed surface morphologies (Figure 5.11(a) and (b)) and with the stylus profiler showing depth and 3D profiles (Figure 5.12(a) and (b)). It is clearly shown that the microchannels are V-shaped with an average depth of about 6 µm. The centre portion of the microchannels is deeper due to the higher power intensity in the centre of the beam. The laser-machined microchannels in both cutting directions are very similar in terms of depth, profile and surface morphologies. The side surfaces have granular structures with no indication of microcracks or melting. Some waviness along the cut edges was observed which was the effect of the stage movement and beam overlaps.

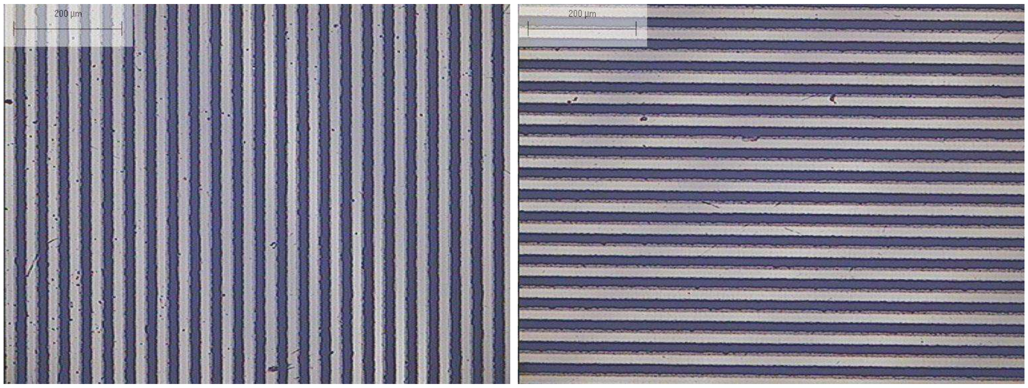

(a) (b)

Figure 5.10: Optical graphs of fs-laser machined microchannels with cutting direction in (a) parallel to p-polarization (y-direction), and (b) perpendicular (x-direction) to polarization. Average fluence: 9 J/cm^2, sample moving speed: 50 µm/s.

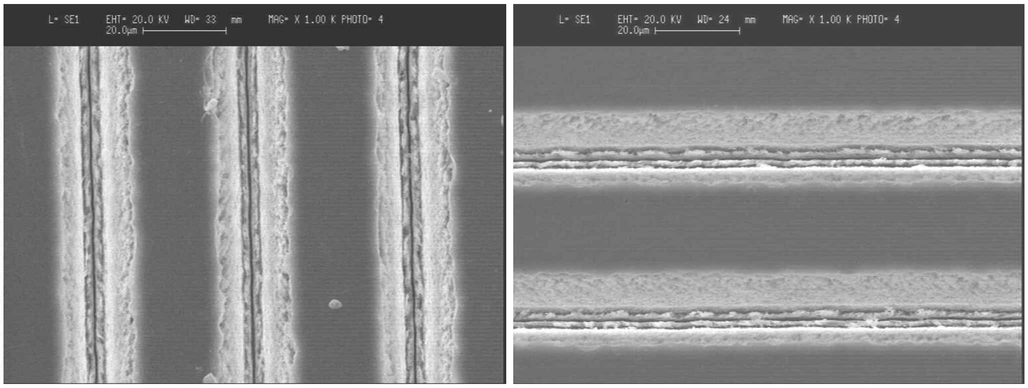

(a) (b)

Figure 5.11: SEM micrographs of fs-laser machined microchannels with cutting direction in (a) parallel to p-polarization (y-direction), and (b) perpendicular (x-direction) to polarization. Average fluence: 9 J/cm^2, sample moving speed: 50 µm/s.

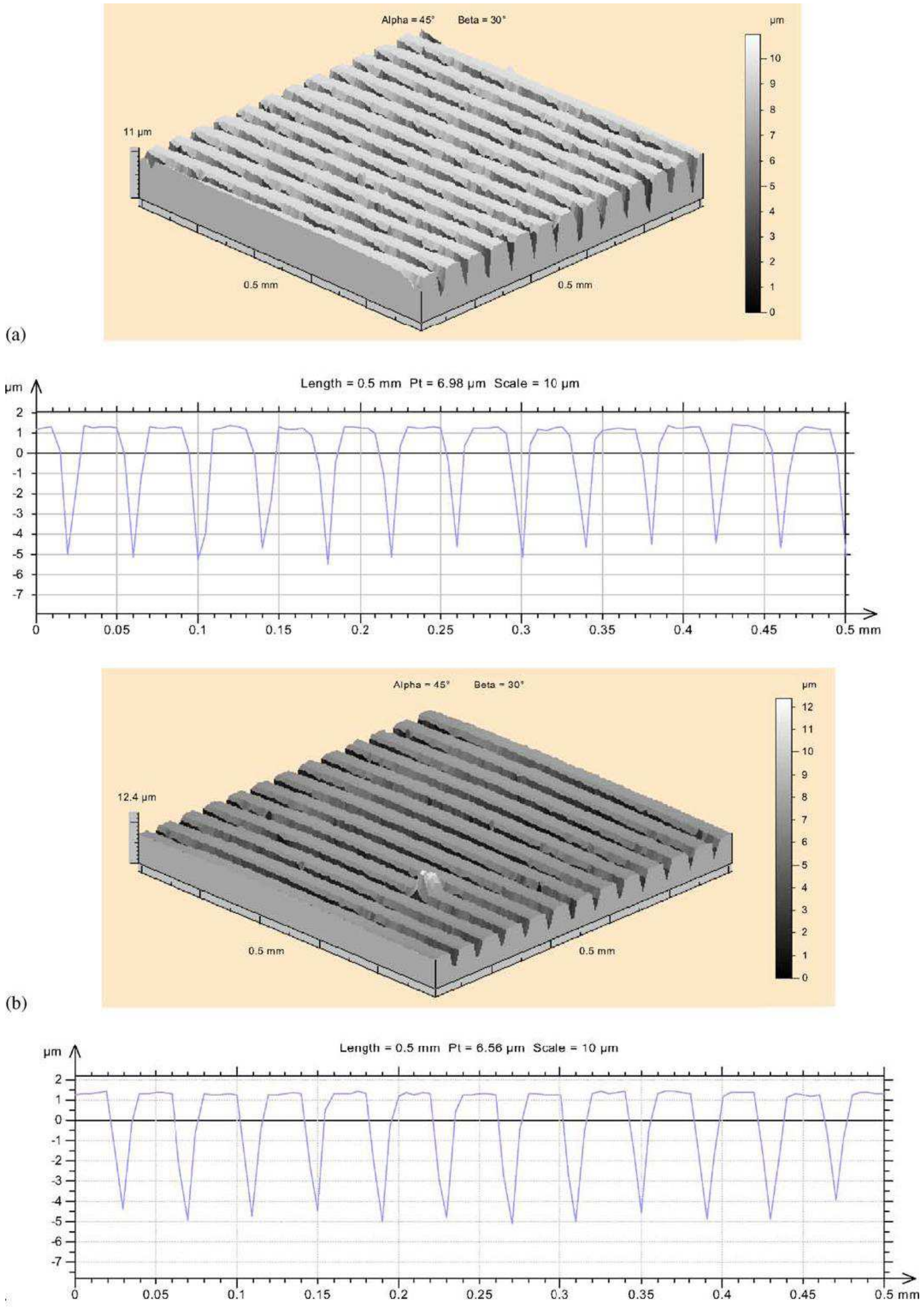

Figure 5.12: (a) 3D and depth profiles of the microchannels shown in Figure 4.3(a), cutting in the direction parallel to beam polarization. (b) 3D profile of microchannels shown in Figure 5.3(b), in the direction perpendicular to beam polarization.

When the microchannels were observed at higher magnifications, it is very interesting to observe regular sub-micron gratings on their side surfaces near the bottom, as shown in Figure 5.13(a) and (b). These gratings have width and spacing of about 400 nm as shown in Figure 5.13(a) and (b), where the cutting directions are different. The exact reason for the formation of the sub-micron gratings is not known. Judging from the feature size that is roughly half of the laser wavelength, these gratings may be the result of beam interference due to multiple reflections from the tapered side-walls and bottom surface as fused silica is transparent to the 775 nm beam during the laser processing.

It was further observed that the electron beams interfered to form interference patterns when scanning over the microchannels though the samples are gold coated to prevent charging effect, as shown in Figure 5.14(a) and 5.14(b). This indicates that the laser-machined microchannels are potentially useful for grating applications.

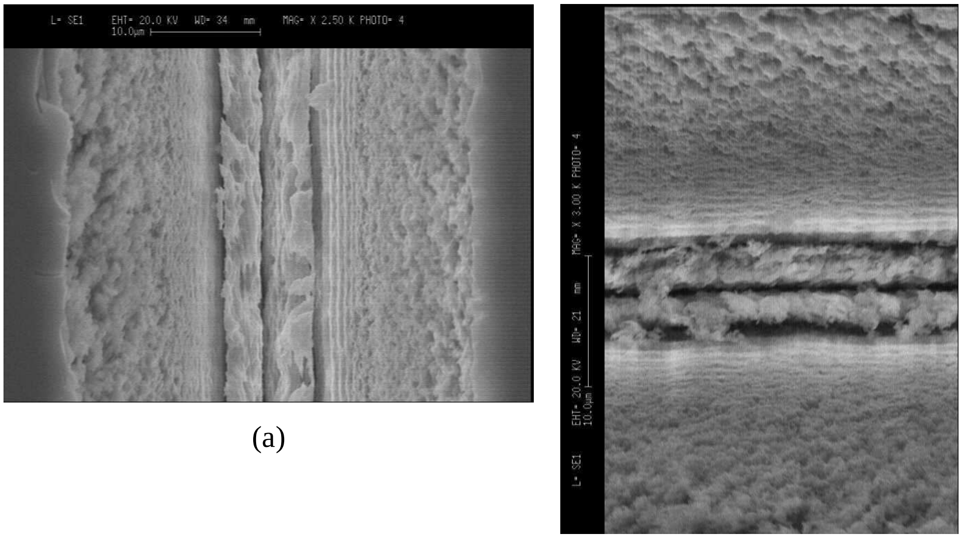

(a)

(b)

Figure 5.13: SEM micrographs showing sub-micron gratings in fs-laser machined microchannels with cutting direction (a) parallel to polarization (y-direction), and (b) perpendicular (x-direction) to polarization. Average fluence: 9 J/cm^2, sample moving speed: 50 µm/s.

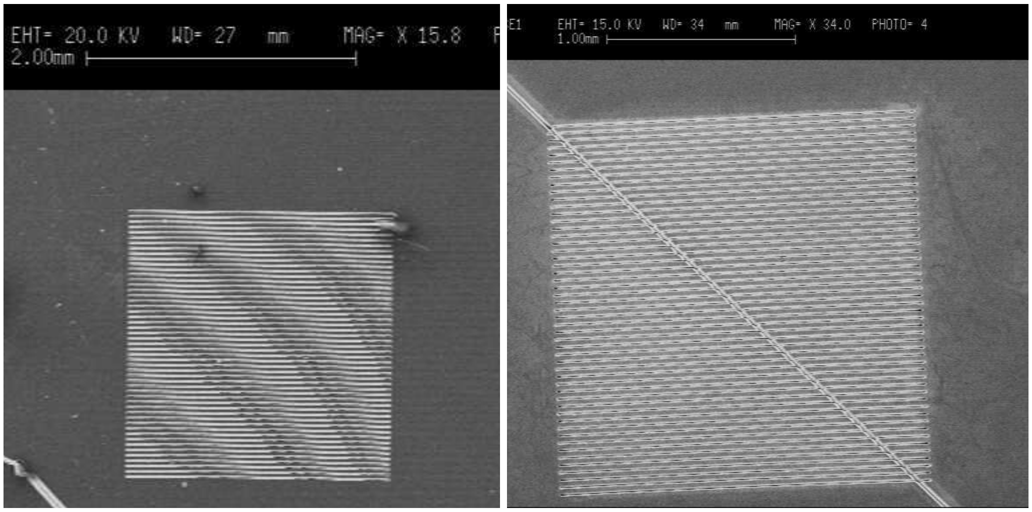

(a) (b)

Figure 5.14: (a) Interference patterns observed during the electron beams scanning over the microchannels, and (b) Interference patterns observed in other microchannels.

5.3.2 Effect of laser fluence and cutting speed

In this section, the effect on the laser fluence and beam overlap in machining of microchannels in fused silica is studied. Grooves were machined using various laser fluences (3.75 J/cm^2 to 125 J/cm^2) and speed ranging from 10μm/sec to 500μm/sec. To first study the effect of fluence, the machining speed is kept constant at 10μm/sec. Cross-sectional profile of the channels was analyzed by cutting the samples using a diamond saw.

Figure 5.15 shows the cross-sectional profile of the grooves machined using various fluences. As expected, using a higher fluence would expect a deep depth of cut. However, better machine quality was achieved when machining was carried out in using a lower fluence. It is also observed that the profile of the grooves tends to get more tapered when the laser fluence is increased. This is due to the higher intensity Moreover using higher fluence can lead to undesirable subsurface damage which is shown in Figure 5.16. The channels were machined using a fluence of 62.5 J/cm^2. The microchannels instead of having a clean cut have a filament at the end of the channels.

The observed filament is a result of self-focusing which is one of the non-linear effects that can occur during laser machining of transparent materials (Bercegol *et al*., 2003; Shah *et al*., 2004). Shah et al (2004) reports that non-linear effect like self focusing can dramatically affect the hole shape and penetration depth. For the self-focusing effect to develop, applied peak power should be greater than the critical power. Several other nonlinear effects can occurs when a femtosecond laser pulses interact with transparent material which include self-phase modulation (Shen, 1984), white-light continuum generation (Corku, *et al*., 1986; Shen, 1984), and material damage. At high laser intensity, the laser pulse first self focused to form a filament, following which white light is emitted from all positions of the filament in the forward direction. The white-light continuum generation is a universal phenomenon in all transparent optical media and is mainly due to self-phase modulation (Yang and Shen, 1984). With the development of very powerful femtosecond laser pulses, generation the white light can occur even without using a focusing lens (Corku, *et al*., 1986). Studies have shown that the generation of white light in noble gases using a weakly focused femtosecond pulses have lead to the suggestion that self-focusing plays a critical role in the process as well (Rothenberg, 1992). The generation of the broad anti-Stokes part of the continuum generation is due to the self-phase modulation of the self-focused pulse in the self-created plasma. The narrow stokes broadening is due to self-phase modulation in the neutral Kerr medium, which also contributes to a narrow part of the anti-Stokes side (See *et al*., 1999; Schaffer, 2001). Also a study has shows that the threshold for continuum generation coincides with the threshold for catastrophic self-focusing (See *et al*., 1999). The Continua generated just above this threshold exhibit a very strong Stokes and anti- Stokes asymmetry (Brodeur and Chin, 1998).

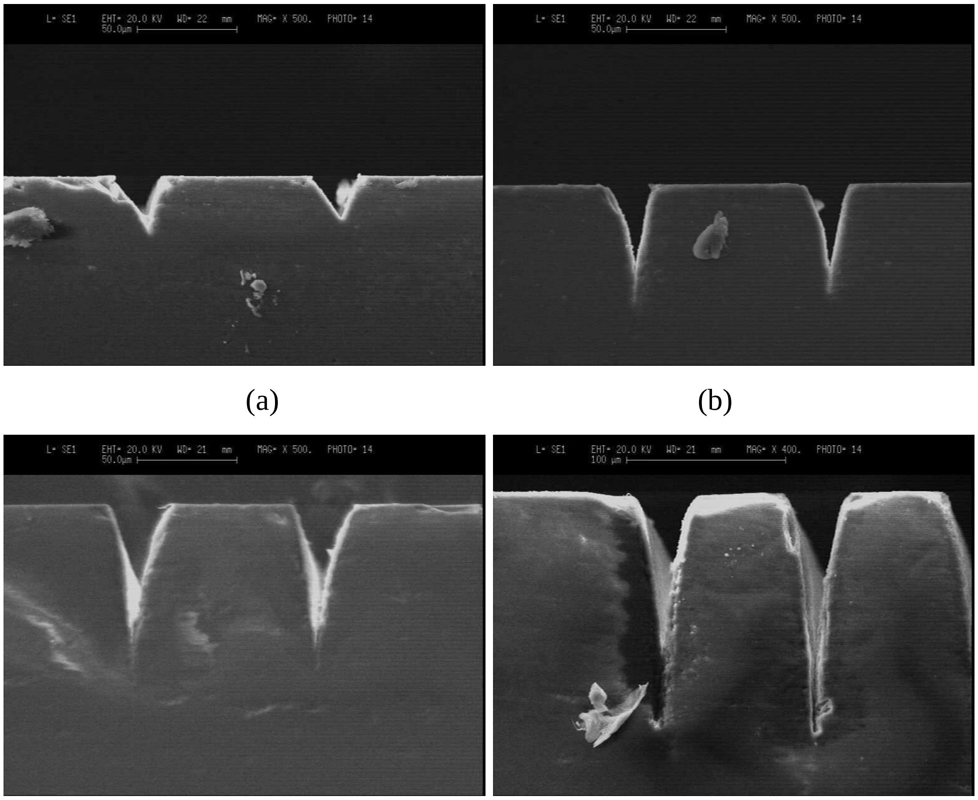

(a) (b)

(c) (d)

Figure 5.15: SEM micrograph showing cross-sectional profile of grooves machined using various fluences. (a) 3.75 J/cm^2, (b) 6.25 J/cm^2, (c) 12.5 J/cm^2 and (d) 25 J/cm^2. The machining speed is 10μm/sec.

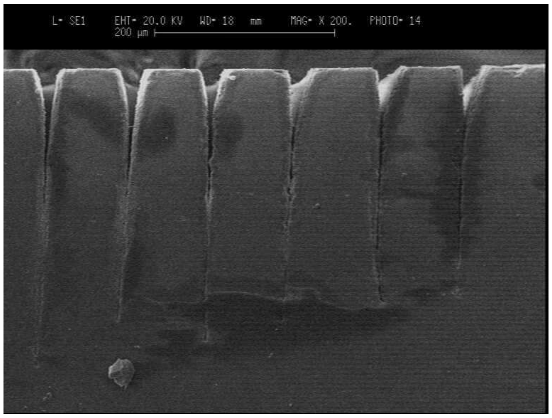

Figure 5.16: SEM micrograph showing cross-sectional profile of grooves machined using a fluence of 62.5 J/cm^2. Filament at the end of the each channel was observed which is a result of self-focusing.

In the next experiment, by varying both the fluence and scanning speed, the dependency on the groove depth is studied. Figure 5.17 shows the mean depth of grooves machined using various fluences and speeds (See Appendix B for raw data). It is known that the ablated depth is governed by the intensity-dependent penetration depth for a femtosecond pulse duration (Bonse *et al*., 2002) and the penetration depth obtained for a pulse of higher energy is much greater than that obtained at lower pulse energy. As observed, the machining depth increases more significantly as compared to the increase observed at lower laser fluence This result is in good agreement with earlier study reported (Borowiec and Haugen, 2004).

However, one undesirable effect of machining of fused silica at high fluence is that cracking of the groove can occur. Similarly to surface drilling, the most probable cause for cracking is likely to be a result of the laser induced breakdown and plasma as well (Vanagas *et al*., 2004; Yoshida *et al*., 2006). A detailed parametric studied on crack formation will be carried out in later chapter.

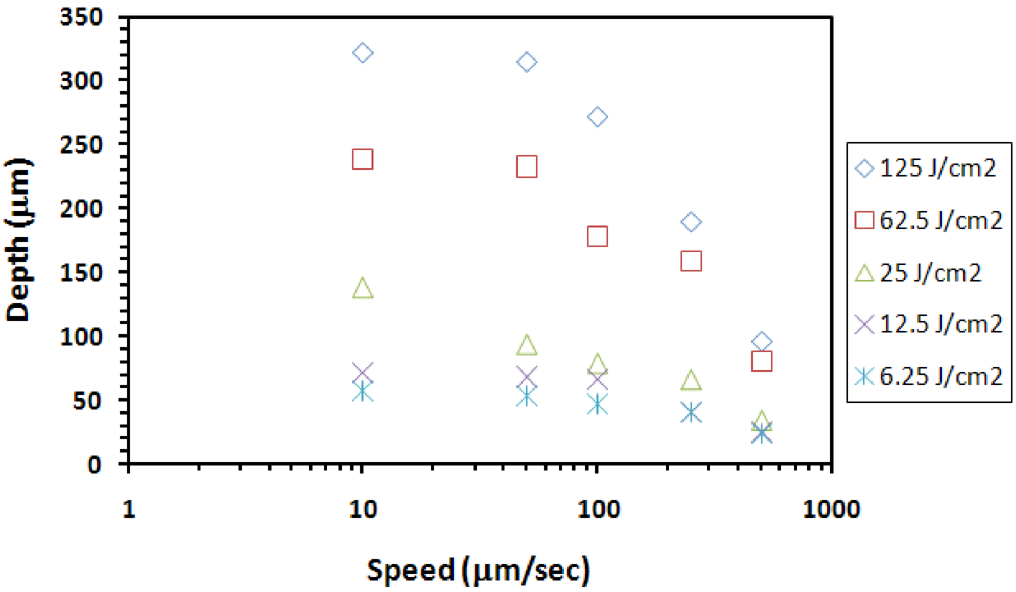

Figure 5.17: Influence of laser fluence on the depth of cut at speed ranging from 10µm/sec to 500µm/sec.

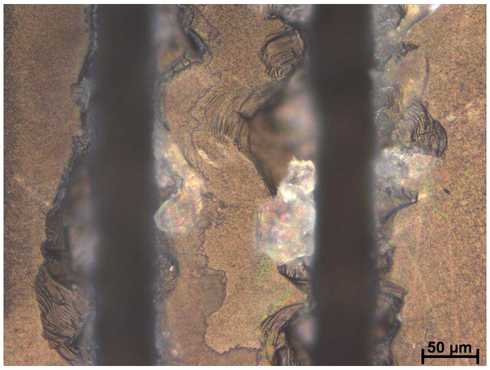

Figure 5.18: Optical micrograph showing cracking around the laser ablated groove. The laser fluence used was 125 J/cm^2.

5.3.3 Effect of multiple passes fabrication

The final experiments were to evaluate whether multiple femtosecond laser passes would increase the aspect ratios of the channels if the same channels were machined multiple times. The channels were cut repeatedly using 1, 2, 4, 8, 10, 25, 50 and 100 times with the machining speed varied, the change in the aspect ratios was studied as well as the dependence on the groove depth. Machining was carried out using two machining speed (50µm/sec and 250µm/sec) and two different polarization (circular and p-polarized beam). The laser fluence was kept constant 12.5 J/cm^2. A low magnification of the channels as shown in Figure 5.19 and their respective close surface profile is shown in Figure 5.20 and Figure 5.21.

For channels machined with a speed of 50µm/sec, it is observed that all the microchannels were straight and the width of the grooves increased when the number of machined passes increases. Similar observations were made for the channels machined at higher speed of 250µm/sec except that for low machined passes, some waviness along the cut edges was observed. However, after several passes, the waviness along the edge was removed. As observed from the optical micrographs, by increasing the number of laser passes over the same channel, there is an increase in the amount of depositions induced on the machined surface. As shown in Figure 5.22, it is observed the width increase with increasing passes and the depth is saturated at 25 passes. Moreover, the ablation rate was observed to decrease with increasing number of passes (See Figure 5.23 and Appendix C for raw data) and this departs from the linear dependence on the number that was observed in femtosecond laser ablation of other materials (Lenzner *et al*., 1998; Ameer *et al*., 1998, Campbell *et al*., 1999).

In this study, the mechanism can be interpreted as follows: As the ablated depth increases, the groove starts to act as a hollow waveguide. The initial pulse first travels to the bottom of the groove, where majority of the ablation takes place. During the pulse propagation through the groove the pulse energy decreases due to scattering and absorption resulting in a diminished energy available for the ablation at the bottom of the groove. At some final depth, the propagation losses are sufficiently high to bring the pulse energy below the ablation threshold, leading to an unavoidable taper. Furthermore, with the increasing depth, the ablated material at the bottom has a greater probability of being redeposited on the walls. Similar behavior has been observed by Campbell et al., (1999) in femtosecond processing of different glasses. They reported three different phenomenons when ablating dielectric materials in the different fluence regimes. In the first regime, where the laser fluence is less than the ablation threshold, long channels with a high aspect ratio can be produced. In the second regime, where the laser fluence is equal to the threshold, they observed two distinct ablation phases, which they describe as the gentle and strong phases. In the third regime where the fluence is less than the threshold, they observed self-focusing of the laser light due to the Kerr effect.

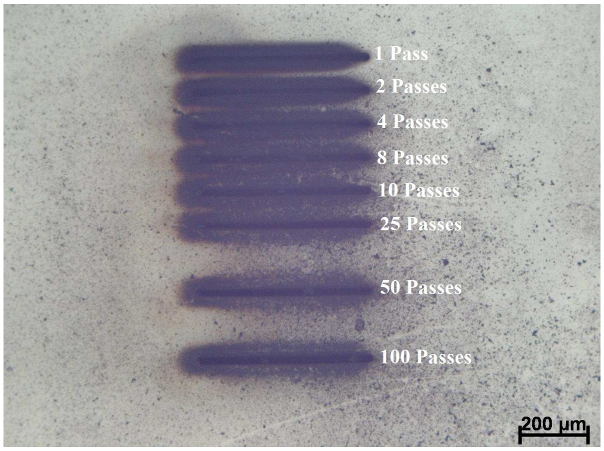

Figure 5.19: Low magnification of Fs laser ablated grooves machined using different number of cutting pass for a fluence of 12.5 J/cm^2.

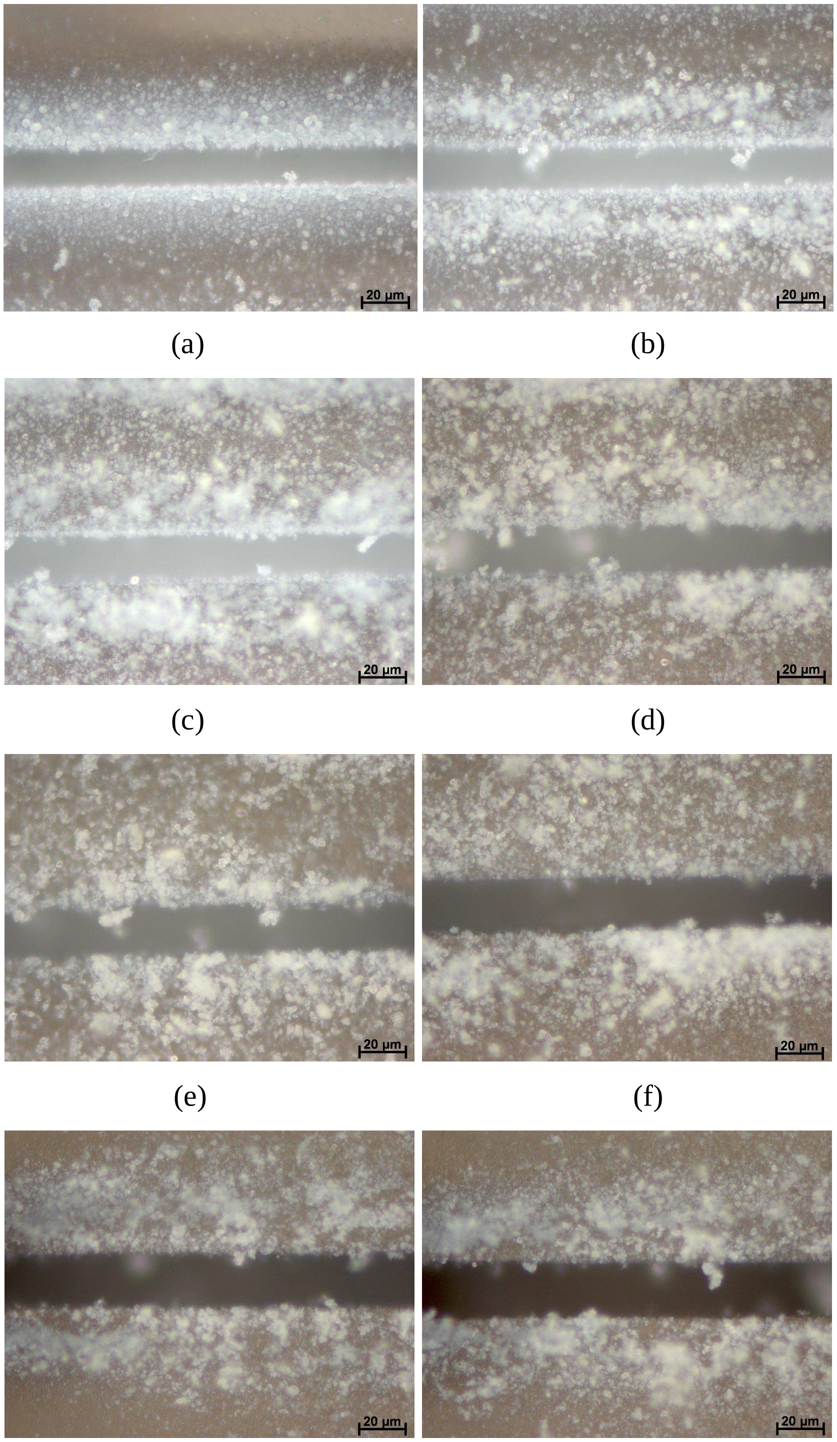

(a) (b)

(c) (d)

(e) (f)

(g) (h)

Figure 5.20: Optical micrograph of grooves machined using different number of cutting pass for a fluence of 12.5 J/cm^2. The machining speed is 50µm/sec. (a) 1 pass, (b) 2passes, (c) 4 passes, (d) 8 passes, (e) 10 passes, (f) 25 passes, (g) 50 passes and (h) 100 passes.

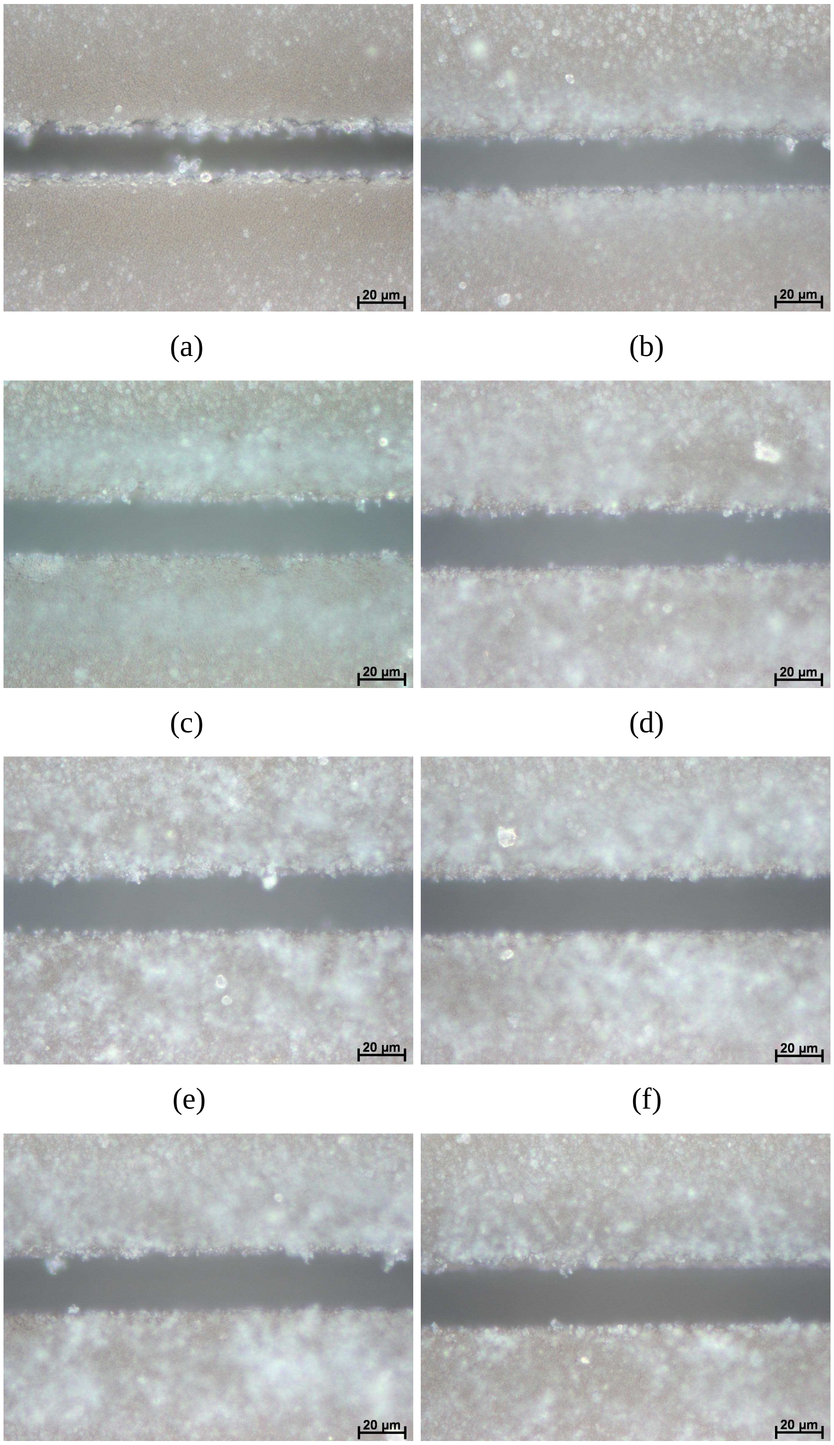

(a) (b)

(c) (d)

(e) (f)

(g) (h)

Figure 5.21: Optical micrograph of grooves machined using different number of cutting pass for a fluence of 12.5 J/cm^2. The machining speed is 250µm/sec. (a) 1 pass, (b) 2passes, (c) 4 passes, (d) 8 passes, (e) 10 passes, (f) 25 passes, (g) 50 passes and (h) 100 passes.

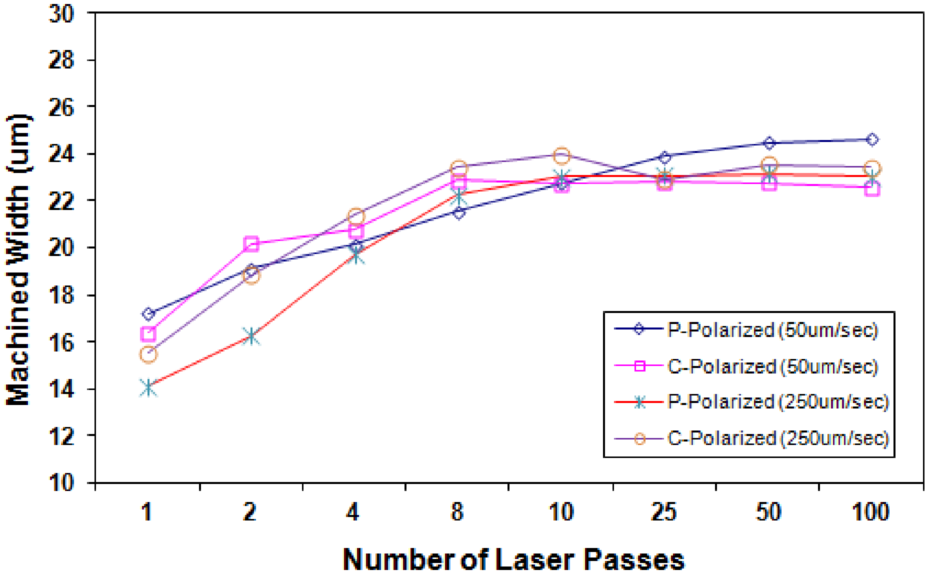

Figure 5.22: Groove width as a function of the number of consecutive passes.

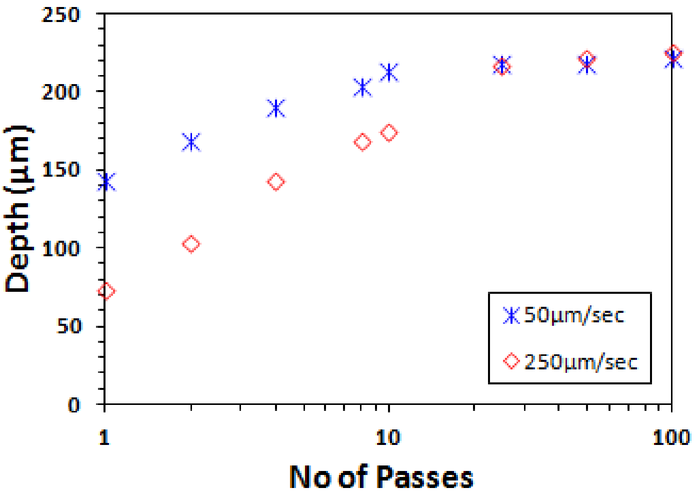

Figure 5.23: Groove depths as a function of the number of consecutive passes. The graph shows a linear portion up to an approximately 10 passes/groove.

5.4 Summary

In summary, effect on machining of microholes and channels was studied by varying a wide range of processing parameters such as polarization, fluence, speed, cutting pass and pulse. In the drilling experiments, two ablation regimes have been identified. It is observed that beam polarization does not have significant influence on the hole profile and machined depth. Side effects such as cracking were observed when drilling at high laser fluence.

In surface channels machining experiment, using lower fluence resulted in better cutting quality as compared to high fluence cutting though high fluence cutting have better machining efficiency. However, high fluence cutting can lead to cracking and subsurface damages like self focusing. Similarly, the beam polarization did not show significant effect on the machined quality in terms of cut width, depth, profiles and surface morphologies. By machining with multiple passes, straight microchannels were realized in fused silica substrates.

Chapter 6 Fs Laser Irradiation Effects on Structures of Crystalline and Amorphous materials

6.1 Introduction

Laser treatment of surfaces has been well known to induce crystallization of amorphous materials. For instance, excimer laser with a pulse duration of about 20 ns is used to crystallize amorphous Si film for thin film transistor (TFT) applications (Loreti *et al*., 2000; Hatano *et al*., 2000). The crystallization is attributed to melting of material and the spontaneous nucleation and crystal growth processes (Demchuk and Labunov, 1995; Loreti *et al*., 2000; Hatano *et al*., 2000). In recent years femtosecond laser-induced crystallization has been reported in a wide range of materials, including Ge (Singh *et al*., 2003), Si (Choi *et al*., 2003; Bonse *et al*., 2004), $Ge_2Sb_2Te_5$ film (Zhang *et al*., 2005) and Fe:$LiNbO_3$ crystal (Cheng *et al*., 2005). Furthermore, Kondo et al. (1998 & 1999) reported selective crystallization in a glass containing special ions such as Ag^+ and Ce^+ when irradiated with femtosecond laser (630 nm, 100 nJ, 500 shots at 1kHz).

In the previous chapter, successful machining of microgrooves has been demonstrated using a femtosecond laser. These microgrooves can be use for fabricating optical gratings (Zheng *et al*., 2004), however, complete or partial crystallization of glass may affect the optical properties in real life application. For example, in glass fiber fabrication, partial crystallization in glass during fiber drawn thermal process can lead to optical scattering loss (Hu *et al*., 2010). Also the mechanical properties of glass such as hardness and fracture strength can be improve by using partial crystallization and phase transformation technique (Daguano *et al*., 2012). Therefore, in this chapter, experiments were performed to understand whether or not femtosecond laser irradiation will induce any chemical or structural change in amorphous UV grade fused silica. To complement the study, crystalline materials like quartz and titanium were also used to study femtosecond laser irradiation effects. The reason why titanium is added into this chapter though it is not an opaque is because the author wants to compare the laser irradiation effect between metal and ceramic having high melting temperature.

6.2 Effect of femtosecond laser irradiation on structure of UV grade fused silica

6.2.1 Surface morphology and chemical composition analysis

Machining of microchannels on fused silica was carried out using the femtosecond laser. The single pulse energy used was 31 mJ and laser fluence was calculated to be 20 J/cm^2. After the laser irradiation, it was observed that the microchannels were straight with consistent cut width of 20 μm, as shown in Figure 6.1. Characterization of the microchannels using a stylus profiler indicates that they are of V-shape with an average depth of about 5 μm, as shown in Figure 6.2. No cracking was detected for the laser parameters used. Energy dispersive spectra (EDS) obtained for non-irradiated and irradiated surface are compared in Figure 6.3 (a) and (b). As expected, there is no change in the chemical concentration due to the femtosecond laser irradiation.

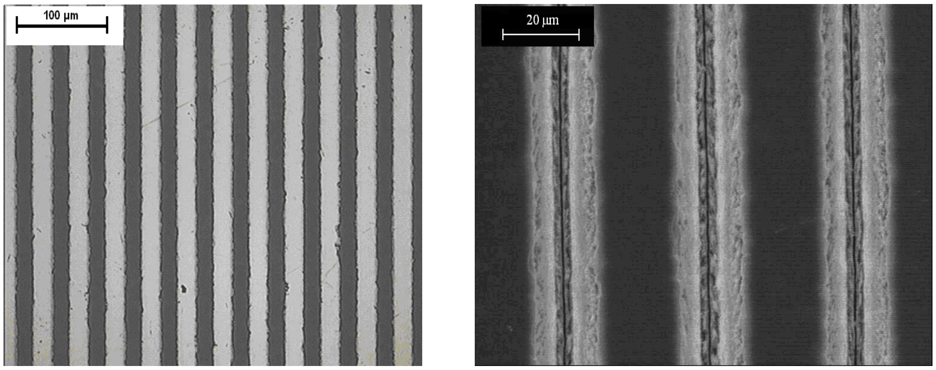

(a) (b)

Figure 6.1: Femtosecond laser machined microchannels with cutting direction parallel to p-polarization. (a) Optical image and (b) SEM image of microchannels.

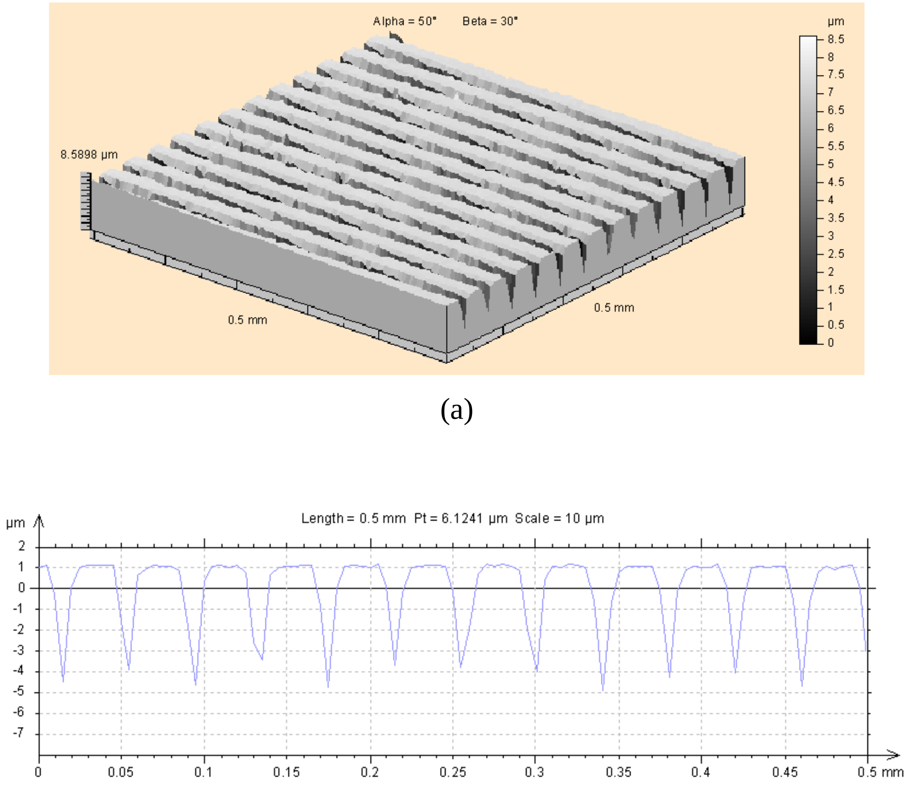

(a)

(b)

Figure 6.2: Surface profile of the microchannels machined on fused silica substrate showing an average depth of 5 µm. (a) 3D image and (b) Depth profile.

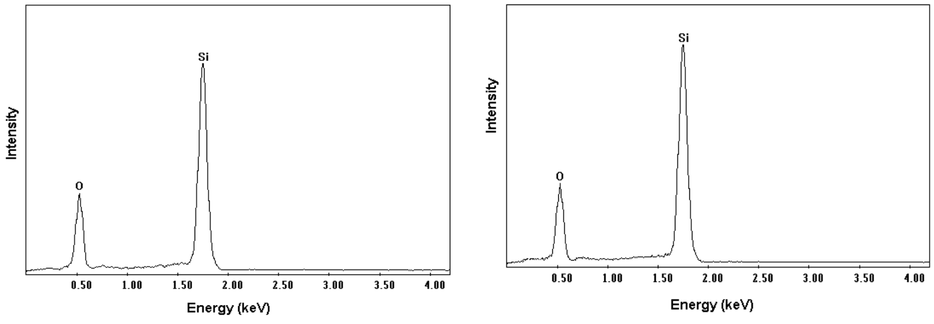

(a)

(b)

Figure 6.3: EDS showing no change of chemical concentration in the fused silica. (a) Non-irradiated surface; and (b) Surface irradiated with femtosecond laser.

6.2.2 XRD characterization

XRD was carried out to obtain the spectra for the non-irradiated and femtosecond laser irradiated surfaces, as shown in Figure 6.4 (a) and (b). The absence of any sharp peaks in the broad band ranging from 0° angle to 100° angle indicates that the fused silica structure was amorphous and remained amorphous after the femtosecond laser irradiation.

However, it should be noted that the XRD results cannot completely exclude the possibility of occurrence of a small amount of crystals due to the laser irradiation. XRD technique may not detect crystalline diffractions if crystal size is small down to nanoscale or its amount is less than a certain critical level. For example, Revesz et al. (2001) reported that there is not much difference in XRD patterns between $Zr_{57}Ti_5$-$Cu_{20}Al_{10}Ni_8$ bulk metallic glass and the partially crystallized sample containing 15% of crystalline phases within the amorphous matrix.

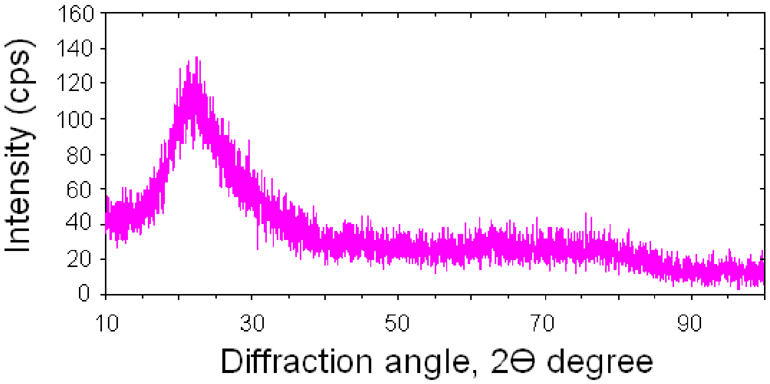

(a)

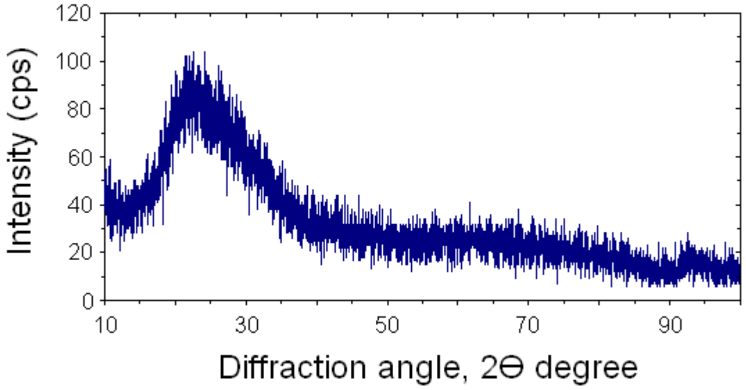

(b)

Figure 6.4: X-Ray diffraction spectra of fused silica, (a) Un-irradiated material and (b) After femtosecond laser irradiation.

6.2.3 TEM analysis of fs laser irradiated fused silica

To further examine whether femtosecond laser irradiation induces crystallization in the fused silica, great effort was expended to prepare cross-sectional TEM samples from the laser irradiated surfaces. It is to note that the samples were not pre-process such as chemically etched or gold coated in order to preserve the original state of the sample. During preparation of the TEM samples, a special technique which was mentioned in Chapter 3, as illustrated in Figure 6.5, was used to protect the irradiated surfaces. Two cross-sectional slices of the microchannels with thickness 1 mm were first sectioned using diamond saw (Figure 6.5(a)) and then glued face-to-face using M-bond adhesive (Figure 6.5(b)). Afterwards, the sample was ground using progressively finer diamond abrasive paper to reduce its thickness to around 20 μm. Finally, the thin sample was transferred onto a TEM grid (Figure 6.5(c)) for ion thinning to make it ready for TEM observation.

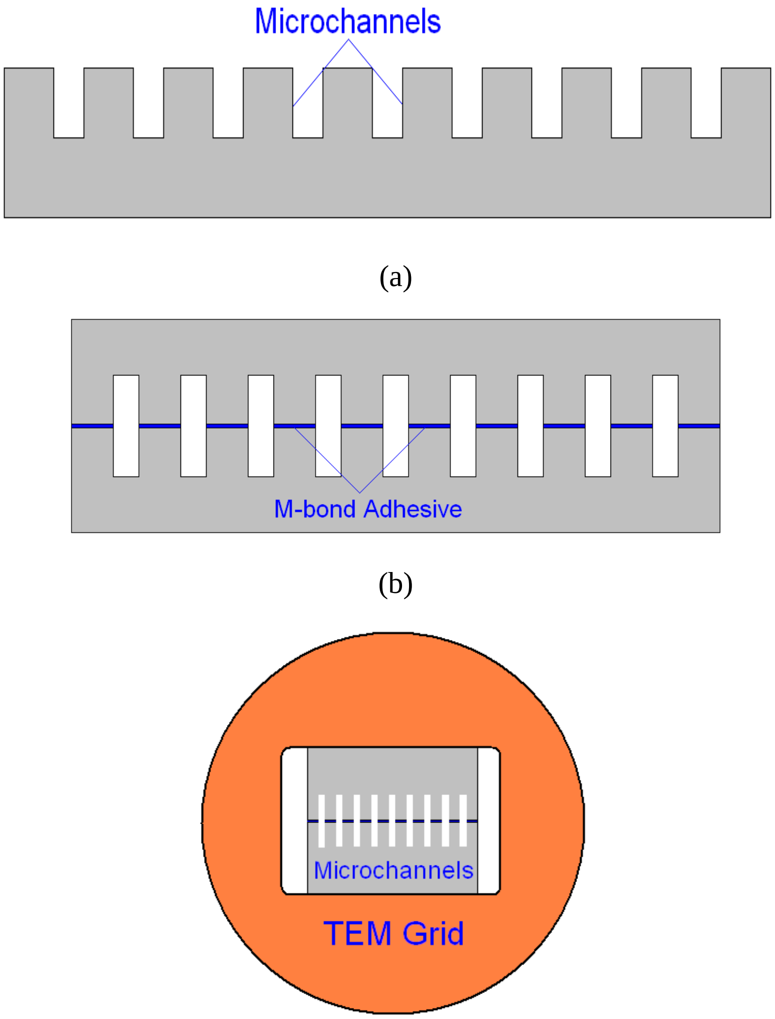

(a)

(b)

(c)

Figure 6.5: Steps in preparation of cross-sectional TEM sample. (a) Cross-sectional slice of microchannels sectioned with diamond saw; (b) Two slices of microchannels glued face to face to protect irradiated surfaces; and (c) Transfer of sample onto TEM grid after grinding.

Examination of the cross-sectional samples was carefully carried out under the TEM to study the effect of femtosecond laser irradiation on the structure of fused silica. Special attention was paid to the walls of the microchannels. The irradiated surfaces were all observed to be amorphous, as shown in Figure 6.6 (a) and (b). Furthermore, electron diffraction was carried out and the selected area diffraction patterns (SADP) show that both non-irradiated and laser irradiated structures are amorphous, as shown in Figure 6.7 (a) and (b).

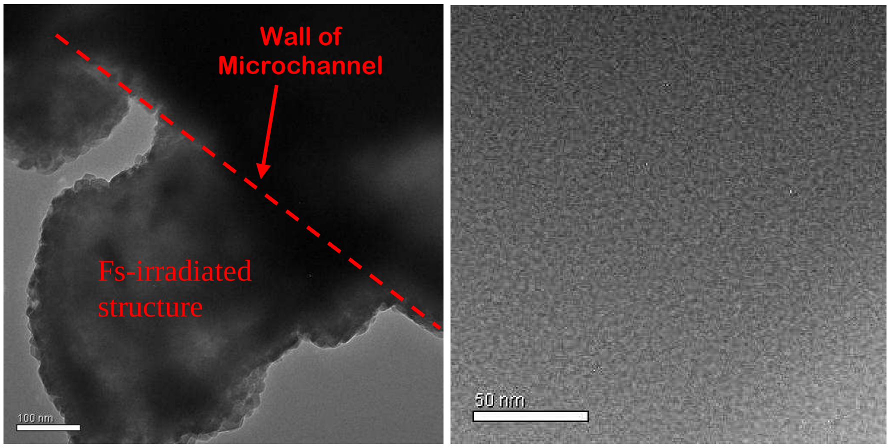

(a) (b)

Figure 6.6: (a) Irradiated structure on the side wall of the microchannels. (b) HRTEM image of the irradiated structure showing it is amorphous.

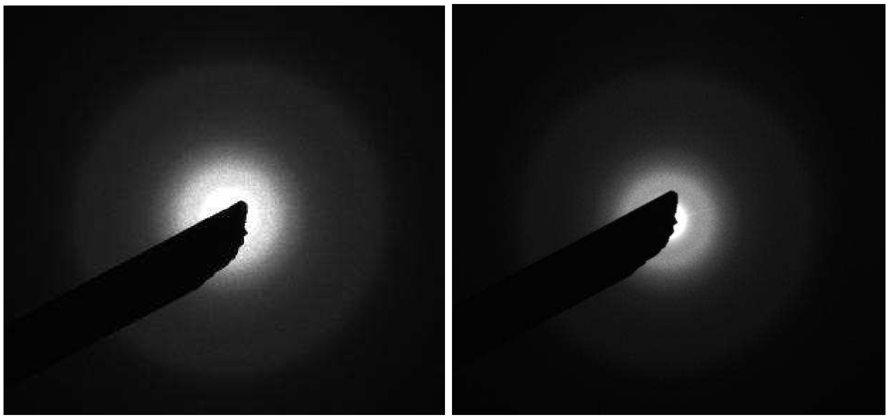

(a) (b)

Figure 6.7: Selected diffraction patterns (SADP). (a) Non-irradiated sample; and (b) Laser irradiated structure on surface of the microchannel.

It should be noted that the study may represent the first direct TEM examination of femtosecond laser irradiated surface of fused silica using cross-sectional TEM samples and this can leads to a better understanding of fs-laser material interaction of fused silica. Kasaai et al. (2001) and Koubassov et al. (2004) investigated surface modifications of fused silica samples and analyzed through X-ray diffraction and TEM the powder ejected during the femtosecond laser irradiation. Their results indicated the presence of melting and crystallization of fused silica. However, it should be noted that they examined the powder rather than the femtosecond laser irradiated surface. Detection of crystallization in the powder ejected during femtosecond laser irradiation does not necessarily mean that crystallization must also occur on the laser irradiated surface. The results obtained by Kasaai et al. (2001) can be used to support this argument. Kasaai et al. (2001) observed crystallization in the ejected powder, but XRD spectrum of the femtosecond laser irradiated surface indicates that the fused silica remained amorphous.

Silica has strong glass forming ability, so it must be cooled very slowly from liquid state to produce crystalline phase. Rapid cooling favors noncrystalline formation since time is not allowed for long-range ordered arrangements of atoms. Femtosecond laser is known to produce very rapid heating and cooling rates, so it is not surprising to observe in the present study that the fused silica remains amorphous after femtosecond irradiation. However, femtosecond laser-induced crystallization and amorphization are complex physical processes which warrant further study in the future.

6.3 Effect of femtosecond laser irradiation on structure of quartz

6.3.1 Surface morphology and chemical composition analysis

Gratings machined on Quartz (111) using the femtosecond laser are shown in Figure 6.8(a) and (b). The laser fluence used was 20 J/cm^2. It is observed that the gratings were straight with consistent width of 25 μm. Some waviness along the machined edges was observed, which was due to the effect of the stage movement and beam overlaps. The side surfaces have granular structures with no indication of microcracks or melting. Characterizing of the gratings using a stylus profiler clearly shows that the gratings are V-shaped with an average depth of about 4 μm, as shown in Figure 6.9. The central portion of the microchannels is deeper due to the higher power intensity in the centre of the beam (Figure 6.9(b)). No surface cracking was detected for the laser parameters used. Energy dispersive spectra (EDS) were also obtained for non-irradiated and irradiated surface of quartz is shown in Figure 6.10 (a) and (b). As observed, no significant change in the chemical composition was detected after femtosecond laser irradiation.

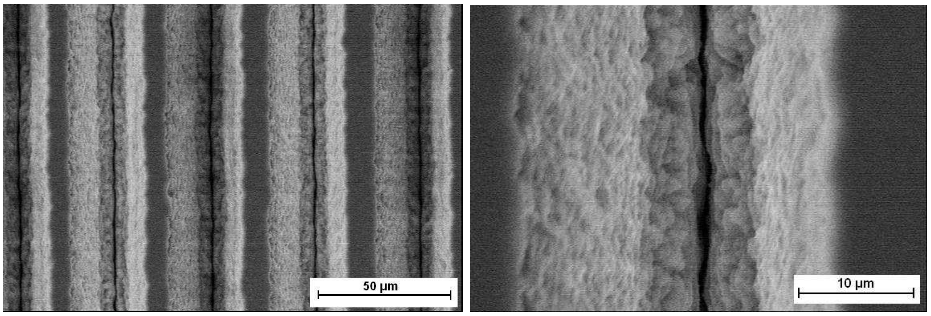

(a) (b)

Figure 6.8: Femtosecond laser machined gratings with cutting direction parallel to p-polarization. (a) SEM image of gratings and (b) Close-up image on the grating wall.

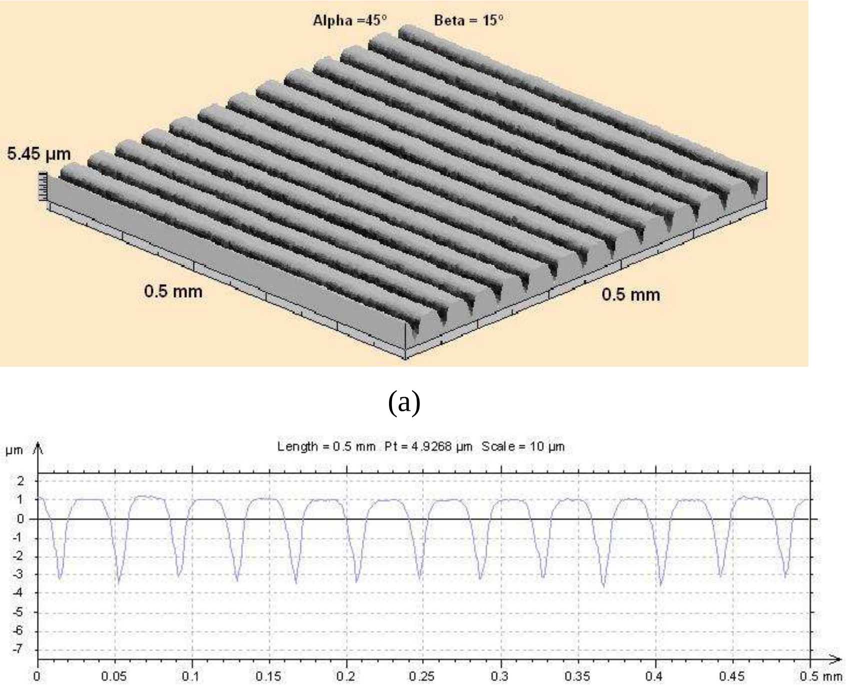

(a)

(b)

Figure 6.9: Surface profiles of the gratings machined on crystalline quartz substrate showing an average depth of 4 μm. (a) 3D image and (b) Depth profile.

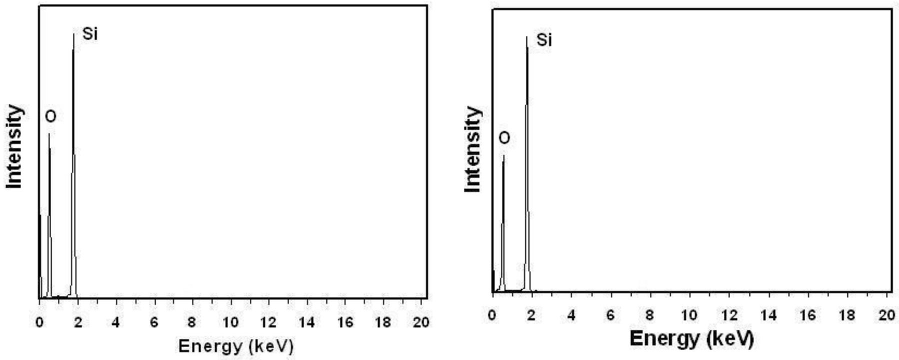

(a) (b)

Figure 6.10: EDS showing no change of chemical composition in the quartz. (a) Non-irradiated surface; and (b) Surface irradiated with femtosecond laser.

6.3.2 XRD characterization

To characterize if there is any structural changes on quartz gratings after femtosecond laser machining, XRD was carried out to obtain spectra for the non-irradiated and femtosecond laser irradiated surfaces, as shown in Figure 6.11 (a) and (b). No significant difference can be observed from the two XRD plots after scanning range of 0° angle to 100° angle. This indicates that no change in the quartz structure after the femtosecond laser irradiation. However, as mentioned earlier, the XRD technique may not be effective to detect crystalline diffractions if crystal size is small down to nanoscale or its amount is less than a certain critical level. Thus we employ a more detailed analysis by TEM.

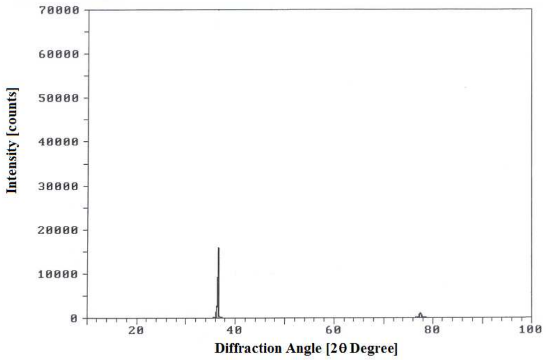

(a)

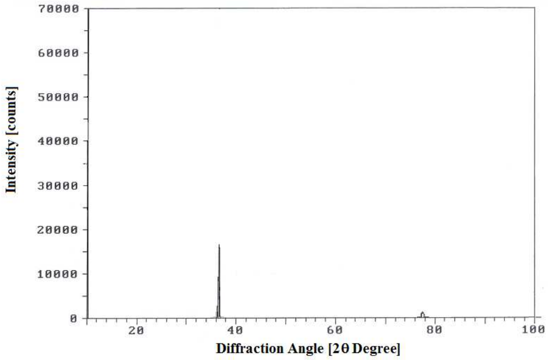

(b)

Figure 6.11: X-Ray diffraction spectra of quartz, (a) Un-irradiated material and (b) After Femtosecond irradiation.

6.3.3 TEM analysis of fs laser irradiated quartz

To examine whether femtosecond laser irradiation induced changes in the structure of quartz, preparation of cross-sectional TEM samples was carried out using the technique demonstrated earlier. Figure 6.12 shows an optical micrograph of a cross-section of the gratings after thinning with broad ion beam. It is observed from the figure that the laser machined grooves, which was thinned by the ion beam appeared to be almost transparent in color. The thinned regions of the machined grooves were then characterized using the transmission electron microscope (TEM).

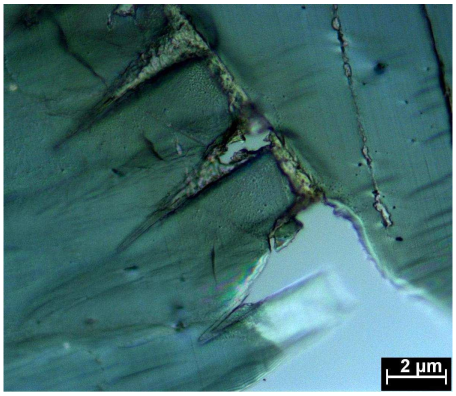

Figure 6.12: Optical micrograph showing a cross-sectional TEM sample of the laser machined gratings. The almost transparent regions were thinned by broad ion beam milling process.

Figure 6.13(a) shows a TEM micrograph of a femtosecond laser machined groove at low magnification while Figure 6.13(b) shows a close-up TEM image of the wall structures. It is observed in Figure 6.13(b) that the structures along the groove have an irregular feature. To evaluate whether femtosecond laser induced structural modification of the machined grooves, selected area diffraction patterns (SADP) were carried out at various positions in the sample starting from the edge of the machined groove and moving into the bulk. The diffraction pattern was taken from the [001] direction. The SADP are shown in Figure 6.14(a) and Figure 6.14(b) which correspond to the regions marked as A and B in Figure 6.13 (b).

From the selected area diffraction pattern, it is observed that the quartz structures in region marked as B in Figure 6.13(b) were amorphized by femtosecond laser irradiation. A dull ring instead of a series of concentrate rings was observed which indicate that the material is amorphous instead of nano crystalline. This amorphous layer was found to vary in width ranging from 200 nm to 300 nm on both sides of the laser machined grooves. However, observation of the structure about 200 nm away from the amorphous region shows a defective crystalline layer indicated by the dotted line in Figure 6.13(b). Examination of the material located 400 nm away from the amorphous zone (the region is marked as A in Figure 6.13(b)) shows that the structure still remains crystalline.

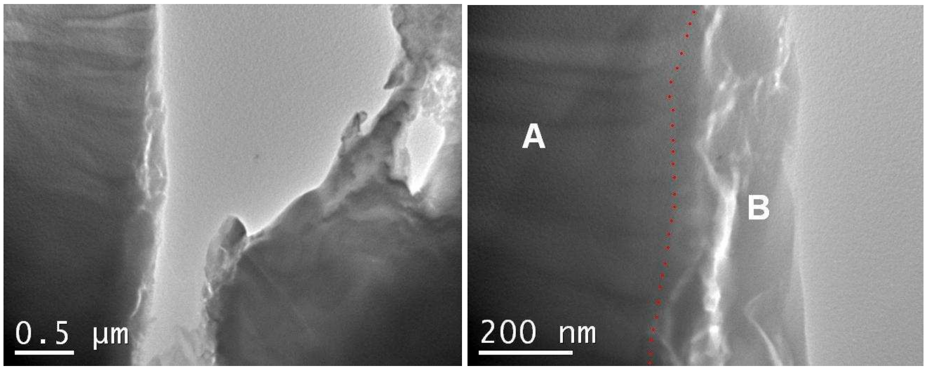

(a) (b)

Figure 6.13: TEM image showing (a) Low magnification of the irradiated structure on the side wall of the microchannels; and (b) Close-up on the structures along the microchannel wall.

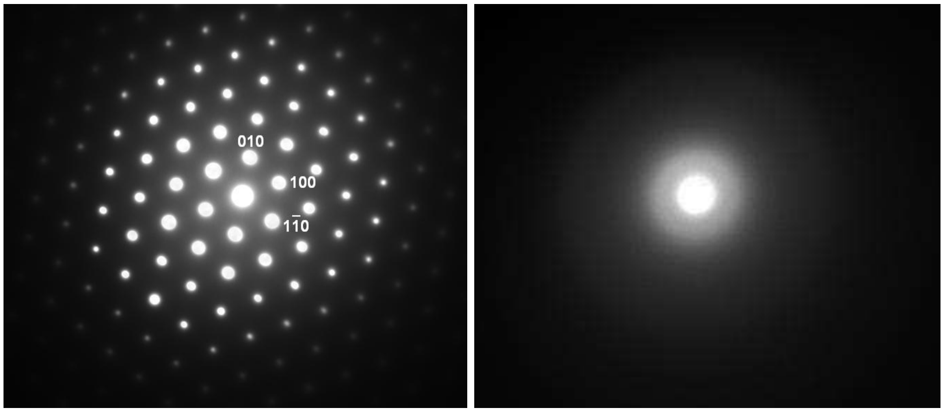

(a) (b)

Figure 6.14: TEM diffraction images showing (a) Non laser irradiated structure on the side wall of the microchannels in region A in Fig. 6.13(b); and (b) Laser irradiated structures in region B in Fig. 6.13(b).

In order to verify that the amorphous region observed within the machined grooves was induced by femtosecond laser, non laser irradiated quartz structures were observed and compared. This comparison was carried out because of the concern that thinning with a board ion beam during the sample preparation might induce amorphization of the material. Figure 6.15(a) shows a TEM micrograph of a non laser irradiated sample. The dotted line in the Figure 6.15(a) shows the boundary between the amorphous and the crystalline zones.

It is observed in the figure that a thin amorphous layer, region marked X was formed along the edge of the non laser irradiated sample after ion beam thinning. Figure 6.15(b) shows the SADP obtained from this region. Observation of the non laser irradiated samples at various locations within the samples show that the amorphous layers induced by ion beam thinning have an average width of about 50 nm. This amorphous region is smaller than the laser irradiated region. Since the damaged region induced by ion milling is smaller, it can be concluded that the amorphous region in Figure 6.13(b) is a result of the femtosecond laser irradiation.

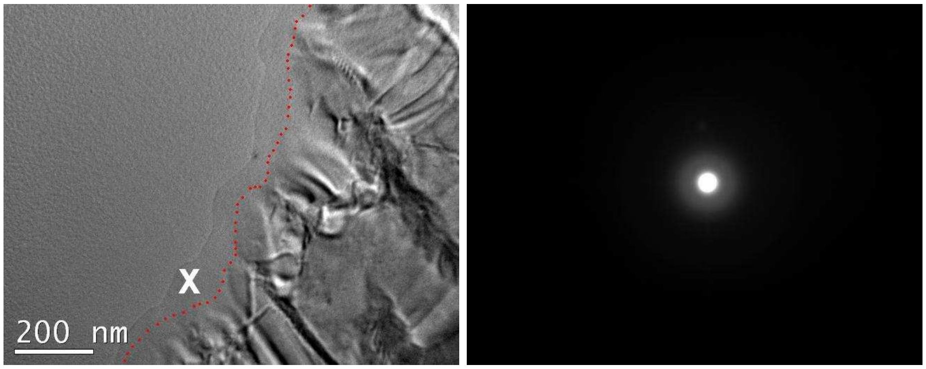

(a) (b)

Figure 6.15: TEM diffraction showing (a) Non laser irradiated quartz structure and (b) TEM diffraction image obtained in region X of the non-irradiated sample.

Femtosecond laser induced crystallization (Cheng *et al*., 2003; Singh *et al*., 2003; Bonse *et al*., 2002 & 2004; Zhang *et al*., 2005) and amorphization (Malshe and Deshpande, 2004; Vazquez *et al*., 2005 Amer *et al*., 2005; Rodenas *et al*., 2006) of materials have been reported for a wide range of materials. Amer *et al.* (2005) carried out machining of silicon using femtosecond laser and estimated the width of amorphous region to be around 150 nm using micro Raman spectroscopy technique. Others such as Malshe and Deshpande (2004) carried out both surface and subsurface machining in $LiNbO_3$ crystal and found that surface machining would induce a smaller amorphous layer having a width of 100 nm as compared to subsurface machining, which has a width ranging from 1 μm to 3 μm. Similar observations were also reported by Gorelik *et al.* (2003) and Matsuo *et al.* (2006) on subsurface structure of quartz. In their reports, the amorphous layer was found to have a width of 1 μm. The amorphous layer observed in this study has a width between 200 nm to 300 nm. It is comparable with the width of amorphous layer in femtosecond laser irradiated surface of $LiNbO_3$ but roughly an order of magnitude less than those of subsurface machined $LiNbO_3$ or quartz. Therefore, it is worthwhile to note that surface machining would induce a smaller amorphous thickness.

Several reasons may be attributed to the amorphization phenomenon observed in quartz. It is known that the high viscosity of pure SiO_2 makes the recrystallization of pure quartz very slow, and that the amorphous–crystalline epitaxial regrowth of quartz is difficult to realize (Gorelik *et al*., 2003). Furthermore, it has been reported that the high-pressure conditions, which occur around the fast-expanding plasma, lead to an amorphization of the crystalline quartz matrix (Gorelik *et al*., 2003).

Another reason is that the thermal conductivity of quartz is ten times higher than that of fused silica, thus the melted volume surrounded by crystalline quartz cools down faster than that in fused silica. Since slower cooling favors crystallization, it is conceivable that the melt in the quartz sample might have cooled down too fast and so no re-crystallization occurred (Koubassov *et al*., 2004). Thus, an amorphous structure rather than a crystalline structure was formed.

An interesting observation was made when carrying out TEM examination of the laser irradiated structures. It was observed that some regions of the quartz surfaces contained a large area of particles of around 10 nm in size. The TEM image and the diffraction pattern of these nanoparticles are shown in Figure 6.16(a) and (b). EDS analysis in this region indicates a high concentration of copper in the particles, as illustrated in Figure 6.16(c). Indexing the diffraction pattern shows that the polycrystalline ring matches the pattern of copper.

It is known that bombardment of solid targets using energetic ions can lead to the production of atomic recoils and defects within the solid and the ejection or sputtering of atoms from the surface with the consequent erosion of the solid (Carter *et al*., 2001). In our experiment, the quartz substrate was attached onto a copper grid to carry out ion thinning. It is believed that the formation of these copper nanoparticles were the sputtered products from the copper grid which had redeposited onto the quartz surface during the ion thinning process. Thus special precaution must be taken when carrying out TEM observation as these nano-artifacts induced by ion milling would lead to misinterpretation of the images.

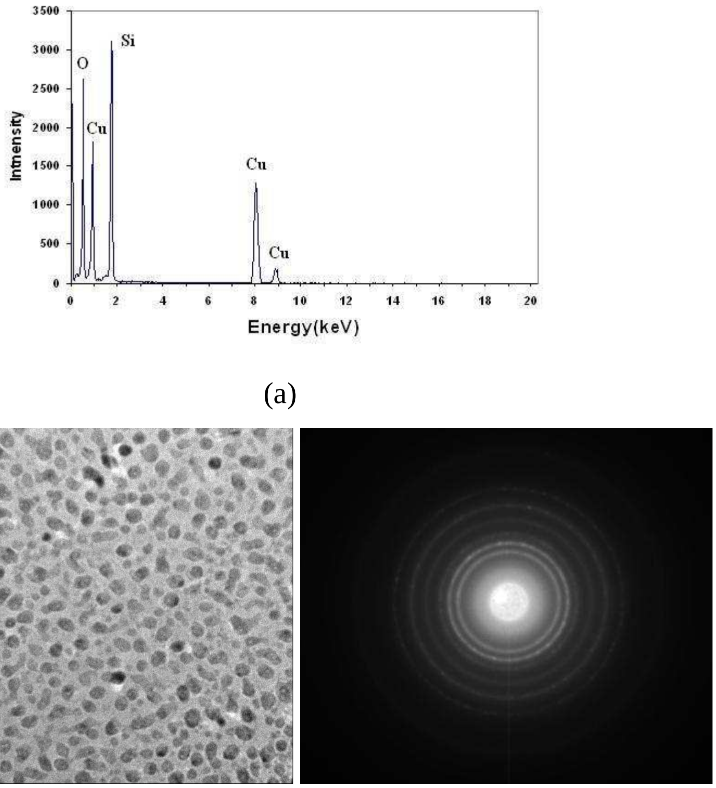

(a)

(b) (c)

Figure 6.16: TEM and EDS analysis of the nanoscale particles on quartz. (a) EDS spectra obtained from the nanoparticles region showing a high concentration of copper. (b) TEM image of the nanoparticles and (c) Diffraction pattern of the nanoparticles on the substrate.

6.4 Effect of femtosecond laser irradiation on structure titanium

6.4.1 Surface morphology and chemical composition analysis

Commercially pure titanium foils (99% pure) having a thickness of 10µm was used for the laser experiment. The foils underwent slight polishing with diamond suspension paste from a grade of 6 µm to 1 µm progressively to remove any scratches or particles on the surface. The foils were then washed with ethanol and followed by rinsing with de-ionized water to remove organic contamination. 3 mm diameter discs were punched out from the foil using a puncher for direct observation of the laser irradiated structures under TEM. The discs were again washed with ethanol and de-ionized water to ensure the surface was free from any organic contamination prior to the laser ablation experiment.

In this experiment, it is noted that thin foil was employed instead of a bulk sample in order to preserve the original laser irradiated surface so that the sample could be directly observed under TEM upon femtosecond ablation without undergoing any sample preparation process. This is especially important when carrying out HR TEM studies as the sample preparation process using ion thinning technique can alter the microstructure if it is not done correctly (Mizeikis *et al*., 2005). Figure 6.17 shows the SEM results of the titanium foil after irradiating with different number of laser pulses. The fluence was calculated to be about 47.7J/cm^2.

From Figure 6.17(a), a melting or splattering pattern is clearly observed around the femtosecond laser ablated crater after irradiating with 10 consecutive pulses. This melting or splattering pattern which is commonly observed on surfaces ablated by long pulse or nanosecond laser is a result of fast thermal melting and solidification (Hoffman 1974; Zhigilei *et al*., 2009). For femtosecond laser machining, though it is often considered to be a non thermal process (Mingareev *et al*., 2006; Watanabe *et al*., 2007), similar melting has been observed and the dynamics for femtosecond laser induced melting have been carried out (Bonse *et al*., 2004; Wai *et al*., 2008).

By taking a closer examination of the splattering pattern around the peripheral of the ablated crater at higher SEM magnification (See Figure 6.17(b)) periodic structures or also commonly known as ripple in many literatures can be observed. By further irradiating the surface with more laser pulses, no ripples can be observed around the ablated crater (See SEM images in Figure 6.17 (c) and (d)). This indicates the ripples formation is dependent on the total cumulative pulse and fluence (Yasumaru *et al*., 2005; Wang *et al*., 2005; Groenendijk *et al*., 2006). Moreover it is observed that the foil was drilled through with little redepositions around the ablated region after 1000 pulses. This indicates that femtosecond laser is an effective tool for micromachining of aerospace materials like titanium.

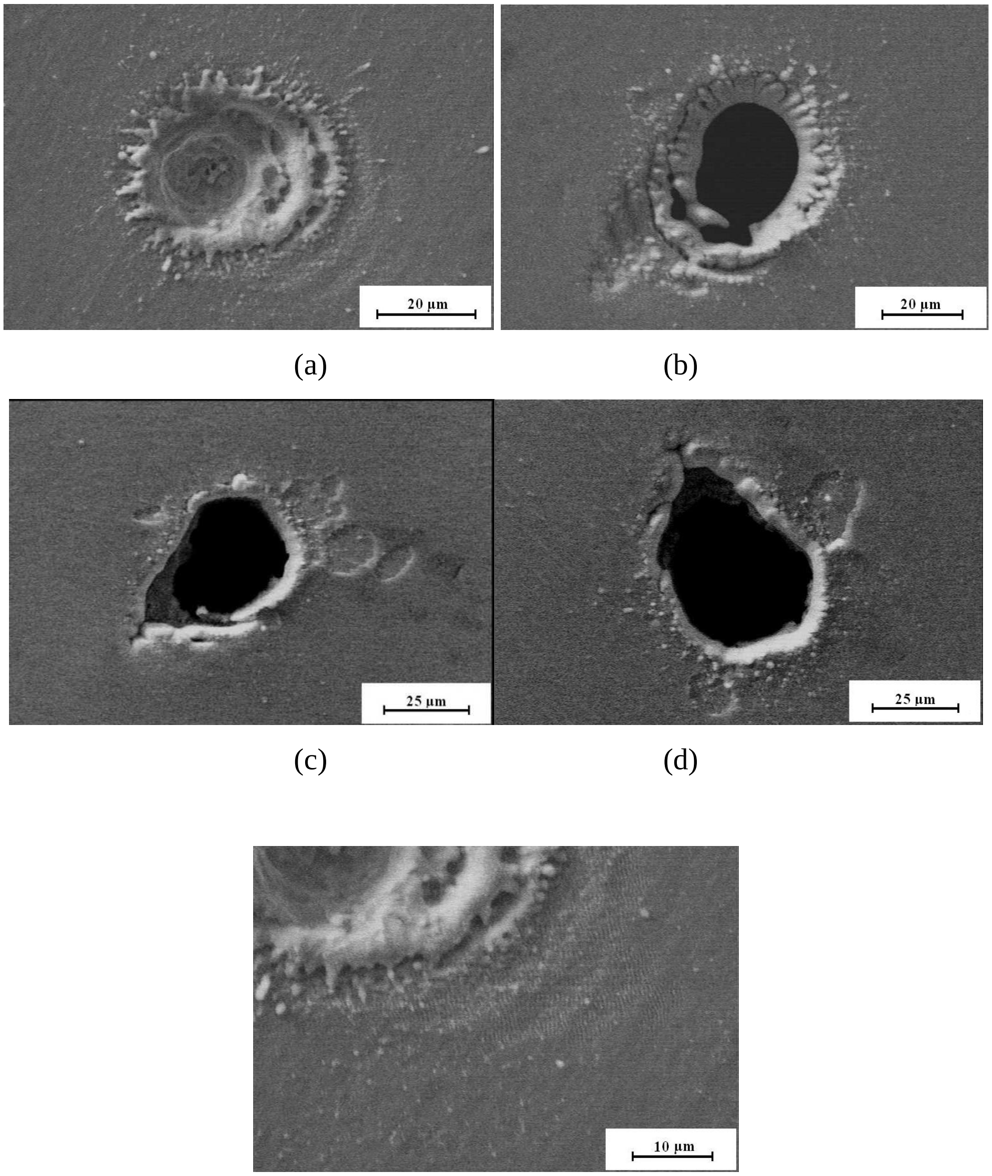

(a) (b)

(c) (d)

(e)

Figure 6.17: SEM micrographs of titanium surface after femtosecond laser irradiation. The numbers of pulses are as follows for (a) 10 pulses, (b) 100 pulses, (c) 1000 pulses, (d) 10000 pulses and (e) Close up of image 1a showing ripples.

Next, to examine whether femtosecond laser irradiation would induce structural changes, the structures around the laser ablated crater was carefully observed under TEM. A comparison was carried out between the laser irradiated and non-laser irradiated foil in term of the crystal structure and chemical compositions. Figure 6.18 shows the Energy dispersive spectra (EDS) results obtained for the non-irradiated and laser irradiated surfaces. No significant change in chemical composition was detected due to femtosecond laser irradiation.

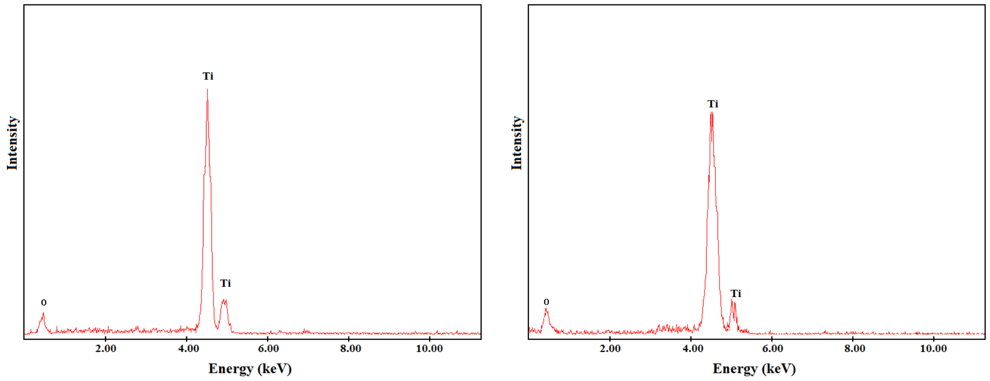

(a) (b)

Figure 6.18: EDS showing no change of chemical composition in the titanium foil. (a) Non-irradiated surface; and (b) Surface irradiated with femtosecond laser.

6.4.2 TEM analysis of fs laser irradiated titanium

Bright-field TEM results of the titanium structures irradiated with 100 and 10000 femtosecond laser pulses are presented in Figure 6.19(a) and (b). Under low TEM magnification, the laser irradiated region for both the samples show many overlapping granular patches with sizes ranging from 10nm to 30nm. The use of low TEM magnification could only give an overview of ablated sample but not the details of their crystal structures. Therefore diffraction analysis of the two samples under high resolution (HR) TEM mode was further carried out. The HR TEM results for 100 and 10,000 pulses are presented in Figure 6.20(a) and (c) while their diffraction patterns in Figure 6.20(b) and (d).

In Figure 6.20(a), the HR TEM image clearly shows that the titanium structure after 1000 pulses consists of both amorphous and crystalline phase as indicated by the wave pattern superimposed on the background of the lattice fringes. Far away from the ablated crater, the material still remains crystalline. Selected diffraction results (See Figure 6.20(b)) show very weak circular rings which further prove the existence of some nano crystals within a highly rich amorphous phase. For sample irradiated with higher laser pulses (10000 pulses), the HR TEM image (See Figure 6.20(c)) only shows a wave pattern which indicates only the presence of amorphous phase. The corresponding diffraction pattern is shown in Figure 6.20(d). From the diffraction pattern, a dull circular ring is observed which shows that the irradiated titanium structure contains only of amorphous phase.

It is estimated that the laser amorphous region measured from the edge of the crater is around 150 nm. This result is quite similar to HAZ length found for femtosecond laser ablation of metals which is found to be a few hundreds of nanometers (Le *et al*., 2002). A non-laser irradiated sample was also used as a comparison against the two laser irradiated samples. TEM image and diffraction results of the non-irradiated titanium are shown in Figure 6.20(e) and (f) respectively. For the non-laser irradiated surface, the HR TEM image shows very clear lattice fringes which are only present for crystalline materials. The diffraction pattern corresponds to a zone axis of [2-1-10] as shown in Figure 6.20(f).

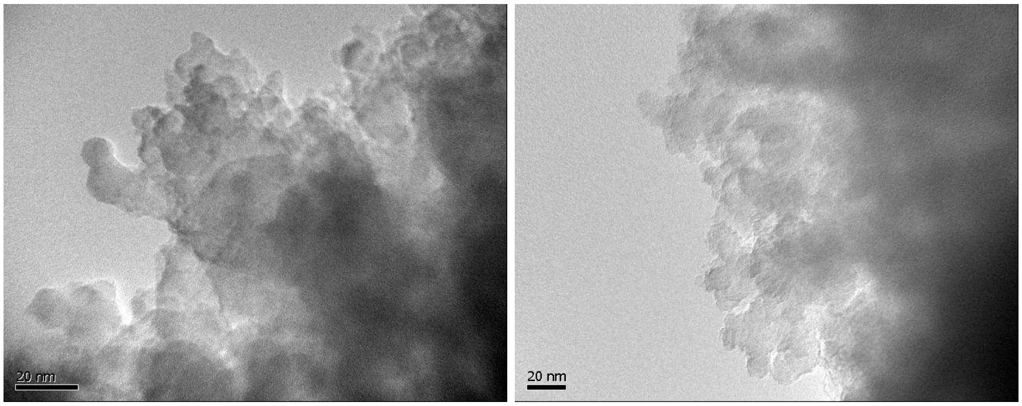

(a) (b)

Figure 6.19: Bright-field TEM images of the titanium structures after femtosecond laser irradiation. (a) 100 pulses and (b) 10000 pulses.

In this study, it is observed that the distribution of the amorphous and crystalline phase depends on the distribution of the laser intensity. The degree of crystallinity of the ablated titanium increases from the unstructured region toward the center of the irradiated zone. Furthermore an increase in the number of laser irradiated pulses leads to a higher degree of the amorphization of the irradiated zones which is explained according to the melt-quenching phenomena. A molecular dynamics simulation study on the heat-affected zone of copper metal ablated with femtosecond laser shows that using higher fluence, the thickness of the heat-affected zone is greater because the laser energy is absorbed into the deep layer due to the high thermal diffusion length compared to the skin depth (Hirayama and Obara, 2005). The residual energy left in the metal, which is not used for ablation will induces a liquid phase thus leading to the amorphous or polycrystalline phase of the metal during re-solidification.

For our case, since increasing melting and solidification is observed with increase cumulative fluence base on the SEM results, it is also presumed that the remaining laser energy did not further contribute to the ablation process. This excess or residual laser energy induced heat and formed a very thin layer of melt around the laser ablated crater (Hirayama and Obara, 2002; Guo, 2006). It is reasonable to assume that femtosecond laser ablation often involves fast heating and cooling due to the very short pulse duration. Therefore, heat from the melting region is quickly absorbed by the large cold surrounding resulting in a rapid quench of the melt when the laser pulses terminate. This results in total amorphous phase around the laser irradiated region. This mechanism is similar to the technique used for fabricating amorphous metal by using melting and fast quenching. In summary, femtosecond laser irradiation can induce amorphization in titanium. The transformation from crystalline to amorphous phase is highly dependent on the number of laser pulses as observed from the TEM results.

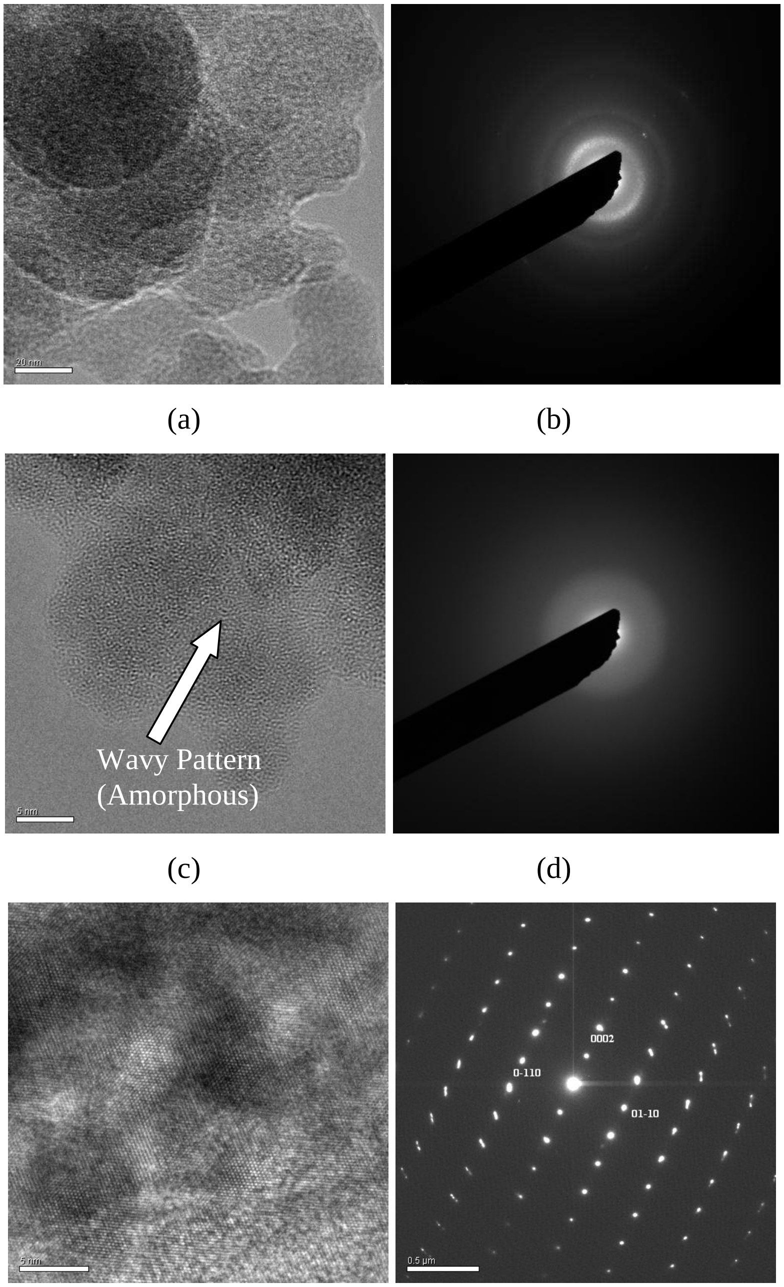

(a) (b)

(c) (d)

(e) (f)

Figure 6.20: Bright field TEM and diffraction patterns of femtosecond laser irradiated and non-irradiated titanium. (a) and (b) are the Bright field TEM and diffraction pattern of titanium irradiated with 100 pulses, (c) and (d) are the Bright field TEM and diffraction pattern of titanium irradiated with 10,000 pulses, (e) and (f) are the Bright field TEM and diffraction pattern of a non-laser irradiated titanium having a Zone Axis of [2-1-10].

6.4.3 In situ TEM analysis of fs laser irradiated titanium

Next, the use of *in-situ* TEM technique was also carried out to study the evolution of amorphous titanium structures upon thermal annealing. It is to note that this may be the first reported *in-situ* study to observe femtosecond laser irradiated titanium structure evolution upon thermal treatment. Similar technique can also be applied to study temperature effect on fs-laser irradiated glass on recrystallization and how it can affect the optical properties. The laser irradiated amorphous sample was placed on a Gatan 652 double-tilt TEM heating holder and subjected to heating. For commercial pure titanium, typical recommended annealing temperature ranges from 650 ºC to 760 ºC while the annealing time can vary from 6 minutes to 2 hours (Harry, 1996). For this experiment, the heating rate was set at 20 ºC per minute and the total heating time was 3 hours. Heating of the sample was carried out from an initial temperature of 25ºC to a final temperature of 600 ºC which is slightly lower than the recommended temperature due to the TEM tool limitation. However, a delta of 50 ºC is still high enough to study the structural evolution.

In-situ characterization on the amorphous titanium structure was carried out constantly by capturing both the bright field TEM images as well as its diffraction patterns throughout the entire annealing process. The objective was to have a better understanding on the recrystallization dynamic of amorphous structure as it often involves complex processes such as crystal nucleation and grain growth.

Selected TEM diffraction results for the entire heat treatment process at different time interval are shown in Figure 6.21 while the bright field TEM images of the pre and post annealed titanium structures are shown in Figure 6.22 respectively. From Figure 6.21(a), the laser irradiated region prior to heating is of total amorphous phase as illustrated by a dull circular ring. However, after the sample was annealed for approximately 15 minutes, several weak concentrated rings are observed (See Figure 6.21(b)). This indicates that nucleation and growth of the nano crystals had occured within the amorphous material. As expected, with a longer heating time (See Figure 6.21(c), the diffraction signal get stronger and this indicates an increase in crystal growth.

The diffraction pattern at the end of the annealing experiment is shown in Figure 6.21(d). The diffraction results correspond close to the zone axis [01-10] of pure titanium though the angle between [0002] and [-2110] is not at 90º angle. This is likely due to the sample not achieving full recrystallization and there is still some distortion within the crystal lattice. The TEM images in Figure 6.22(b) confirm the diffraction results. It is observed that the sample has not been fully recrystallized as the regular lattice array has not completely developed.

One interesting observation made is that the crystal growth seems to initiate from the edge of the sample rather than the centre region clearly as indicated in Figure 6.22(a) and (b) by the arrow. From some literature, this phenomenon where crystal growth is initiated from the sample edge is likely attributed to the free surface energy. Jung *et al*. (2001) reported that the both the grain boundaries and surface energy also play a very important role in determining grain growth. In the same report, they commented that the free surface energy will only play an active role in driving grain growth when the grain size is comparable to the film thickness. In another report by Schumacher and Wahi (1998), they observed that the nucleation of the crystals in amorphous $Pd_{81}Si_{19}$ initiated faster from the thinner part of the sample. They related their observation to both the surface and interfacial free energies. In this study, since our observation is similar to Schumacher and Wahi (1998) where the nucleation is initiated from the edge. It is speculated that the driving force for the recrystallization process of amorphous titanium upon heat treatment is most likely due to the free surface energy as well.

Since the fs laser irradiated sample can be directly observed under TEM, the thickness should be around one hundred nanometre or lesser. This thickness is much smaller than the original grain size in several micron scale. As such, the effect of free surface energy is likely to be very prominent as commented by Schumacher and Wahi (1998). However, recrystallization from amorphous structure is often a complex process and crystal structures evolution may varies with different processing parameters and this warrant further studies. It is hope that the above results can simulate research interest in studying microstructure evolution on laser irradiated material.

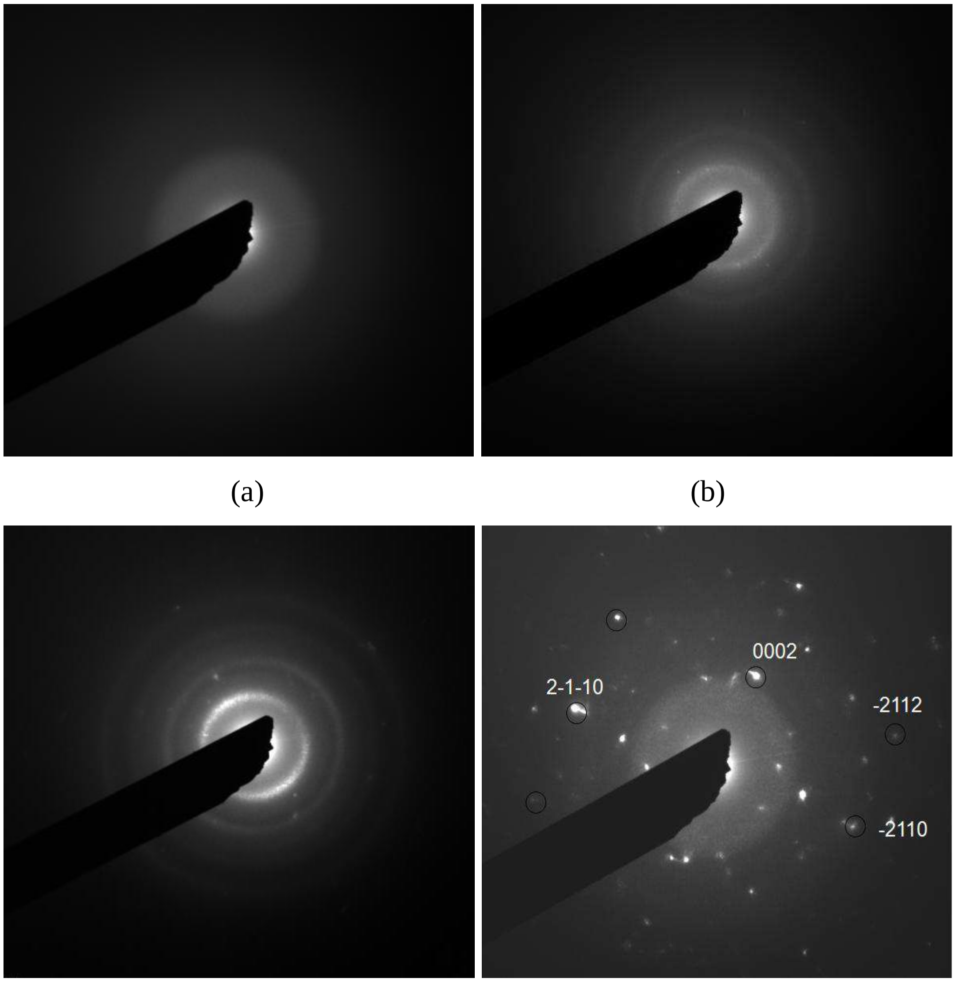

(a) (b)

(c) (d)

Figure 6.21: TEM diffraction patterns showing the formation of nano crystals with time (a) Before annealing, (b) 15 minutes, (c) 80 minutes & (d) After 180 minutes. [01-10].

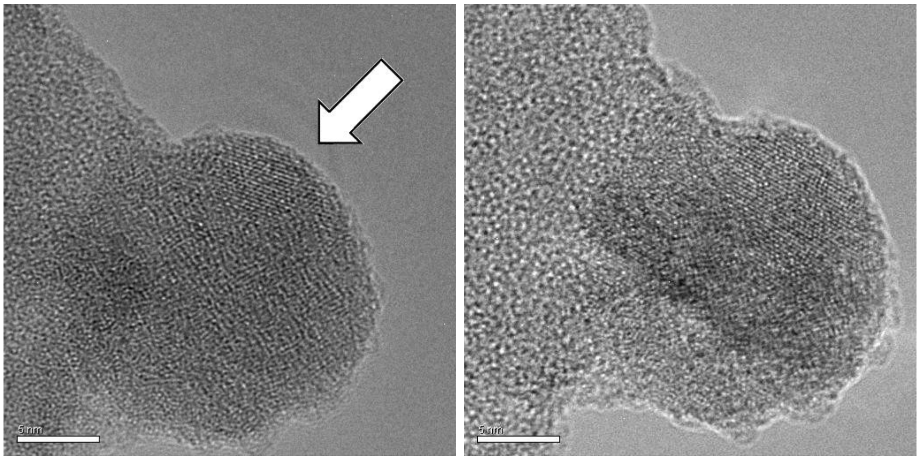

(a) (b)

Figure 6.22: Bright field TEM images showing the growth of the crystal lattice when subjected to thermal annealing (a) 15minutes and (b) 180 minutes.

6.5. Summary

A study on femtosecond laser irradiation effects on the structures of crystalline and amorphous materials has been carried out. For amorphous material like fused silica, the XRD spectra and TEM observation reveal that structure remain amorphous after femtosecond laser irradiation. For irradiation effects on crystalline quartz, the structures of microchannels walls revealed that the femtosecond laser pulses induced an amorphous zone layer ranging from 200 to 300 nm in width, which is about an order of magnitude less than the width of amorphous layer in the case of subsurface machining. In titanium metal, it was demonstrated that the formation of amorphous and crystalline carbon depends on the distribution of the laser intensity and that the use of high number of pulses lead to higher degree of amorphization of the irradiated zones according to the melt-quenching phenomena. Lastly, *in situ* TEM characterization on the laser irradiated titanium structure during thermal annealing process revealed the recrystallization dynamics of amorphous metal. This technique can be also applied to study temperature effect on fs-laser recrystallization of glass.

Chapter 7 Crack Formation in Fs Laser Micromachining of Fused Silica

7.1 Introduction

Precision machining of micro holes and channels in transparent materials has attracted great interest due to its high potential for the development of integrated micro-optics and biochip devices in the MEMS industries (Lee *et al*., 2001; Giannone *et al*., 2010). The femtosecond laser ablation technique is has been widely use for fabricating microstructures on many materials with minimal collateral damage (Stuart *et al*., 1997; Yang *et al*., 2010).

However in recent years, there is an increase in reports on detrimental defects (cracks) induced by femtosecond laser in machining of transparent materials like ruby (Chiwon *et al*., 2009) glass (Kuriyama and Ito, 2003; Wang *et al*., 2004), diamond (Kononenko *et al*., 2008), ruby (Moon *et al*., 2009) and quartz (Budiman *et al*., 2010). For practical engineering applications, material cracking must not be allowed as it will cause failure to the product. Although some studies have suggested that using high laser fluence (Qi *et al*., 2010) and higher machining speed (Ito *et al*., 2003; Low *et al*., 2005) can induce cracking and should be avoided. However, there are no systematic studies carried out in understanding the cracking mechanisms as well as the conditions for cracking to occur during femtosecond laser machining of fused silica.

In this chapter, the laser parameters and their effects on crack formation in drilling and surface machining of fused silica is reported. Through a series of systematic and detailed design of experiments (DOE), a safe process window (without cracking) is also proposed for drilling and surface machining of fused silica. Lastly, the mechanism for femtosecond laser induced cracking of fused silica is discussed.

7.2 Crack formation in fs laser drilling of fused silica

The relationship between the applied fluence and pulses and its influence on cracking during fs laser drilling is important. A simple DOE which is based on the concept of full factorial method was setup using 3 different laser fluences ranging from slightly above to many times above the threshold fluence of fused silica. It is to note that base on the full factorial method, 4 different combinations of fluence and pulses are needed when irradiated with 2 different parameters. However, for this case we use more than 4 combinations is used to improve the accuracy of the experiment. The laser fluence used correspond to 4.77 J/cm^2, 23.87 J/cm^2 and 95.48 J/cm^2 respectively. The fluence was calculated based on single pulse energy divided by the featured diameter (D). These fluence values correspond to 1.5, 7, and 27 times above the threshold fluence of fused silica for a 1mm thick substrate. Drilling of microholes was carried out at different pulses ranging from 1 to 10000.

Figure 7.1 to Figure 7.3 illustrates the optical micrographs of the top profiles of the fs laser drilled holes using the above conditions. As observed from the optical micrographs in Figure 7.1, drilling using a fluence of 4.77 J/cm^2 did not induce any surface cracks for the range of pulses applied. However when the drilling was performed using the next higher fluence at 23.87 J/cm^2, some micro cracks were observed around the peripheral of the hole only after 10 consecutive applied pulses$^.$ The length of the crack is approximately 10 μm and the crack length continues to increase with more laser pulses until it saturates to a length almost or equal to the diameter of the laser ablated crater. The last set of fluence (23.87J/cm^2) observed severe cracking at a low number of applied pulses (See figure 7.3). A crack profile measured by AFM is shown in Figure 7.4(a) and a sectional analysis of the crack in Figure 7.4(b). It can be observed that the crack induced a step height about 100 nm above the surface as measured by AFM.

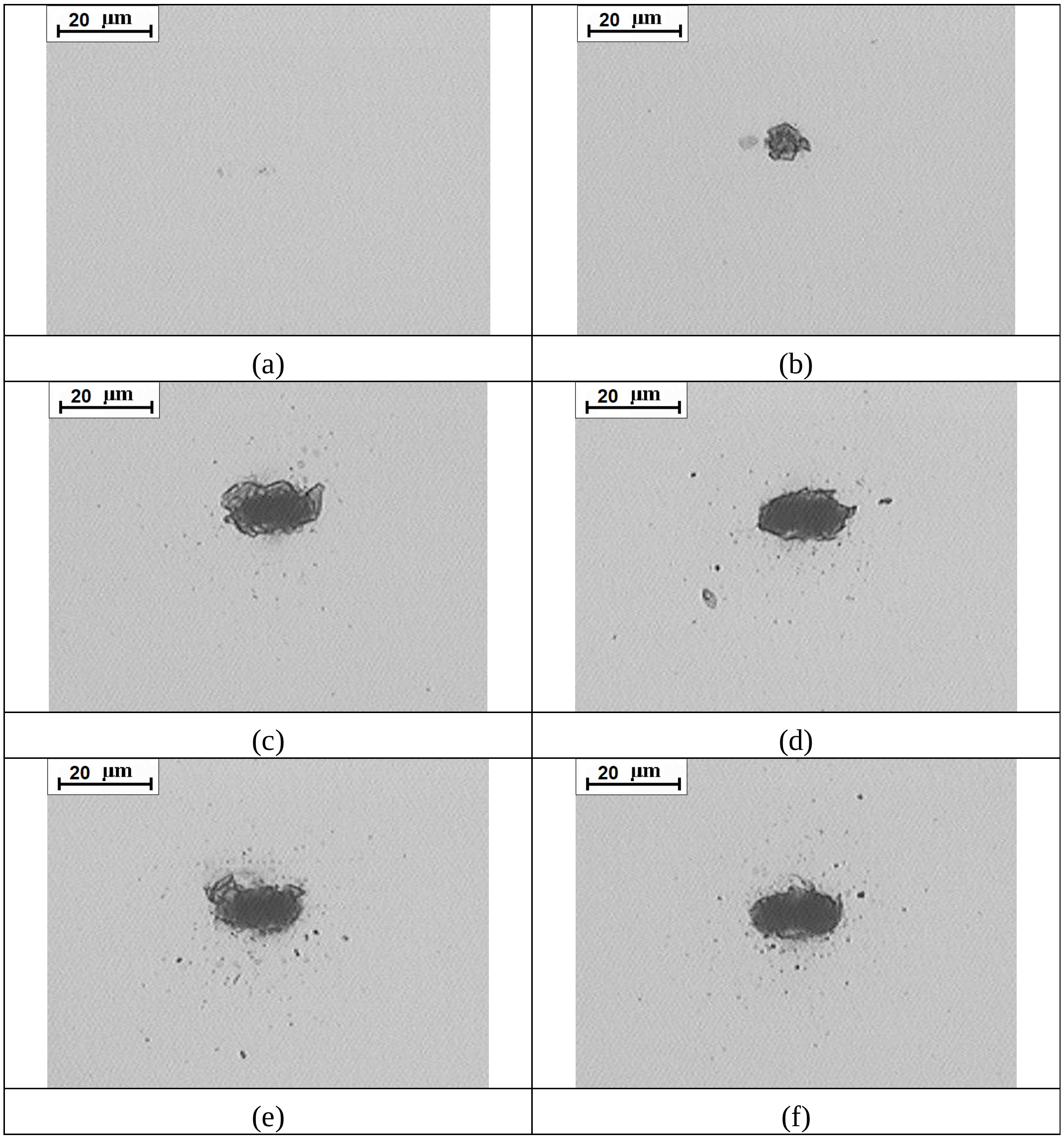

(a) (b) (c) (d) (e) (f)

Figure 7.1: Optical micrographs of fs laser drilled holes using a fluence of 4.77 J/cm^2. The laser pulses are as follows (a) 1 pulse, (b) 10 pulses, (c) 50 pulses, (d) 100 pulses, (e) 1000 pulses and (f) 10000 pulses.

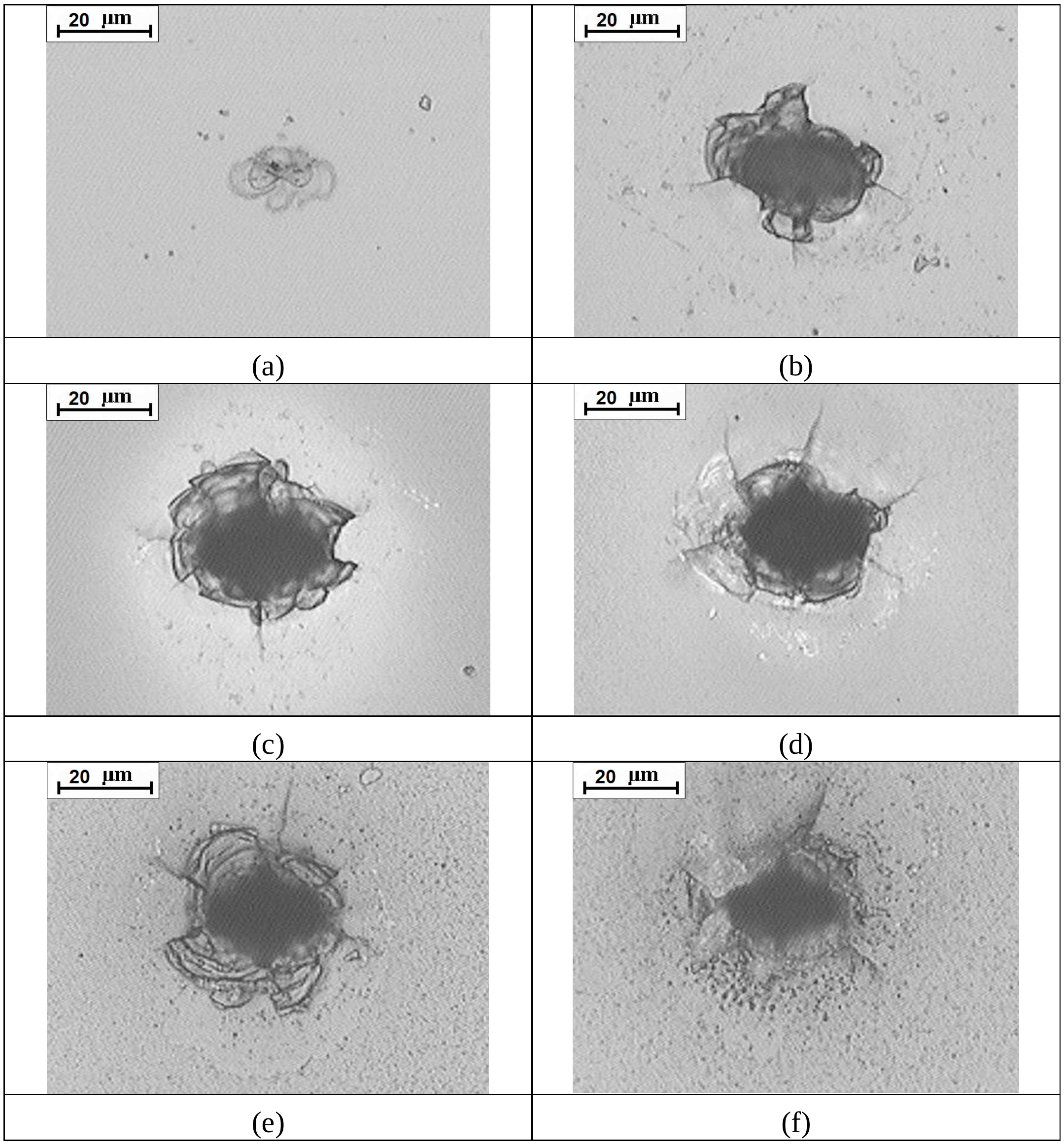

(a) (b)

(c) (d)

(e) (f)

Figure 7.2: Optical micrographs of fs laser drilled holes using a fluence of 23.87 J/cm^2. The laser pulses are as follows (a) 1 pulse, (b) 10 pulses, (c) 50 pulses, (d) 100 pulses, (e) 1000 pulses and (f) 10000 pulses.

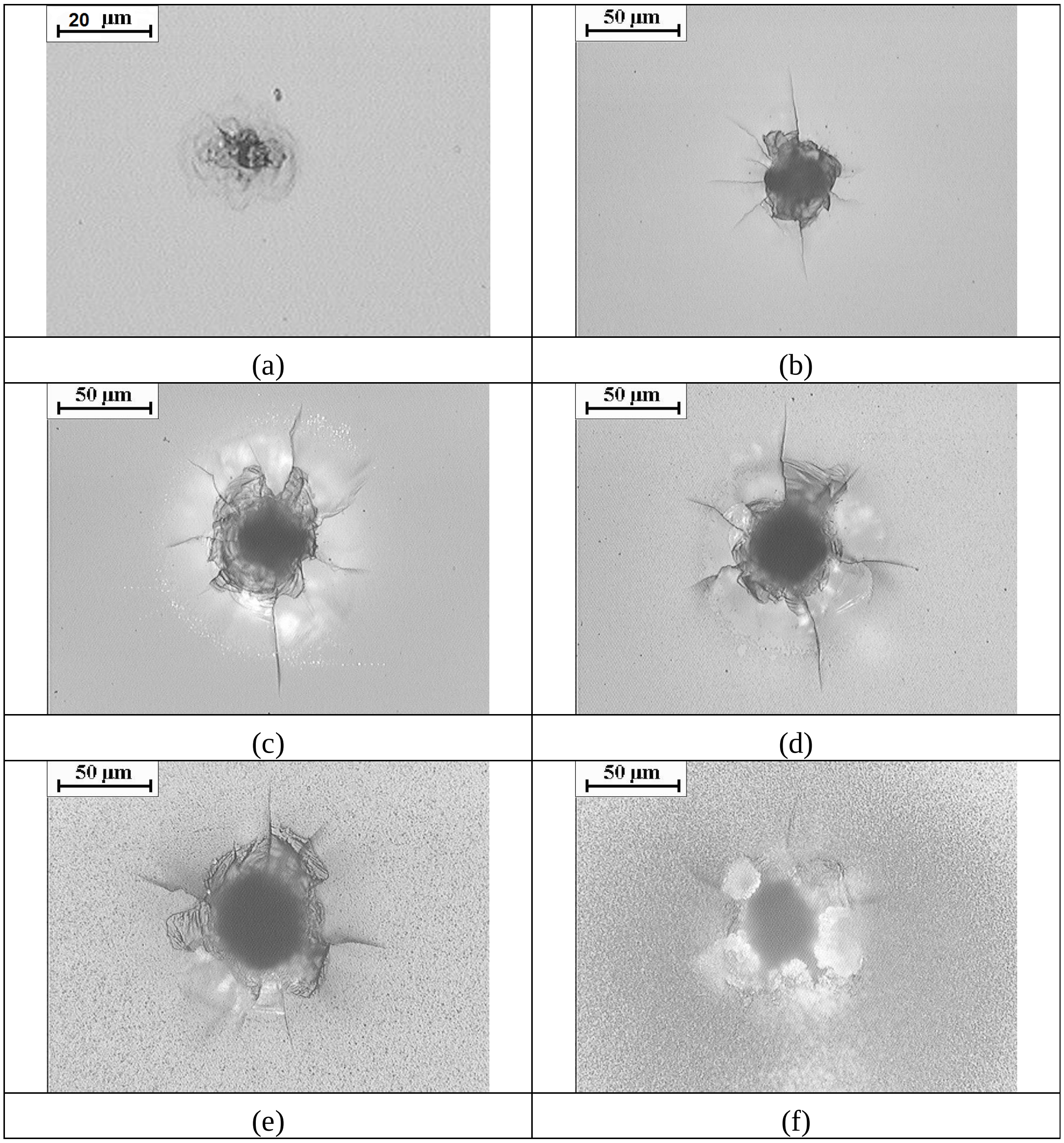

(a) (b)

(c) (d)

(e) (f)

Figure 7.3: Optical micrographs of fs laser drilled holes using a fluence of 95.48 J/cm^2. The laser pulses are as follows (a) 1 pulse, (b) 10 pulses, (c) 50 pulses, (d) 100 pulses, (e) 1000 pulses and (f) 10000 pulses.

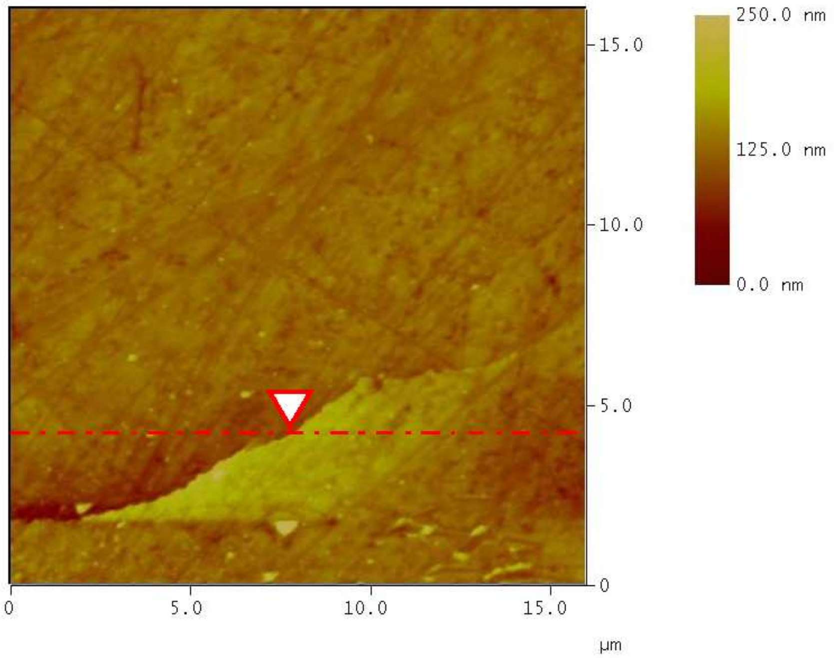

(a)

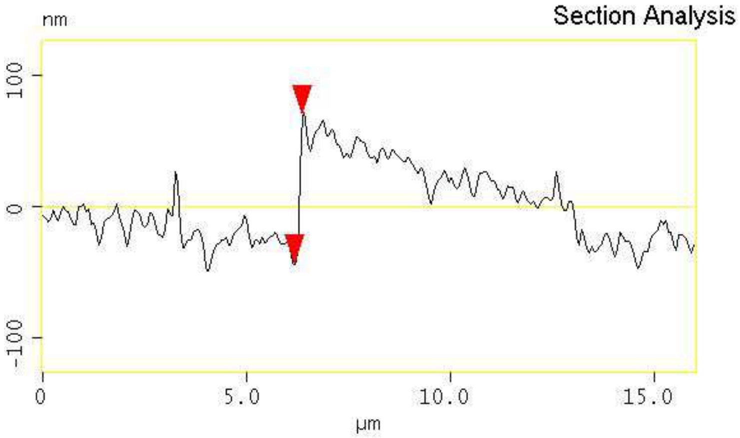

(b)

Figure 7.4: AFM images showing (a) Top profile of a crack (b) Sectional analysis of the crack profile. The laser fluence and pulses used are 23.87 J/cm^2 and 10 pulses.

From the above results, it can be concluded that cracking of fused silica during femtosecond laser drilling process is highly dependent on the applied laser fluence and pulses. Therefore it would be useful to find a safe process window where the drilling can be safely carried out without any cracking. To find the optimum processing window, a second set of laser drilling experiments was conducted. It should be noted that this second drilling experiment was carried out using the full factorial design method but in a more detailed manner as compared to the first experiment. A wider fluence range but with a smaller step size between the pulse ranges is used so as to find the cracking boundary.

The laser fluence for the second experiments was 3.18 J/cm^2 to 190.6 J/cm^2 and pulse ranging from 1 to 50,000. The laser drilled holes for each set of parameters were observed under the optical microscope for any sign of cracks. A pictorial model based on the optical observations is summarized and shown in Figure 7.5. From this figure, it can be observed that femtosecond laser drilling of fused silica can be classified into 2 different zones: (i) No cracking and (ii) Cracking zone. The crack boundary occurs around a fluence of 15.9 J/cm$^{2.}$ This fluence corresponds to about 4.5 times the threshold fluence of fused silica. Exceeding this value would result in a direct cracking scenario during the drilling process. It is worth noting that the above results may represent the first parametric study of the effect of laser influence and pulses on crack formation of femtosecond laser drilling of fused silica.

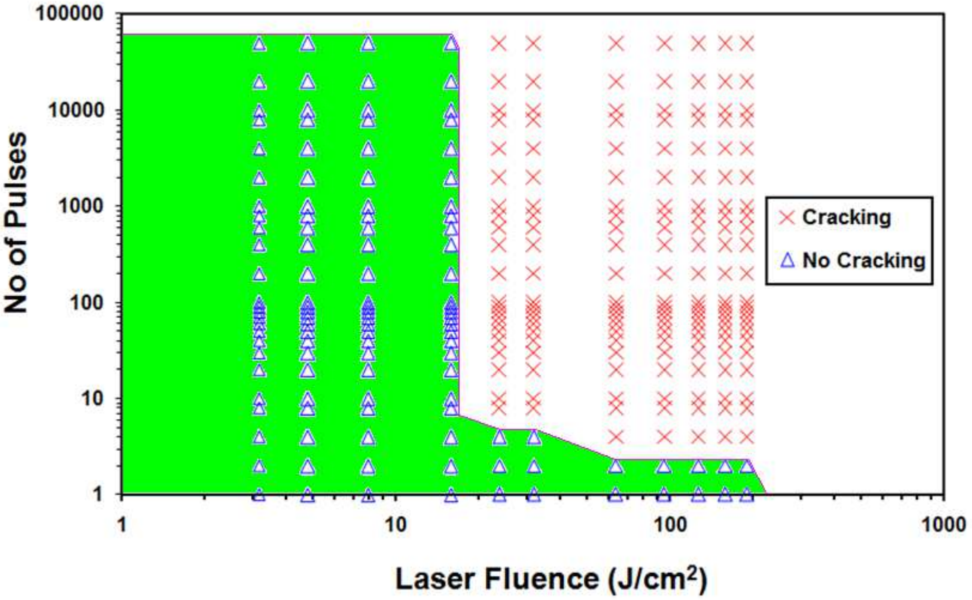

Figure 7.5: Illustrate 2 different zones in Fs laser drilling.

Next by plotting the crack length as a function pulses at different fluence, it is observed that the crack length exhibit a logarithmic dependence on the applied fluence and pulses which is shown in Figure 7.6. A relationship between the crack length and the applied fluence and pulse can be derived from the graph and can be fitted into a simple empirical expression as follows:

$$l_c = 0.1 F_{ap} In(P_a) \tag{7.1}$$

where (l_c) is the crack length, (P_a) is the applied pulses and (F_{ap}) is the applied fluence. It is to note that the empirical expression is only valid if the applied fluence is greater than 4.5 times the threshold fluence of fused silica.

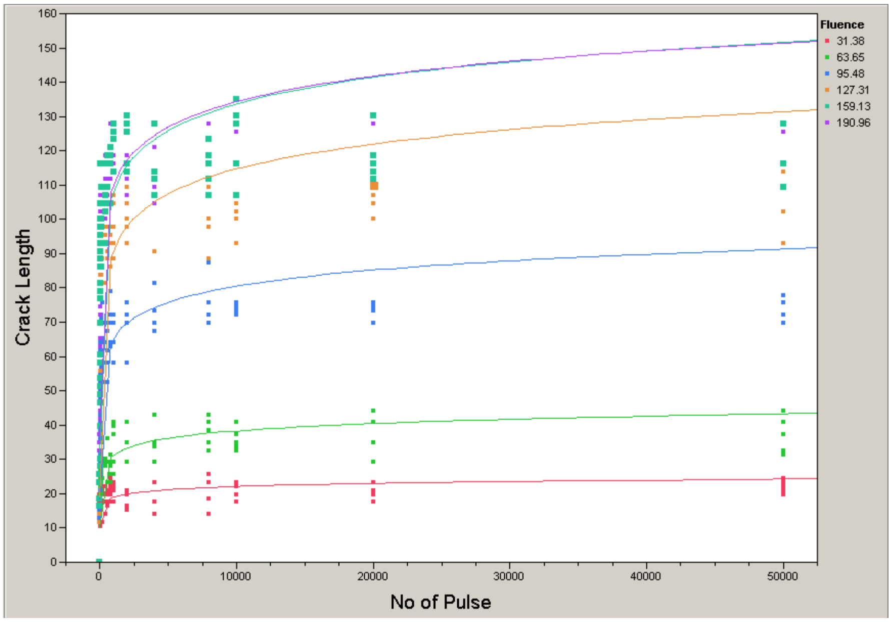

Figure 7.6: Crack Length as a function of pulses at different fluence.

However, one question still remains why cracking would still occur even though fs-laser machining is widely considered to be a non-thermal machining process. In this study, the hypothesis adopt for the crack formation of fused silica is a result of fs-laser induced shock pressure cracking. When transparent dielectric like fused silica is subjected to intense fs-laser irradiation, the electrons near the surface will be excited via nonlinear multi-photon absorption and subsequent avalanche ionization process (Momma *et al*., 1996; Glezer *et al*., 1997; Lenzner *et al*., 1998; Perry *et al*., 1999). The laser energy is then transferred to the lattice upon reaching critical pulse energy and a strong plasma is generated at the material interface. As the plasma expands, it induced a violent recoil pressure that causes material removal (Chen *et al*., 2006; Mak *et al*., 2011). At the same instance, the recoil pressure develops an impact force at the vapor to solid interface generating a high magnitude of plastic wave (shock wave) that propagates towards the surrounding and into the bulk. A schematic of plasma induced recoil force is shown in Figure 7.7.

During shock wave loading of solid materials, the material is subjected to high strain rates. The most widely studied of these processes is probably spall fracture (Antoun *et al*., 2002) which arises from tensile stresses generated by the interaction of release waves within the material upon reflection of a compressive pulse from a free surface or from an interface with a layer of lower acoustic impedance. If such tensile stresses exceed the dynamic strength of the material, they cause the nucleation and growth of micro-voids or micro-cracks which may eventually coalesce to form a macroscopic fracture and lead to the ejection of one or several fragments (spalled layers) from the sample (Thibuat *et al*., 2010).

Griffith proposes that all brittle material contain a population of small cracks and flaws that varies in sizes, geometries and orientation. Facture occurs when the tensile stress exceed the theoretical cohesive strength of the material at the tip of one of these flaws (Callister, 2000). To verified that the fs-laser induced tensile stresses has exceed the dynamic strength of fused silica ~ (104 MPa) that resulted in material fracture, the critical stress (σ_c) is calculated based on a crack length of 10 µm shown in Figure 7.2 using

$$K_c = Y\left(\frac{l_c}{W}\right)\sigma_c\sqrt{\pi l_c} \qquad (7.2)$$

Where (K_c)is the fracture toughness, (Y) is a dimension parameters or function that depend on both the crack and specimen sizes and geometries, as well as the manner of loading, (l_c) is the crack length and (W) is the sample width. For fused silica, the fracture toughness is given as 0.79 x 10^6m$^{0.5}$ and $Y\left(\frac{l_c}{W}\right)$ is approximately equal to 1.1 for a very wide plane and short crack. The critical stress is calculated to be 128 MPa which is greater than the theoretical strength of fused silica at 104 MPa, thus cracking occur.

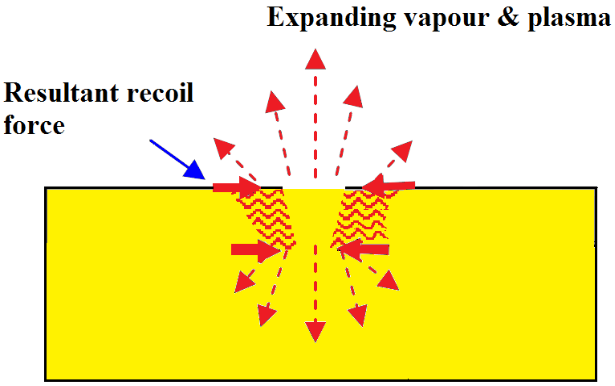

Figure 7.7: Schematic showing plasma induced recoil force.

Lee et al. (2004) reported that the recoil pressure can reach a range of 40 x 10^9 to 200 x 10^9 Pa when irradiating the surface of silicon using a nanosecond laser with a peak power at 10^{11} W/cm^2. Bernath et al. (2006) also reported that pressure of aluminum irradiated with high intensity fs-laser beam can induce pressures of tens of GPa with electron temperatures approaching 30eV. In the same report, they also reported that that the pressure inside the plasma can increase to >100 GPa, with electron temperatures of tens of thousands of keV at irradiances greater than 10^{14} W/cm and have demonstrated that fracture of silicon dioxide could occur due to shockwave. For our experiment, the recoil pressure P (kbar) in the ambient air can be estimated using the following equation by treating air as an ideal gas (Fabbro *et al*., 1990):

$$P = 32.2\left(\frac{\xi}{2\xi+3}\right)^{2/3}(4\rho)^{1/3} I_a^{2/3} \qquad (7.3)$$

Here, ξ is the ratio between the thermal and the internal energy, which is equal to 1 in the case of an ideal gas. ρ is the density of air . (0.0011 g/cm^3) and I_a is the absorbed intensity of the laser beam in GW/cm^2. For our laser drilling experiments, the recoil pressure is calculated to be in the range of 1.3 x 10^{11} to 9 x 10^{12} Pa. Such enormous pressure generation could easily induce cracking for material like fused silica as the material has small value of thermal conductivity (1.38 Wm^{-1}K^{-1}), thermal expansion (0.55 x 10^{-6}K^{-1}) and defect accumulation (Tsai *et al*., 2003).

7.3 Crack formation in Fs laser machining of fused silica

Next, evaluation on defect formation in scribing grooves on the fused silica using a moving femtosecond laser beam was carried out. The key objective is to understand the dynamics of defect formation when a moving femtosecond beam is applied in machining as compared to a stationary beam. Moreover, it is hoped that through a series of DOE, a set of optimum cutting parameters can be introduced for machining of grooves on the fused silica is so that defects like cracking or chipping can be avoided.

By varying two of the most used machining parameters such as the laser fluence and feed rate, a simple DOE using full factorial design method was first set up to evaluate if defects could occur under three different machining conditions. Scribing of grooves using a single pass was carried out using a speed ranging from 10μm/sec to 500 μm/sec for three different sets of laser fluence which are 7.96 J/cm^2, 15.9 J/cm^2 and 31.8 J/cm^2. Figures 7.8 to 7.10 shows the optical results of the microgrooves machined using the three different sets of laser fluence at different feed rates.

For the grooves machined with a fluence of 7.96 J/cm^2, it is observed from the optical micrographs in Figure 7.8(a) that machining with a low feedrate of 10 μm/sec produced clean edges without any material cracks or chipping observed. Similarly, scanning at the next two higher speeds of 50 and 100 μm/sec produced clean edges as well. However, it is observed that as the machining speed progressively became higher, some waviness along the edge of the grooves can be observed as shown in Figure 7.8 (d). At a speed of 500 μm/sec (See Figure 7.8 (e)), slight chipping can be observed on the edge. For grooves machined with a fluence of 15.9 J/cm^2, similar observations are made except that the chipping gets more severe when higher fluence is applied. For the third set of applied fluence (31.8 J/cm^2), highest among the three, it is observed that the chipping signature tend to occurs earlier at even lower machining speed which is at 250 μm/sec. At speeds ranging from 10 μm/sec to 100 μm/sec, no chipping or cracking is observed.

To obtain a safe process window for machining of grooves in fused silica, more grooves were machined using a wider fluence range as compared to the first DOE. Figure 7.11 shows a summary of the results obtained for a wider fluence range. From the graph, it is observed that machining in both the high and low fluence regime can induce defects formation when the fused silica sample is translated at a highest feedrate of 500 μm/sec. These defects can be in the form of only material chipping when machining in the low fluence regime, or consist of both chipping and cracking when machining in the high fluence regime. Thus it is recommended that machining of fused silica using high federate should be avoided and the feedrates should be kept below 100 μm/sec to avoid material cracking based on the results obtained.

In summary, it can be concluded that the fs laser machined grooves on fused silica is highly dependent on the applied laser fluence and machining speed. Moreover, it is also observed that higher machining speeds seems to promote even more chipping or even cracking. This observation is in contrast with dielectric material machined using long pulse lasers (Tsai *et al*., 2003). For machining with long pulse lasers, using a higher machining speed would reduce the tendency of cracking due to a reduction of thermal stress.

For femtosecond laser machining of fused silica, material cracking or chipping is more likely to be a result of thermal shock rather than recoil pressure force created by the expanding plasma (Kongsuwan *et al*., 2012). By translating the sample with higher peak power and higher scanning speed results in a higher peak temperature and greater thermal gradient surrounding the absorption volume, respectively. Once the thermal stress overcomes the fracture stress of the material, cracks are initiated in the material as clearly observed from the results in Figure 7.12.

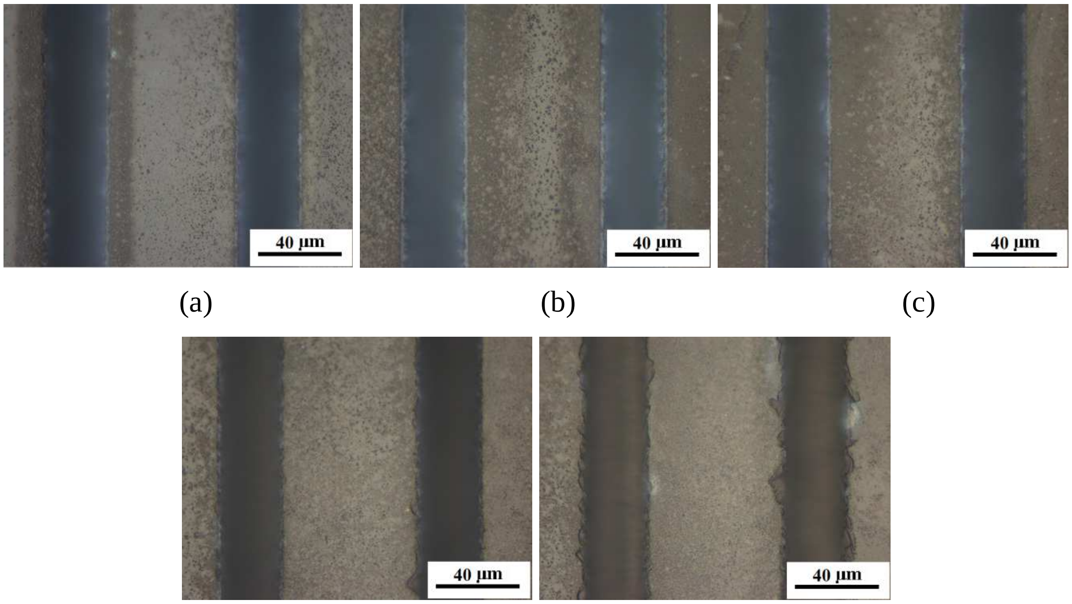

(a) (b) (c)

(d) (e)

Figure 7.8: Optical micrographs of fs laser machined grooves using a fluence of 7.96 J/cm^2. The machining speed are as follows (a) 10 µm/sec (b) 50 µm/sec (c) 100 µm/sec (d) 250 µm/sec and (e) 500 µm/sec.

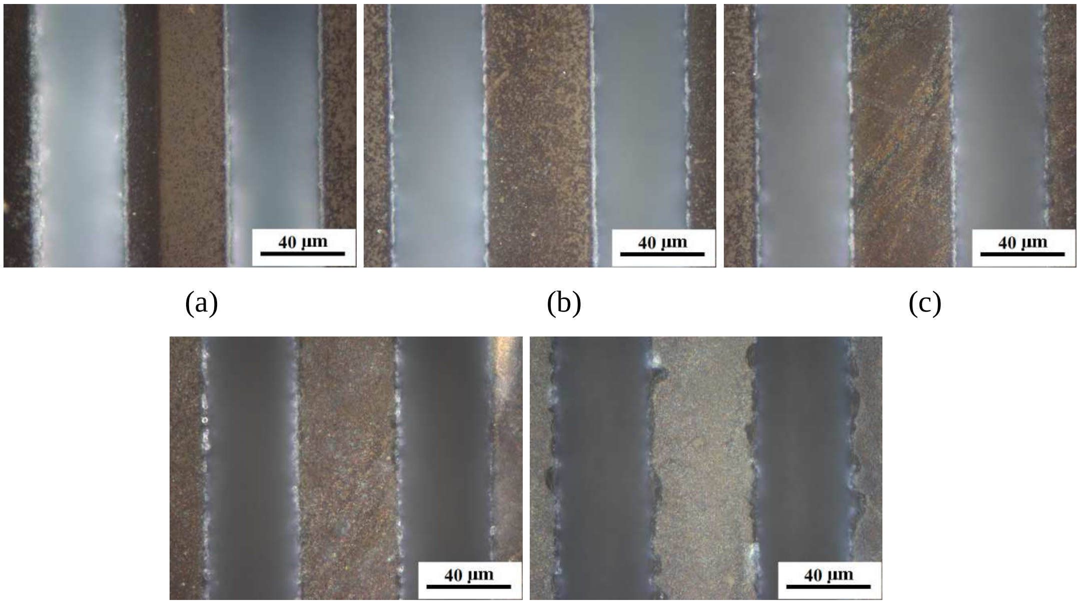

(a) (b) (c)

(d) (e)

Figure 7.9: Optical micrographs of fs laser machined grooves using a fluence of 15.9 J/cm^2. The machining speed are as follows (a) 10 µm/sec (b) 50 µm/sec (c) 100 µm/sec (d) 250 µm/sec and (e) 500 µm/sec.

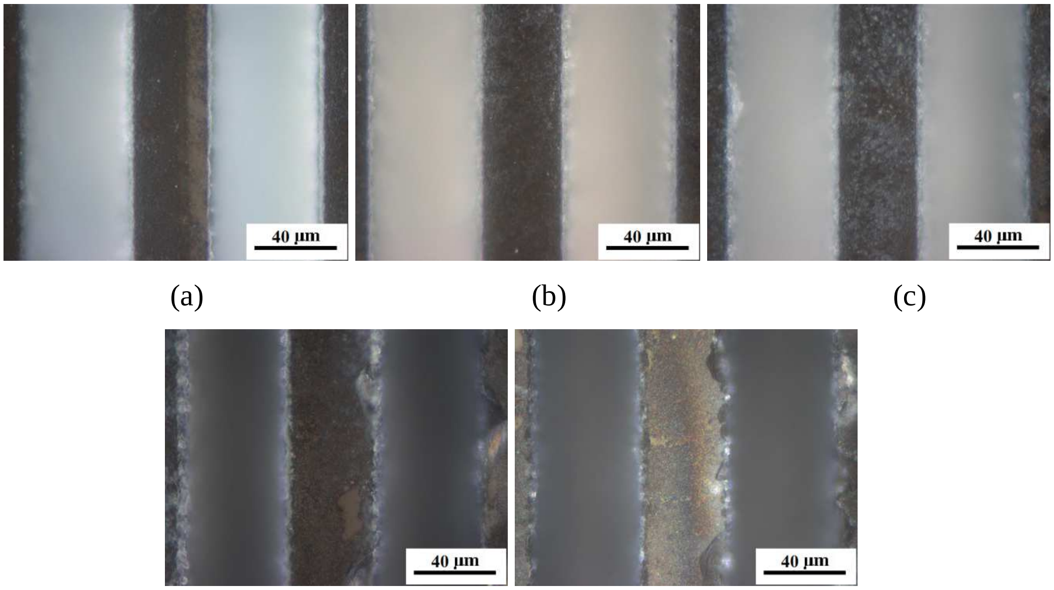

(a) (b) (c)

(d) (e)

Figure 7.10: Optical micrographs of fs laser machined grooves using a fluence of 31.8 J/cm^2. The machining speed are as follows (a) 10 µm/sec (b) 50 µm/sec (c) 100 µm/sec (d) 250 µm/sec and (e) 500 µm/sec.

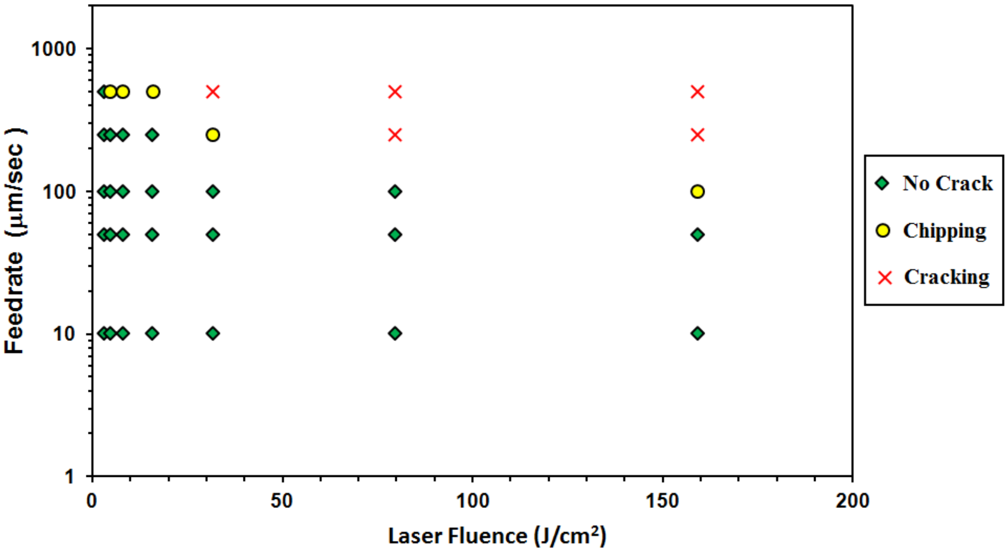

Figure 7.11: Summary of cracking Vs no cracking region in fs laser machining grooves using different fluence and federate.

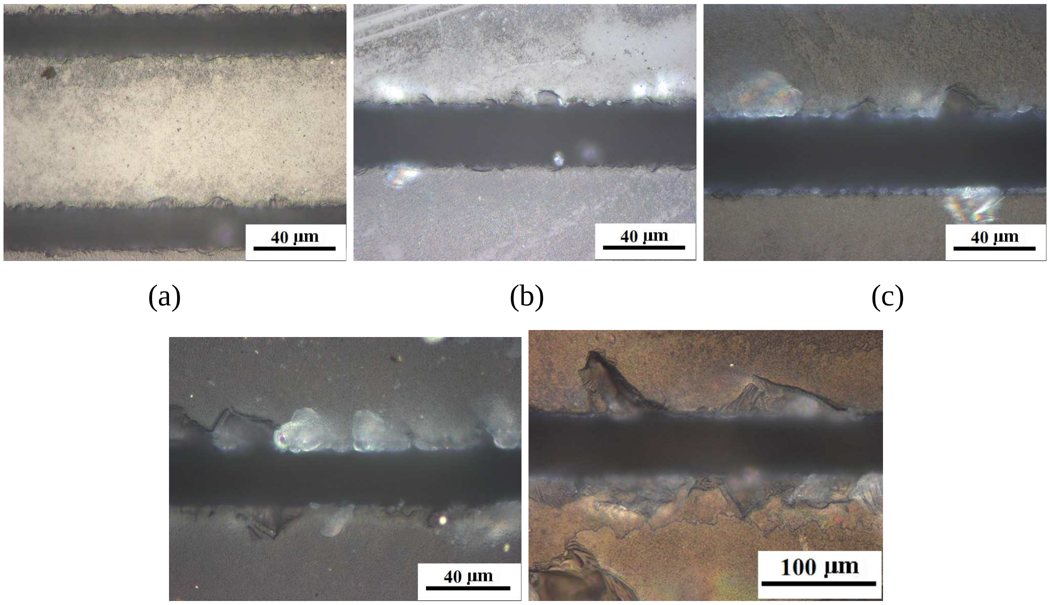

(a) (b) (c)

(d) (e)

Figure 7.12: Optical micrographs of fs laser machined grooves using a speed of 500 µm/sec. The laser fluence are as follows (a) 7.96 J/cm^2 (b) 15.9 J/cm^2 (c) 31.8 J/cm^2 (d) 79.57 J/cm^2 and (e) 159.1 J/cm^2.

7.4 Summary

A systematic investigation on the effect of laser fluence, pulse and feedrate in crack formation during fs laser drilling and machining of fused silica is carried out. For drilling of contact holes in fused silica, an optimum process window has been identified which is to use a fluence level not more than 4.5 times the threshold value so that cracking can be prevented. A simple empirical expression to predict the crack length base on applied fluence and pulse has been developed. For machining of surface channels, it is recommended that high federate should be avoided to reduce the tendency of defect formation and the federate should be kept below 100 µm/s. The developed micromachining process has potential application in manufacturing blind contact holes and channels on fused silica substrate based bio and optical devices.

Chapter 8 Conclusions and Future work

8.1 Summary

Femtosecond laser beam interaction with fused silica has been investigated and the aim of this research is to understand irradiation effects, phenomenon and machining parameters affecting the quality of fused silica. Starting from low fluence irradiation, the thesis begins by reporting results of ripple formation. Using higher fluence, femtosecond laser micromachining of holes and channels was demonstrated and the effects of process parameters were studied and discussed. Following which, in-depth characterizations on the laser irradiated structures were performed since femtosecond laser irradiation can induce structural change. Lastly, an investigation on an engineering problem was carried out which is the cracking of fused silica during femtosecond laser machining. The overall experimental conclusions and research contributions is summarized in the below sections:

8.1.1 Pattern formation upon femtosecond laser irradiation of fused silica

The formation of laser induced periodic surface structures in fused silica upon irradiating with a linearly polarized fs-laser beam (τ~<150fs, λ=775nm) in air was studied theoretically and experimentally. It was found that ripples having two different orientations, one parallel (coarse ripple) and the other perpendicular (fine ripple) to beam polarization can be formed on the surface of fused silica. Both the ripples periods were observed to be smaller than the wavelength of the femtosecond laser and the mechanism on the ripple formation cannot be explained using both the classical interference model or by using the self-organization theory. Instead the origin of the coarse ripple is proposed to be a result of frozen capillary waves upon the ultrafast melting and solidification of fused glass, while the fine ripples is a result of harmonica wave generation. By varying the experimental parameters such as fluence, pulses and beam polarization, it is found that orientation and period of these ripples structures can be controlled experimentally. Also it is found that the ripple is highly dependent on the defect orientation but not on material crystallographic orientation when irradiated using crystalline quartz having different crystallographic orientations. The above results have shed new lights on the role of beam polarization, defect density and crystal structure of silica glass on the ripple formation. This will play a key role in the development of new optical devices such as gratings or similar.

8.1.2 Femtosecond laser micromachining of fused silica

The feasibility of using femtosecond laser in carrying out micromachining of holes and channels were studied using a wide range of experimental parameters. The result presented is the first detailed parametric study in machining of fused silica. In drilling of microholes, two ablation regimes have been identified and discussed. In the first regime (Pulses <100), a steep increase in the ablation rate was observed until the drilling enters into the second regime (Pulses >100), where the ablation rate began to slow down. The decrease in ablation rate was attributed to the plasma shielding effect. Effect of beam polarization in drilling of holes that has never been investigated on fused silica has been studied. It was observed that the beam polarization not have any significant effect in terms of the hole profile and machined depth. Cracking phenomenon that was rarely observed is found to occur in the high fluence regime when drilling micro holes with a fs-laser beam.

In machining of surface grooves, lower machining power results in better cutting quality but a decrease in machining efficiency. Though using high power and high machining speed can result in a faster and deeper cut but it can also lead to cracking and subsurface damages. Similar, beam polarization effect which has never been investigated was observed to not have any significant effects on the machined quality in terms of cut width, depth, profiles and surface morphologies. By machining the same groove multiple times, straight microchannels can be achieved.

8.1.3 Femtosecond laser irradiation effects on structures of crystalline and amorphous material

To study femtosecond laser irradiation effects, several key engineering materials were chosen ranging from single crystal quartz to poly crystalline titanium and amorphous material like fused silica. On the study of fused silica, the result presented is the first direct cross-sectional TEM examination on the silica grooves structures irradiated with a femtosecond laser beam. The fused silica structure is observed to remain amorphous after the femtosecond laser irradiation. In the studying of fs-laser irradiated single crystal quartz, amorphization of the quartz sample was observed after femtosecond laser irradiation. The amorphous region was found to be in a range of 200 to 300 nm in width.

For titanium thin foil, the structure around the laser irradiated region can be partially or fully amorphized depending on the number of applied laser pulses. Using thin foil to study the laser irradiated structure has advantage over bulk sample as the sample can be directly observed under TEM without further sample preparation. The use of in-situ TEM heating technique can be used to reveal the recrystallization dynamics of amorphous metal. The above study has led to a better understanding on fs-laser material interaction.

8.1.4 Crack formation in Fs laser micromachining of fused silica

Cracking of fused silica during femtosecond machining has been systematic studied. The laser parameters were studied for process optimization. A crack-free process window for micromachining of fused silica has been proposed together with an empirical expression to predict the crack length base on the applied fluences and pulses has been developed. In drilling of contact holes in fused silica, it is found that the applied fluence must not greater than 4.5 times the ablation threshold of fused silica in order to avoid a cracking scenario. The mechanism for the fs-laser induced crack is proposed to be a result of the recoil pressure and shock, generating stresses greater than strength of fused silica material. For machining of microchannels, the use of high feedrate should be avoided and should be kept below 100 μm/s as it can increase the defect formation. The developed micromachining process has potential application in fabricating lab-on-chip biomedical, optical and microelectronic devices.

8.2 Future Work

As summarized above, the results reported in this research study has help to advance the field of femtosecond laser material interaction and microfabrication in several aspects; however several questions and challenges still remain which warrant further investigation.

(1) Ripples can be used for a wide range of applications. However, controlling ripples growth especially producing very regular ripples over a large region can be very difficult. Thus further research work can be undertaken to explore fabricating ripples with very regular feature size over a large area such as using diffraction technique.

(2) In-depth studies on surface machining of fused silica have been performed using a wide range of parameters. However, femtosecond laser can also be used to carryout subsurface machining as well. Similarly, further in-depth studies for process optimization can be carried out to study subsurface machining of fused silica for practical applications like waveguides and microfludic channels.

(3) Femtosecond irradiation effect has been carried out using TEM. However, a clear relationship on how experimental various parameters can affect structure change is still not yet fully understood. This is especially important as the material properties vary with different crystal structures. By understand these effects; one can alter laser irradiated structures to the suit a specific design or application. Thus further experiments can be carried out using a wide range of parameters to study the recrystallization and amorphization dynamic of various materials. Also the use of modelling software may be explore to model the femtosecond laser irradiation effects of material to gain a better understanding of phase change in material.

(4) Though cracking of fused silica can be avoided using appropriate process parameters and the mechanism of crack formation is discussed. However, the use modelling or simulation work may help to develop a better understanding on femtosecond cracking mechanism on various materials. This area of study can be further explored.

List of Publications

(1) H. Y. Zheng, W. Zhou, H. X. Qian, **T. T. Tan**, and G.C. Lim, Polarisation-Independence of Femtosecond Laser Machining of Fused Silica, *Applied Surface Science*, Elsevier Science, USA, Sept. 2004, Vol. 236, Nos. 1-4, pp. 114-119.

(2) W. Zhou, **T.T. Tan,** H.Y. Zheng, S. Zhu and L.M. Wang**,** Effect of Femtosecond Laser Irradiation on Structure of UV Grade Fused Silica, *Optics Express*, *2006*, Vol. 14, no. 20, pp. 9217-9222.

(3) H.Y. Zheng, **T.T. Tan** and W. Zhou. Studies of KrF laser-induced long periodic structures on polyimide, *Optics and Lasers in Engineering*, Jan. 2009, Vol. 47, no. 1, pp. 180-5.

References

Aggoune, S., Vidal, F. and Amara, E. H. (2010). “Influence of pressure on aluminium plasma expansion produced by a nanosecond laser pulse: a numerical study”. *Proceedings of the 36th International MATADOR Conference*. Pp 481-484.

Alekhin, A.A., Ionin, A.A., Kozhushko, S.E., Kourylyova, I.M., Kudryashov, S.I., Kuz'min, K.K., Likhvansteva, V.G., Samoylov, M.V., Seleznev, L.V., Sinitsyn, D.V. and Zakharov, S.D. (2010). “In vitro femtosecond laser subsurface micro-disruption inside human cornea and pre-cleared sclera”. *Laser Physics Letters*. Vol. 7, no. 6, pp. 463-6.

Ameer-Beg, S., Perrie, W., Rathbone, S., Wright, J., Weaver, W. and Champoux, H. (1998). “Femtosecond laser microstructuring of materials”. *Applied Surface Science*. Vol. 127-129, pp. 875-80.

Amer, S., El-Ashry, M.A., Dosser, L.R., Hix, K.E., Maguire, J.F. and Bryan, I. (2005). “Femtosecond versus nanosecond laser machining: comparison of induced stresses and structural changes in silicon wafers”. *Applied Surface Science*. Vol. 242, no. 1-2, pp. 162-7.

Ams, M., Dekker, P., Marshall, G.D., Little, D.J. and Withford, M.J. (2010). “Directly written DFB waveguide lasers using femtosecond laser pulses”. *AIP Conference Proceedings*. Vol. 1278, pp. 438-45.

An, R., Li, Y., Dou, Y.P., Fang, Y., Yang, H. and Gong, Q.H. (2004). “Laser micro-hole drilling of soda-lime glass with femtosecond pulses”. *Chinese Physics Letters*. Vol. 21, no. 12, pp. 2465-8.

Andreev, A.A., Platonov, K.Yu., Okada, T. and Toraya, S. (2003). “Nonlinear absorption of a short intense laser pulse in a nonuniform plasma”. *Physics of Plasmas*. Vol. 10, no. 1, pp. 220-226.

Antoun, T., Seaman, L., Curran, D.R., Kanel, G.I., Razorenov, S.V. and Utkin, A.V. (2002). “Spall fracture”. *Ed. Springer*, ISBN 0-387-95500-3.

Anthony, T.R. and Cline, H.E. (1977). “Surface rippling induced by surface tension gradient during laser surface melting and alloying”. *Journal of Applied Physics*. Vol. 48, no. 9, pp. 3888-3894.

Ashkenasi, D., Lorenz, M., Stoian, R. and Rosenfeld, A. (1999). “Surface damage threshold and structuring of dielectrics using femtosecond laser pulses: the role of incubation”. *Applied Surface Science*. Vol. 150, no. 1, pp. 101-106.

Banks, P.S, Stuart, B.C., Perry, M.D., Feit, M.D., Rubenchik, A.M., Armstrong, J.P., Nguyen, H., Roeske, F., Lee, R.S., Myers, B.R. and Sefcik, J.A. (1998). “Femtosecond laser machining”. *Technical Digest. Summaries of Papers Presented at the Conference on Lasers and Electro-Optics. Conference Edition. 1998 Technical Digest Series*. Vol. 6, no.98CH36178, pp. 510.

Baudach, S., Bonse, J. and Kautek, W. (1999). “Ablation experiments on polyimide with femtosecond laser pulses”. *Applied Physics A (Materials Science Processing)*. Vol. A69, suppl., pp. 395-8.

Baudach, S., Kruger, J. and Kautek, W. (2001). “Femtosecond laser processing of soft materials”. *Review of Laser Engineering*. Vol. 29, no. 11, pp. 705-9.

Bellouard, Y. and Madani, G. (2010). “Femtosecond laser micromachining of fused silica molds”. *Optics Express*. Vol. 18, no. 21, pp. 21826-21840.

Bercegol, H., Lamaignère, L., Le Garrec, B., Loiseau, M. and Volto, P. (2003). “Self-focusing and rear surface damage in a fused silica window at 1064 nm and 355 nm”. *Proceedings of SPIE - The International Society for Optical Engineering*. Vol. 4932, pp. 276-285.

Bernath, R., Brown, C.G., Aspiotis, J., Fisher, M. and Richardson, M. (2006). “Shock-wave generation in transparent media from ultra-fast lasers”. *Proceedings of the SPIE - The International Society for Optical Engineering*. Vol. 6219, no. 1, pp. 62190A-1-5.

Bilger, H.R. and Habib, T. (1985). "Knife-edge scanning of an astigmatic Gaussian beam". *Applied Optics*. Vol. 24, no. 5, pp. 686-690.

Birnbaum, M. (1965). "Semiconductor surface damage produced by ruby lasers". *Journal of Applied Physics*. Vol. 36, no. 11, pp. 3688-3689.

Bitter, J. G. A. (1953). "A study of erosion phenomena Part I". *Wear*. Vol.6, pp.5-21.

Blamires, N.G. and Totterdell, D.H.J. (1983). "Orientation dependent surface damage observed in laser irradiated cadmium telluride". *Journal of Physics D (Applied Physics)*. Vol. 16, no. 12, pp. 2361-5.

Bohme, R.,Vass, C., Hopp, B. and Zimmer, K. (2008). "Sub-wavelength ripples in fused silica after irradiation of the solid/liquid interface with ultrashort laser pulses". *Nanotechnology*. Vol. 19, no. 49, pp. 495301 (6 pp).

Bonse, J., Baudach, S., Kruger, J., Kautek, W. and Lenzner, M. (2002). "Femtosecond laser ablation of silicon-modification thresholds and morphology". *Applied Physics A (Materials Science Processing)*. Vol. A74, no. 1, pp. 19-25.

Bonse, J., Brzezinka, K.W. and Meixner, A.J. (2004). "Modifying single-crystalline silicon by femtosecond laser pulses: an analysis by micro Raman spectroscopy, scanning laser microscopy and atomic force microscopy". *Applied Surface Science*. Vol. 221, no. 1-4, pp. 215-30.

Bonse, J., Rosenfeld, A. and Krüger, J. (2009). "On the role of surface plasmon polaritons in the formation of laser-induced periodic surface structures upon irradiation of silicon by femtosecond-laser pulses". *Journal of Applied Physics*. Vol. 106, no. 10, p 104910 (5 pp).

Bonse, J., Rudolph, P., Kruger, J., Baudach, S. and Kautek, W. (2000). "Femtosecond pulse laser processing of TiN on silicon". *Applied Surface Science*. Vol. 154-155, pp. 659-63.

Bonse, J., Wiggins, S.M. and Solis, J. (2004). “Dynamics of femtosecond laser-induced melting and amorphization of indium phosphide”. *Journal of Applied Physics*. Vol. 96, no. 4, pp. 2352-8.

Bonse, J., Wrobel, J.M., Kruger, J. and Kautek, W. (2001). “Ultrashort-pulse laser ablation of indium phosphide in air.” *Applied Physics A (Materials Science Processing)*. Vol. A72, no. 1, pp. 89-94.

Bonse, J., Munz, M. and Sturm, H. (2005). “Structure formation on the surface of indium phosphide irradiated by femtosecond laser pulses”. *Journal of Applied Physics*. Vol. 97, no. 1, pp. 13538-1-9.

Brodeur, A. and Chin, S.L. (1998). “Band-gap dependence of the ultrafast white-light continuum”. *Physical Review Letters*. Vol. 80, no. 20, pp. 4406-4409.

Borowiec, A. and Haugen, H.K. (2003). “Subwavelength ripple formation on the surfaces of compound semiconductors irradiated with femtosecond laser pulses”. *Applied Physics Letters*. Vol. 82, no. 25, pp. 4462-4.

Borowiec, A. and Haugen, H.K. (2004). “Femtosecond laser micromachining of grooves in indium phosphide.” *Applied Physics A (Materials Science Processing)*. Vol. A79, no. 3, pp. 521-529.

Brodeur, A. and Chin, S.L. (1998). “Band-gap dependence of the ultrafast white-light continuum”. *Physical Review Letters*. Vol. 80, no. 20, pp. 4406-9.

Brugger, J., Berenschot, J.W., Kuiper, S., Nijdam, W., Otter, B. and Elwenspoek, M. (2000). “Resistless patterning of sub-micron structures by evaporation through nanostencils”. *Microelectronic Engineering*. Vol. 53, no. 1-4, pp. 403-5

Budiman, M., Hsu, E.M., Haugen, H.K. and Botton, G.A. (2010). “Cross-sectional study of femtosecond laser bulk modification of crystalline α-quartz”. *Applied Physics A: Materials Science and Processing*. Vol. 98, no. 4, pp. 849-853.

Cai, W. and Piestun, R. (2007). “Low pulse-energy micromachining in bulk glass with a short-cavity femtosecond oscillator”. *Optical Engineering*. Vol. 46, no. 12, pp. 124301-1-5

Callister, W.J. (2000). "Materials Science and Engineering - An Introduction”. *John Wiley and Sons Inc*., New York, (5th ed.)

Campbell, E.E.B., Ashkenasi, D. and Rosenfeld, A. (1999). “Ultra-short-pulse laser irradiation and ablation of dielectrics”. *Materials Science Forum*. Vol. 301, pp. 123-44.

Campbell, S., Dear, F.C., Hand, D.P. and Reid, D.T. (2005). “Single-pulse femtosecond laser machining of glass”. *Journal of Optics A: Pure and Applied Optics*. Vol. 7, no. 4, pp. 162-168.

Carr, C.W., Feit, M.D., Rubenchik, A.M., De Mange, P., Kucheyev, S.O., Shirk, M.D., Radousky, H.B. and Demos, S.G. (2005). “Radiation produced by femtosecond laser-plasma interaction during dielectric breakdown”. *Optics Letters*. Vol. 30, no. 6, pp. 661-663.

Carter, G. (1997). "Theory of ripple topography inhibition in depth profiling with sample rocking". *Applied Physics Letters*. Vol. 71, no.21, pp. 3066-3068.

Carter, G. (2001). “The physics and applications of ion beam erosion”. *Journal of Physics D (Applied Physics)*. Vol. 34, no. 3, pp. R1-22.

Cerny, R., Chab, V., Ivlev, G., Gatskevich, E. and Prikryl, P. (1999). “Modeling the phase-change processes in pulsed laser-irradiated InSb”. *Physical Review B (Condensed Matter)*. Vol. 59, no. 16, pp. 10685-90.

Chen, C.S, Liu, A.H, Sun, G., He, J.L., Wei, X.Q., Liu, M., Zhang, Z.G. and Man, B.Y. (2006). “Analysis of laser damage threshold and morphological changes at the surface of a HgCdTe crystal”. *Journal of Optics A: Pure and Applied Optics*. Vol. 8, no. 1, pp. 88-92.

Chen, X.Y., Lu, Y.F., Cho, B.J., Zeng, Y.P., Zeng, J.N. and Wu, Y.H. (2002). "Pattern-induced ripple structures at silicon-oxide/silicon interface by excimer laser irradiation". *Applied Physics Letters*. Vol. 81, no. 7, pp. 1344-6.

Cheng, C.W., Shen, W.C., Lin, C.Y., Lee, Y.J., Chen, J.S. (2010). "Fabrication of micro/nano crystalline ITO structures by femtosecond laser pulses". *Applied Physics A: Materials Science & Processing*. Vol. 101, no. 2, pp. 243-8.

Cheng, G.G., White, J.D., Qing, L., Wang, Y.S., Zhao, W. and Chen, G.F. (2003). "Microstructure on surface of $LiNbO_3$:Fe induced by a single ultra-short laser pulse". *Chinese Physics Letters*. Vol. 20, no. 8, pp. 1283-5.

Chichkov, B.N., Momma, C., Nolte, S., Alvensleben, F. and Tunnermann, A. (1996). "Femtosecond, picosecond and nanosecond laser ablation of solids". *Appied. Physics A*. Vol. 63, pp. 109-115.

Chiwon, M., Kanehira, S., Nishi, M., Miura, K., Nakaya, T., Tochigi, E., Shibata, N., Ikuhara, Y. and Hirao, K. (2009). "Crack Propagation in a Ruby Single Crystal by Femtosecond Laser Irradiation". *Journal of the American Ceramic Society*. Vol. 92, no. 12, pp. 3118-21.

Choi, T.Y., Hwang, D.J. and Grigoropoulos, C.P. (2003). "Ultrafast laser-induced crystallization of amorphous silicon films". *Optical Engineering*. Vol. 42, no. 11, pp. 3383-8.

Christov, I.P., Kapteyn, H.C., Murnane, M.M., Huang, C.P. and Zhou, J. (1995). "Space-time focusing of femtosecond pulses in a Ti:sapphire laser".*Optics Letters*. Vol. 20, pp. 309-311.

Corkum, P.B., Rolland, C., Srinivasan-Rao, T. (1986). "Supercontinuum generation in gases". *Physical Review Letters*. Vol. 57, no. 18, pp. 2268-71.

Costa, L., Terekhov, A., Rajput, D., Hofmeister, W., Jowhar, D., Wright, G. and Janetopoulos, C. (2011). "Femtosecond laser machined microfluidic devices for imaging of cells during chemotaxis". *Journal of Laser Applications*. Vol. 23, no. 4, pp. 042001 (5 pp.).

Costache, F., Henyk, M. and Reif, J. (2003). "Surface patterning on insulators upon femtosecond laser ablation". *Applied Surface Science*. Vol. 208-209, no.1, pp. 486-491.

Couillard, M., Borowiec, A., Haugen, H.K., Preston, J.S., Griswold, E.M. and Botton, G.A. (2007). "Subsurface modifications in indium phosphide induced by single and multiple femtosecond laser pulses: A study on the formation of periodic ripples". *Journal of Applied Physics*. Vol. 101, no. 3, pp. 33519-1-8.

Craig, B. (1998). "Ultrafast pulses promise better processing of fine structures". *Laser Focus World*. Pp. 79-88.

Crawford, T.H.R., Borowiec, A., and Haugen, H.K. (2003). "Femtosecond laser micromachined grooves cut in silicon with 400 nm and 800 nm pulses". *OSA Trends in Optics and Photonics Series*. Vol. 88, pp. 1969-1971.

Daguano, J.K.M.F., Strecker, K., Ziemath, E.C., Rogero, S.O., Fernandes, M.H.V. and Santos, C. (2012). "Effect of partial crystallization on the mechanical properties and cytotoxicity of bioactive glass from the 3CaO.P2O5-SiO2-MgO system". *Journal of the Mechanical Behavior of Biomedical Materials*. Vol. 14, pp. 78-88.

Das, D.K. and Pollock, T.M. (2009). "Femtosecond laser machining of cooling holes in thermal barrier coated CMSX4 superalloy". *Journal of Materials Processing Technology*. Vol. 209, no. 15-16, pp. 5661-8.

Demchuk, A.V. and Labunov, V.A. (1995). "Surface morphology and structure modification of silicon layers indused by nanosecond laser irradiation". *Applied Surface Science*. Vol. 86, pp. 353-8.

Demos, S.G., Kozlowski, M.R., Staggs, M., Chase, L.L., Burnham, A. and Radousky, H.B. (2001). “Mechanisms to explain damage growth in optical materials”. *Proceedings of SPIE - The International Society for Optical Engineering*. Vol. 4347, pp. 277-284.

Deng, J. and Lee, T. (2002). “Ultrasonic machining of alumina-based ceramic composites”. *Journal of the European Ceramic Society*. Vil. 22, no. 8, pp. 1235-1241.

Deshpande, D.C., Malshe, A.P., Stach, E.A., Radmilovic, V., Alexander, D., Doerr, D. and Hirt, D. (2005). “Investigation of femtosecond laser assisted nano and microscale modifications in lithium niobate”. *Journal of Applied Physics*. Vol. 97, no. 7, pp. 74316-1-9.

Dong, Y. and Molian, P. (2004). “Coulomb explosion-induced formation of highly oriented nanoparticles on thin films of 3C-SiC by the femtosecond pulsed laser”. *Applied Physics Letters*. Vol. 84, no. 1, pp. 10-12.

Doremus, R. H. (1994). “Glass science”. *John Wiley and Sons Inc*., New York, 2nd ed.

Duan, J., Man, H.C. and Yue, T.M. (2001). “Modelling the laser fusion cutting process: III. Effects of various process parameters on cut kerf quality”. *Journal of Physics D (Applied Physics)*. Vol. 34, no. 14, pp. 2143-50.

Dufft, D., Rosenfeld, A., Das, S.K., Grunwald, R. and Bonse, J. (2009). “Femtosecond laser-induced periodic surface structures revisited: A comparative study on ZnO”. *Journal of Applied Physics*. Vol. 105, no. 3, pp. 034908 (9 pp).

Emel'yanov, V.I., Konov, V.I., Tokarev, V.N. and Seminogov, V.N. (1989). “Formation of periodic surface ripples under the action of pulsed carbon dioxide radiation on fused silica”. *Journal of the Optical Society of America B (Optical Physics)*. Vol. 6, no. 1, pp. 104-14.

Emmony, D.C., Howson, R.P. and Willis, L.J. (1973). “Laser mirror damage in germanium at 10.6 μm”. *Applied Physics Letters*. Vol. 23, no. 11, pp. 598-600.

Engels, P. J. (1978). “Impact wear of materials”. *Finnie, Elsevier*. Chapter 4.

Fabbro, R., Fournier, J., Ballard, P., Devaux, D. and Virmont, J. (1990). **“**Physical study of laser-produced plasma in confined geometry”. *Journal of Applied Physics*. Vol. 68, no. 2, pp. 775-84.

Ferna´ndez-Pradas, J.M., Serrano, D., Morenza, J.L. and Serra, P. (2011). “Microchannel formation through Foturan® with infrared femtosecond and ultraviolet nanosecond lasers”. *Journal of Micromechanics and Microengineering*. Vol. 21, no. 2, pp. 025005 (8 pp).

Finlay, C and Frank, G. (2009). “Laser cutting strengthens thin-film glass panel”. *Global Photovoltaic Business Magazine, INTER PV*. Pp. 66-68.

Firester, A.H., Heller, M.E. and Sheng, P. (1977) “Knife-edge scanning measurements of subwavelength focused light beams”. *Applied Optics*. Vol. 16, no. 7, pp. 1971-1974.

Fork, R.L., Shank, C.V., Hirlimann, C., Yen, R. and Tomlinson, W.J. (1983). “Femtosecond white-light continuum pulses”. *Optics Letters*. Vol. 8, no. 1, pp. 1-3.

Fork, R.L., Martinez, O.E. and Gordon, J.P. (1984). “Negative dispersion using pairs of prisms”. *Optics Letters*. Vol. 9, pp. 150-152.

Gamaly, E.G., Rode, A.V., Luther-Davies, B. and Tikhonchuk, V.T. (2002). “Ablation of solids by femtosecond lasers: Ablation mechanism and ablation thresholds for metals and dielectrics”. *Physics of Plasmas*. Vol. 9, no. 3, pp. 949-57.

Garibotti, D.J. (1963). “Dicing of micro-semiconductors”. *US Patent*. 3,112,850.

Gedvilas, M., Raciukaitis, G. and Regelskis, K. (2008). “Self-organization in a chromium thin film under laser irradiation”. *Applied Physics A: Materials Science and Processing*. Vol. 93, no. 1, pp. 203-208.

Giannone, D., Kazmierczak, A., Dortu. F., Vivien, L. and Sohlstrom, H. (2010). "High performance multichannel photonic biochip sensors for future Point of Care diagnostics: An overview on two EU-sponsored projects". *Proceedings of the SPIE - The International Society for Optical Engineering.* Vol. 7715, pp. 77150U (12 pp.).

Glezer, E.N. and Mazur, E. (1997) "Ultrafast-laser driven micro-explosions in transparent materials". *Applied Physics Letters*. Vol. 71, no. 7, pp. 882-4.

Glezer, E.N., Milosavljevic, M., Hunag, L., Finlay, R.J., Her, T.H., Callan J.P. and Mazur, E. (1996). "Three-dimensional optical storage inside transparent materials". *Optics Letters*. Vol. 21, pp. 2023-2025.

Gorelik, T., Will, M., Nolte, S., Tuennermann, A. and Glatzel, U. (2003). "Transmission electron microscopy studies of femtosecond laser induced modifications in quartz". *Applied Physics A: Materials Science and Processing*. Vol. 76, no. 3, pp. 309-311.

Gottmann, J., Wortmann, D. and Horstmann-Jungemann, M. (2009). "Fabrication of sub-wavelength surface ripples and in-volume nanostructures by fs-laser induced selective etching". *Applied Surface Science*. Vol. 255, no. 10, pp. 5641-6.

Groenendijk, M.N.W. and Meijer, J. (2006). "Surface microstructures obtained by femtosecond laser pulses". *CIRP Annals - Manufacturing Technology*. Vol. 55, no. 1, pp. 183-186.

Guo, C. (2006). "Thermal effects in femtosecond laser ablation of metals". *Proceedings of the SPIE - The International Society for Optical Engineering*. Vol. 6118, pp. 611808-1-14.

Guosheng, Z., Fauchet, P.M., and Siegman, A.E. (1982). "Growth of spontaneous periodic surface structures on solids during laser illumination". *Physical Review B (Condensed Matter)*. Vol. 26, no. 10, pp. 5366-81.

Guy, S., Joubert, M.F., Jacquier, B. and Bouazaoui, M. (1993). “Excited-state absorption in $BaY_2F_8:Nd^{3+}$**”.** *Physical Review B (Condensed Matter)*. Vol. 47, no. 17, pp. 11001-6.

Han, Y., Zhao, X. and Qu, S. (2011). “Polarization dependent ripples induced by femtosecond laser on dense flint (ZF_6) glass”. *Optics Express*. Vol. 19, no. 20, pp. 19150-5.

Han, Y.H., Qu, S.L., Wang, Q.G., Zhong, Y. and Chen, X.J. (2009). “Controllable grating fabrication by three interfering replicas of single femtosecond laser pulse”. *Chinese Physics B*. Vol. 18, no. 12, pp. 5331-5335.

Hanada, Y.,Sugioka, K., Obata, K., Takase, H., Takai, H., Miyamoto, I. and Midorikawa, K. (2004).” Micromachining of transparent materials by laser-induced plasma-assisted ablation (LIPAA)”. *Proceedings of the SPIE - The International Society for Optical Engineering*. Vol. 5662, no. 1, pp. 526-31.

Harry, C. (1996). “Heat treater's guide: Practices and procedures for nonferrous alloys”. *ASM International*. Pp. 467.

Hashish, M. (1989). “A model for abrasive water jet machining”. , *Journal of Engineering. Materials and Technology*. Vol.111, pp.154

Hatano, M., Moon, S., Lee,M., Suzuki, K. and Grigoropoulos, C.P. (2000). “Excimer laser-induced temperature field in melting and resolidification of silicon thin films”. *Journal of Applied Physics*. Vol. 87, no. 1, pp. 36-43.

He, F., Sun, H., Huang, M., Xu, J., Liao, Y., Zhou, Z., Cheng, Y., Xu, Z., Sugioka, K. and Midorikawa, K. (2009). “Rapid fabrication of optical volume gratings in Foturan glass by femtosecond laser micromachining”. *Applied Physics A: Materials Science & Processing*. Vol. 97, no. 4, pp. 853-7.

He, F., Xu, H., Cheng, Y., Ni, J., Xiong, H., Xu, Z., Sugioka, K. and Midorikawa, K. (2010). “Fabrication of microfluidic channels with a circular cross section using spatiotemporally focused femtosecond laser pulses”. *Optics Letters*. Vol. 35, no. 7, pp. 1106-8.

Hermanns, C. (2000). “Laser cutting of glass”. *Proceedings of the SPIE - The International Society for Optical Engineering*. Vol. 4102, pp. 219-26.

Hirayama, Y. and Obara, M. (2002). “Heat effects of metals ablated with femtosecond laser pulses”. *Applied Surface Science*. Vol. 197-198, pp. 741-5.

Hirayama, Y. and Obara, M. (2005). “Molecular dynamics simulation of heat-affected zone of copper metal ablated with femtosecond laser”. *Proceedings of the SPIE - The International Society for Optical Engineering*. Vol. 5714, no. 1, pp. 271-82.

Hiroaki, M. and Saulius, J. (2006). “3D Laser microfabrication: Principles and Applications.” *Wiley-VCH*. Pp. 157.

Ho, C.Y., Tsai, Y.H., Chen, C.S. and Wen, M.Y. (2011). “Ablation of aluminum oxide ceramics using femtosecond laser with multiple pulses”. *Current Applied Physics*. Vol. 11, no. 3 SUPPL., pp. S301-S305.

Ho¨che, T., Ruthe,D., Frost, F. and T. Petsch. (2003). “Nanostructural investigations on ripples Prepared by femtosecond laser treatment of silicon”. *Proceedings of the ICALEO*. Pp. A33–A37.

Hoffman, C.G. (1974). “Laser- target interactions”. *Journal of Applied Physics*. Vol. 45, no. 5, pp. 2125-8.

http://en.wikipedia.org/wiki/Glass

http://www.cmxr.com

http://www.memsjournal.com

Hsu, S.T., Wang, H., Satoh, G. and Lawrence, Y.Y. (2011). “Applications of surface structuring with lasers. *30th International Congress on Applications of Lasers and Electro-Optics, ICALEO*. Pp. 1095-1104.

Hu, J., Feng, N.N., Carlie, N., Petit, L., Agarwal, A., Richardson, K. and Kimerling, L. (2010). "Optical loss reduction in high-index-contrast chalcogenide glass waveguides via thermal reflow". *Optics Express*. Vol. 18, no. 2, pp. 1469-1478.

Huang, M., Zhao, F., Cheng, Y., Xu, N. and Xu, Z. (2009). "Origin of laser-induced near-subwavelength ripples: Interference between surface plasmons and incident laser". *ACS Nano*. Vol. 3, no. 12, pp. 4062-4070.

Iga, Y., Watanabe, W., Ishizuka, T., Yan Li, Nishii, J. and Itoh, K. (2003). "Fabrication of micro-holes in silica glass by femtosecond laser pulses". *Proceedings of the SPIE - The International Society for Optical Engineering*. Vol. 5063, no. 1, pp. 129-132.

Ihlemann, J., Wolff, B. and Simon, P. (1992). "Nanosecond and femtosecond excimer laser ablation of fused silica". *Applied Physics A (Solids and Surfaces)*. Vol. A54, no. 4, pp. 363-8.

Ionita, I. and Zamfirescu, M. (2010). "Teeth material ablation by femtosecond laser". *Proceedings of the SPIE - The International Society for Optical Engineering*. Vol. 7715, pp. 77151S (11 pp.).

Ionita, I. and Zamfirescu, M. (2011). "Femtosecond laser: the finest tool for hard tissue ablation". *Proceedings of the SPIE - The International Society for Optical Engineering*. Vol. 8092, pp. 80921D (8 pp.).

Ippen, E.P. (1994). "Principles of passive mode locking". *Applied Physics B*. Vol. 58, pp.159-170.

Ito, Y., Kuroi, K. and Hayakawa, K. (2003) "Fabrication of holes and grooves on glass by a femtosecond laser". *Proceedings of the SPIE - The International Society for Optical Engineering*. Vol. 5063, no. 1, pp. 338-41.

Izawa, Y., Tokita, S., Fujita, M., Nakai, M., Norimatsu, T. and Izawa, Y. (2009). "Ultrathin amorphization of single-crystal silicon by ultraviolet femtosecond laser pulse irradiation". *Journal of Applied Physics*. Vol. 105, no. 6, pp. 064909 (4 pp.).

Jasapara, J., Nampoothiri, A.V.V., Rudolph, W., Ristau, D. and Starke, K. (2001). "Femtosecond laser pulse induced breakdown in dielectric thin films". *Physical Review B: Condensed Matter*. Vol. 63, no. 4, p 045117/1-5.

Jiang, L. and Tsai, H.L. (2006). "Plasma modeling for ultrashort pulse laser ablation of dielectrics". *Journal of Applied Physics*. Vol.100, no. 2, pp.023116 (7pg).

Jiang, L. and Tsai, H.L. (2011). "Femtosecond Lasers Ablation: Challenges and Opportunities". *Femtosecond NSF Worksshop.pdf.*

Jung, J.K, Park, Y.J., Hwang, N.M. and Joo, Y.C. (2001). "Tertiary grain growth driven by surface energy". *Scripta Materialia*. Vol. 45, no. 3, pp. 267-72.

Kam, D.H., Shah, L. and Mazumder, J. (2011). "Femtosecond laser machining of multi-depth microchannel networks onto silicon". *Journal of Micromechanics and Microengineering*. Vol. 21, no. 4, pp. 045027 (8 pp.).

Kamata, M. and Obara, M. (2004). "Control of the refractive index change in fused silica glasses induced by a loosely focused femtosecond laser". *Applied Physics A (Materials Science Processing)*. Vol. A78, no. 1, pp. 85-8.

Kanemitsu, Y., Kuroda, H. and Shionoya, S. (1984). "Formation of periodic ripple structures in picosecond pulsed laser annealing of ion-implanted silicon". *Japanese Journal of Applied Physics, Part 1 (Regular Papers & Short Notes)*. Vol. 23, no. 8, pp. 1060-4.

Kasaai, M.R., Kacham, V., Theberge, F. and Chin, S.L. (2003). "The interaction of femtosecond and nanosecond laser pulses with the surface of glass**".** *Journal of Non-Crystalline Solids*. Vol. 319, no. 1-2, pp. 129-135.

Kasaai, M.R., Lagace, S., Boudreau, D., Forster, E., Muller, B. and Chin, S.L. (2001). "Creation of micro-holes on glass surface by femtosecond laser through the ejection of molten material". *Journal of Non-Crystalline Solids*. Vol. 292, no. 1-3, pp. 202-9.

Kawahara, K., Kurogi, Y., Matsuo, N., Sawada, H., Yokotani, A. and Kurosawa, K. (2002). "Morphological characterization of various kinds of materials in femtosecond laser micromachining". *Proceedings of the SPIE - The International Society for Optical Engineering*. Vol. 4426, pp 86-89.

Kestenbaum, A., D'Amico, J.F., Blumenstock, B.J. and DeAngelo, M.A. (1990). "Laser drilling of microvias in epoxy-glass printed circuit boards". *IEEE Transactions on Components, Hybrids, and Manufacturing Technology*. Vol. 13, no. 4, pp. 1055-1062.

Kim, J., Na, S., Cho, S, Chang, W. and Whang, K. (2008). "Surface ripple changes during Cr film ablation with a double ultrashort laser pulse". *Optics and Lasers in Engineering*. Vol. 46, no. 4, pp. 306-10.

Kondo, Y., Miura, K., Suzuki, T., Intuye, H., Mitsuyu, T. and Hirao, K. (1999). "Three-dimensional arrays of crystallites within glass by using non-resonant femtosecond pulses". *Journal of Non-Crystalline Solids*. Vol. 253, pp. 143-56.

Kongsuwan, P., Satoh, G. and Yao, Y.L. (2012). "Transmission welding of glass by femtosecond laser: mechanism and fracture strength". *Journal of Manufacturing Science and Engineering.* Vol. 134, no. 1, p. 011004 (11 pp).

Konishi, M, Santo, H., Hongo, Y., Tajima, K., Hosoi, M. and Saiki, T. (2010). "Ultrafast amorphization in $Ge_{10}Sb_2Te_{13}$ thin film induced by single femtosecond laser pulse". *Applied Optics*. Vol. 49, no. 18, pp. 3470-3.

Kononenko, T.V., Meier, M., Komlenok, M.S., Pimenov, S.M., Romano, V., Pashinin, V.P. and Konov, V.I. (2008). "Microstructuring of diamond bulk by IR femtosecond laser pulses". *Applied Physics A: Materials Science Processing*. Vol. 90, no. 4, pp. 645-51.

Koubassov, V., Laprise, J.F, Theberge, F., Forster, E., Sauerbrey, R., Muller, B., Glatzel, U. and Chin, S.L. (2004). "Ultrafast laser-induced melting of glass". *Applied Physics A: Materials Science and Processing*. Vol. 79, no. 3, pp. 499-505.

Krüger, J., Kautek, W., Lenzner, M., Sartania, S., Spielmann, C. and Krausz, F. (1997). "Structuring of dielectric and metallic materials with ultrashort laser pulses between 20 fs and 3 ps". *Proceedings of SPIE - The International Society for Optical Engineering*. Vol. 2991, pp. 40-47.

Kuriyama, N. and Ito, Y. (2003). "Micro-hole drilling on glass plates by femtosecond laser pulses". *Proceedings of the SPIE - The International Society for Optical Engineering*. Vol. 4830, pp. 567-72.

Ladieu, F., Martin, P. and Guizard, S. (2002). "Measuring thermal effects in femtosecond laser-induced breakdown of dielectrics". *Applied Physics Letters*. Vol. 81, no. 6, pp. 957-9.

Lai, H.Y., Huang, P.H. and Fang, T.H. (2007). "Microscopic spallation mechanisms induced by a pulse laser at the solid-state interface". *Applied Physics A: Materials Science and Processing*. Vol. 86, no. 4, pp. 497-503.

Lam, Y.C., Tran, D.V., Zheng, H.Y., Murukeshan, V.M., Chai, J.C. and Hardt, D.E. (2005). "Femtosecond laser-induced damage morphologies of crystalline silicon by sub-threshold pulses". *Optics and Lasers in Engineering*. Vol. 43, no. 9, pp. 977-986.

Lambert, E., Lambert, J.L. and Longueville, B.D. (1976). "Severing of glass or vitrocrystalline bodies". *US Patent*. 3,935,419.

Lan, B., Hong, M.H., Ye, K.D.,Wang, Z.B. and Chong, T.C. (2003). "Laser microfabrication of glass substrates by pocket scanning". *Proceedings of the SPIE - The International Society for Optical Engineering*. Vol. 5063, no. 1, pp. 133-6.

Ladieu, F., Martin, P. and Guizard, S. (2002). "Measuring thermal effects in femtosecond laser-induced breakdown of dielectrics". *Applied Physics Letters*. Vol. 81, no 6, pp. 957-959

Lane, D.W. (1990). “The optical properties and laser irradiation of some common glasses”. *Journal of Physics D (Applied Physics)*. Vol. 23, no. 12, pp. 1727-34.

Le Harzic, R., Huot, N., Audouard, E., Jonin, C., Laporte, P., Valette, S., Fraczkiewicz, A. and Fortunier, R. (2002). “Comparison of heat-affected zones due to nanosecond and femtosecond laser pulses using transmission electronic microscopy”. *Applied Physics Letters*. Vol. 80, no. 21, pp. 3886-8.

Lee, D. and Jeong, S.H. (2004). “Analysis of recoil force during Nd : YAG laser ablation of silicon”. *Applied Physics A (Materials Science Processing)*. Vol. A79, no. 4-6, pp. 1341-4.

Lee, Y.S and Kang, W.H. (2001). “Laser micro-machining and applications of glasses in optoelectronics”. *Advances in Electronic Materials and Packaging.* (Cat. No.01EX506), pp. 93-5.

Lenzner, M., Kruger, J., Kautek, W. and Krausz, F. (1999). “Precision laser ablation of dielectrics in the 10-fs regime”. *Applied Physics A (Materials Science Processing)*. Vol. 68, no. 3, pp. 369-71.

Lenzner, M., Kruger, L.J., Sartania, S., Cheng, Z., Spielmann, C., Mourou, L.G, Kautek, W. and Krausz, F. (1998). “Femtosecond optical breakdown in dielectrics”. *Physical Review Letters*. Vol. 80, no. 18, pp. 4076-9.

Levchenko, I., Kumar, S., Yajadda, M.M.A., Han, Z.J., Furman, S. and Ostrikov, K. (2011). “Self-organization in arrays of surface-grown nanoparticles: characterization, control, driving forces” *Journal of Physics D, Applied Physics*. Vol. 44, no. 17, pp 174020-174028.

Li, Y., Liu, D., Qi, F., Yang, H. and Gong, Q. (2007). “Femtosecond laser micromachining and microfabrication in transparent materials”. *Proceedings of the SPIE - The International Society for Optical Engineering*. Vol. 6825, pp. 68250K-1-10.

Liu, H.T. (2010). "Waterjet technology for machining fine features pertaining to micromachining". *Journal of Manufacturing Processes*. Vol. 12, no. 1, pp. 8-18.

Liu, J.M. (1982). "Simple technique for measurements of pulsed Gaussian-beam spot sizes." *Optics Letters*. Vol. 7, no. 5, pp. 196-198.

Liu, W.D., Ye, L.M. and Liu, K.X. (2011). "Micro-nano scale ripples on metallic glass induced by laser pulse". *Journal of Applied Physics*. Vol. 109, no. 4, pp. 043109 (5 pp.).

Liu, X., Du, D. and Mourou, G. (1997). "Laser ablation and micromachining with ultrashort laser pulses". *IEEE Journal of Quantum Electronics*. Vol. 33, no. 10, pp. 1706-16.

Loreti, S., Sala, D.D. and Garozzo, M. (2000). "Morphological and structural effects of excimer laser treatment of amorphous silicon". *Micron*. Vol. 31, pp. 299-307.

Low, D.K., Xie, H., Xiong, Z. and Lim, G.C. (2005). "Femtosecond laser direct writing of embedded optical waveguides in aluminosilicate glass". *Applied Physics A: Materials Science and Processing*. Vol. 81, no. 8, pp. 1633-1638.

Luo, L., Wang, D., Li, C., Jiang, H., Yang, H and Gong, Q. (2002). "Formation of diverse form microstructures in wide-bandgap materials by tight-focusing femtosecond laser pulses". *Journal of Optics A: Pure and Applied Optics*. Vol. 4, no. 1, pp. 105-10.

Lumley, R.M. (1969). "Controlled separation of brittle materials using a laser". *American Ceramic Society Bulletin*. Vol.48, no.9, pp. 850–854.

Ma, L., Shi, S., Cheng, G., Zhao, W. and Chen, G. (2006). "Precise processing of transparent material with femtosecond laser pulses". *Proceedings of the SPIE - The International Society for Optical Engineering*. Vol. 6149, pp. 614935-1-6.

Mak, G.Y., Lam, E.Y. and Choi, H.W. (2011). “Liquid-immersion laser micromachining of GaN grown on sapphire”. *Applied Physics A: Materials Science & Processing*. Vol. 102, no. 2, pp. 441-7.

Malek, C.K., Robert, L., Boy, J.J. and Blind, P. (2007). “Deep microstructuring in glass for microfluidic applications”. *Microsystem Technologies*. Vol. 13, no. 5-6, pp. 447-53.

Malshe, A. and Deshpande, D. (2004). “Nano and microscale surface and sub-surface modifications induced in optical materials by femtosecond laser machining”. *Journal of Materials Processing Technology*. Vol. 149, no. 1-3, pp. 585-90.

Matsuo, S., Tabuchi, Y., Okada, T., Juodkazis, S. and Misawa, H. (2006). “Femtosecond laser assisted etching of quartz: microstructuring from inside”. *Applied Physics A: Materials Science and Processing*. Vol. 84, no. 1-2, pp. 99-102.

Matthew S.A. (2001). “The back-end process: Step 11 - Scribe and break”. *Advance Packaging Article*.

Mazur, E., Maxwell, I. and Chung, S. “Nanoprocessing of subcellular targets using femtosecond laser pulses”. (2005). *Medical Laser Application*. Vol. 20, no. 3, pp. 193-200.

McLellan G. W. and Shand, E. B. (1984). “Glass Engineering Handbook”. *McGraw-Hill*, Inc., 3rd ed.

Mingareev, I., Horn, A. and Kreutz, E.W. (2006). “Observation of melt ejection in metals up to 1 μs after femtosecond laser irradiation by a novel pump-probe photography setup”. *Proceedings of the SPIE - The International Society for Optical Engineering*. Vol. 6261, pp. 62610A-1-8.

Mizeikis, V., Kimura, S., Surovtsev, N.V., Jarutis, V., Saito, A., Misawa, H. and Juodkazis, (2009). “Formation of amorphous sapphire by a femtosecond laser pulse induced micro-explosion”. *Applied Surface Science*. Vol. 255, no. 24, pp. 9745-9.

Momma, C., Chichkov, B.N., Nolte, S., Alvensleben, F., Tunnermann, A., Welling, H. and Wellegehausen, B. (1996). “Short-pulse laser ablation of solid targets”. *Optics Communications*. Vol. 129, no. 1-2, pp. 134-42.

Mongeot, F.B.D., Costantini, G., Boragno, C. and Valbusa, U. (2000). "Ripple rotation in multilayer homoepitaxy". *Physical Review Letters*. Vol. 84, no. 11, pp. 2445-2448.

Moon, C., Kanehira, S., Nishi, M., Miura, K., Nakaya, T., Tochigi, E., Shibata, N., Ikuhara, Y. and Hirao, K. (2009). “Crack propagation in a ruby single crystal by femtosecond laser irradiation”. *Journal of the American Ceramic Society*. Vol. 92, no 12, pp. 3118-3121.

Morou, G. (1997). “The ultrahigh-peak-power laser: present and future”. *Applied Physic B*. Vol. 65, pp. 205-211.

Nath, C., Lim, G.C. and Zheng, H.Y. (2012). “Influence of the material removal mechanisms on hole integrity in ultrasonic machining of structural ceramics”. *Ultrasonics*. Vol. 52, no. 5, pp. 605-613.

Nayak, B.K. and Gupta, M.C. (2010). “Ultrafast laser-induced self-organized conical micro/nano surface structures and their origin”. *Optics and Lasers in Engineering*. Vol. 48, no. 10, pp. 966-73.

Nikumb, S., Li, C. and Wong, F. (2006). “An optimal process of femtosecond laser cutting of NiTi shape memory alloy for fabrication of miniature devices”. *Optics and Lasers in Engineering*. Vol. 44, no. 10, pp. 1078-87.

Niziev, V.G. and Nesterov, A.V. (1999). “Influence of beam polarization on laser cutting efficiency”. *Journal of Physics D (Applied Physics)*. Vol. 32, no. 13, pp. 1455-61.

Nolte, S., Momma, C., Kamlage, G., Ostendorf, A., Fallnich, C., Von Alvensleben, F. and Welling, H. (1999). “Polarization effects in ultrashort-pulse laser drilling”. *Applied Physics A: Materials Science and Processing*. Vol. 68, no. 5, p 563-567.

Olsen, F.O. (1982). “Studies of sheet metal cutting with planepolarised CO2 laser”. *Proceedings of the Fifth Annual Congress of Opto-Electronics in Engineering (Laser-81)*. Pp. 227–231.

Ostendorf, A., Kulik, C. and Barsch B. (2003). “Processing thin silicon with ultrashort-pulse lasers: creating an alternative to conventional sawing techniques”. *Proceedings of the ICALEO*. Pp. A20–A28.

Ozkan, A.M. and Migliore, L. (2003). “Glass processing using femtosecond and nanosecond pulsed lasers”. *Proceedings of the SPIE - The International Society for Optical Engineering*. Vol. 4978, no. 1, pp. 162-8.

Pattathil, R.P., Hnatovsky, C., Vedula, R.B., Simova, E., Taylor, R.S., Rayner, D.M. and Corkum, P.B. (2005). “Femtosecond laser-induced nanostructures in fused silica”. *Proceedings of the SPIE - The International Society for Optical Engineering*. Vol. 5971, no. 1, pp. 59711D-1-10.

Peng, Y., An, C., Hong, M., Lu, Y. and Chong, T. (2003). “CO_2-laser-induced regular periodic structures on glass substrates”. *Japanese Journal of Applied Physics, Part 1 (Regular Papers, Short Notes & Review Papers)*. Vol. 42, no. 11, pp. 6920-5.

Perez, D. and Lewis, L.J. (2003). “Molecular-dynamics study of ablation of solids under femtosecond laser pulses”. *Physical Review B (Condensed Matter and Materials Physics)*. Vol. 67, no. 18, pp. 184102-1-15.

Perry, M.D., Stuart, B.C., Banks, P.S., Feit, M.D., Yanovsky, V. and Rubenchik, A.M. (1999). “Ultrashort-pulse laser machining of dielectric materials”. *Journal of Applied Physics*. Vol. 85, no. 9, pp. 6803-10.

Pratap Singh, A., Kapoor, A. and Tripathi, K.N. (2003). “Recrystallization of germanium surfaces by femtosecond laser pulses”. *Optics and Laser Technology*. Vol. 35, no. 2, pp. 87-97.

Pronko, P.P., Dutta, S.K., Squier, J., Rudd, J.V. and Mourou, G. (1995). "Machining of sub-micron holes using a femtosecond laser at 800 nm". *Optics Communications*. Vol. 114, no. 1-2, pp. 106-10.

Pronko, P.P.,Van Rompay, P.A., Horvath, C., Liu, X., Juhasz, T. and Mourou, G. (1998). "Avalanche ionization and dielectric breakdown in silicon with ultrafast laser pulses". *Physical Review B (Condensed Matter)*. Vol.58, no. 5, pp. 2387-90.

Qi, L., Nishii, K., Yasui, M., Aoki, H. and Namba Y. (2010). "Femtosecond laser ablation of sapphire on different crystallographic facet planes by single and multiple laser pulses irradiation". *Optics and Lasers in Engineering*. Vol. 48, no. 10, pp. 1000-7.

Qian, H.X, Zhou, W. and Zheng, H.Y. (2005). "Ripple formation on InP surface irradiated with femtosecond laser". *International Journal of Nanoscience*. Vol. 4, no. 4, pp. 779-784.

Qiu, J., Miura, K., and Hirao, K. (2004). "Fabrication of micro-optical components by using a femtosecond laser". *Proceedings of SPIE - The International Society for Optical Engineering, Optical Component and Materials*. Vol. 5350, pp. 1-12.

Qiu, J., Miura, K. and Hirao, K. (2008). "Femtosecond laser-induced microfeatures in glasses and their applications". *Journal of Non-Crystalline Solids*. Vol. 354, no. 12-13, pp. 1100-1111.

Quere, F., Guizard, S. and Martin, Ph. (2001). "Time-resolved study of laser-induced breakdown in dielectrics". *Europhysics Letters*. Vol. 56, no. 1, pp. 138-44.

Rayner, D.M., Naumov, A. and Corkum, P.B. (2005). "Ultrashort pulse non-linear optical absorption in transparent media". *Optics Express*. Vol. 13, no. 9, pp. 3208-3217.

Regelskis, K., Raciukaitis, G. and Gedvilas, M. (2007). "Ripple formation in the chromium thin film during laser ablation". *Applied Surface Science*. Vol. 253, no. 15, pp. 6584-7.

Reif, J., Costache, F., Henyk, M., and Pandelov, S.V. (2002). “Ripples revisited: Non-classical morphology at the bottom of femtosecond laser ablation craters in transparent dielectrics”. *Applied Surface Science*. Vol. 197-198, pp. 891-895.

Reif, J., Costache, F., Henyk, M. and Pandelov, S. (2002). “Surface morphology after femtosecond laser ablation of insulators”. *Proceedings of the SPIE - The International Society for Optical Engineering*. Vol. 4760, pp. 980-5.

Reif, J., Varlamova, O. and Costache, F. (2008). “Femtosecond laser induced nanostructure formation: Self-organization control parameters”. *Applied Physics A: Materials Science and Processing*. Vol. 92, no. 4, pp. 1019-1024.

Revesz, A., Ochin, P., Donnadieu, P., Simon, J.P. and Guyot, P. (2001). “Nanocrystallization in a $Zr_{57}Ti_5Cu_{20}Al_{10}Ni_8$ bulk metallic glass”. *Philosophical Magazine Letters*. Vol. 81, no. 11, pp. 767-75.

Rodenas, A., Jaque, D., Torchia, G.A., Mendez, C., Arias, I., Roso, L., Moreno, P. and Agullo-Rueda, F. (2006). “Femtosecond laser induced micromodifications in Nd: SBN crystals: Amorphization and luminescence inhibition”. *Journal of Applied Physics*. Vol. 100, no. 11, pp. 113517-1-7.

Roeske, F., Benterou, J., Lee, R. and Roos, E. (2003). “Cutting and machining energetic materials with a femtosecond laser”. *Propellants, Explosives, Pyrotechnics*. Vol. 28, no. 2, pp. 53-57.

Rohlloff, M., Das, S.K., Ho¨hm, S., Grunwald, R., Rosenfeld, A., Kru¨ger, J. and Bonse, J. (2011). “Formation of laser-induced periodic surface structures on fused silica upon multiple cross-polarized double-femtosecond-laser-pulse irradiation sequences”. *Journal of Applied Physics*. Vol. 110, no. 1, pp. 014910 (4 pp).

Rolo, A., Coelho, J. and Pires, M. (2005). “Laser glass marking - Influence of pulse characteristics”. *Proceedings of SPIE - The International Society for Optical Engineering.* Vol. 5958, pp. 1-8.

Roso, L., San Román, J., Sola, I.J., Ruiz, C., Collados, V., Pérez, J.A., Méndez, C., De Aldana, J.R., Arias, I. and Plaja, L. (2008). “Propagation of terawatt laser pulses in the air”. *Applied Physics A: Materials Science and Processing*. Vol. 92, no. 4, pp. 865-871.

Rothenberg, J.E. (1992). “Pulse splitting during self-focusing in normally dispersive media”. *Optics Letters*. Vol. 17, no. 8, pp. 583-585.

Rothschild, M., Bloomstein, T.M., Kunz, R.R., Liberman, V., Switkes, M., Palmacci, S.T., Sedlacek, J.H.C., Hardy, D. and Grenville, A. (2004). “Liquid immersion lithography: Why, how, and when”. *Journal of Vacuum Science and Technology B: Microelectronics and Nanometer Structures*. Vol. 22, no. 6, pp. 2877-2881.

Roundy, C.B. (1999). “Maximizing laser beam effectiveness by beam analysis”. *Laser Physics*. Vol. 9, no. 3, pp. 692-698.

Salihoglu, O., Ku¨ru¨m, U., Gul Yaglioglu, H., Elmali, A. and Aydinli, A. (2011). “Femtosecond laser crystallization of amorphous Ge”. *Journal of Applied Physics*. Vol. 109, no. 12, pp. 123108 (6 pp.).

Schade, M., Varlamova, O., Reif, J., Blumtritt, H., Erfurth, W. and Leipner, H.S. (2010). “High-resolution investigations of ripple structures formed by femtosecond laser irradiation of silicon”. *Analytical and Bioanalytical Chemistry*. Vol. 396, no. 5, pp. 1905-1911.

Schumacher, G. and Wahi, R.P. (1998). “Surface energy driven crystallization of amorphous $Pd_{81}Si_{19}$”. *Materials Research Society Symposium – Proceedings*. Vol. 481, pp. 477-482.

Schille, J. (2010). ‘Fast, precise, and reliable 3D laser microstructuring”. *SPIE News Room*. 10.1117/2.1201011.003171.

Serna, R., Afonso, C.N., Petford-Long, A.K. and Long, N.J. (1994). “Structural ripple formation in Ge/Sb multilayers induced by laser irradiation”. *Applied Physics A (Solids and Surfaces)*. Vol. A58, no. 2, pp. 197-202.

Seydoux-Guillaume, A.M., Freydier, R., Poitrasson, F., D'Abzac, F.X., Wirth, R. and Datas, L. (2010). “Dominance of mechanical over thermally induced damage during femtosecond laser ablation of monazite”. *European Journal of Mineralogy*. Vol. 22, no. 2, pp. 235-44.

Shah, L., Tawney, J., Richardson, M. and Richardson, K. (2004). “Self-focusing during femtosecond micromachining of silicate glasses”. *IEEE Journal of Quantum Electronics*. Vol. 40, no. 1, pp. 57-68.

Shieh, J.M., Chen, Z.H., Dai, B.T., Wang, Y.C., Zaitsev, A. and Pan, C.L. (2004). “Near-infrared femtosecond laser-induced crystallization of amorphous silicon”. *Applied Physics Letters*. Vol. 85, no. 7, pp. 1232-4.

Shirk, M.D. and Molian, P.A. (1998). “Review of ultrashort pulsed laser ablation of materials”. *Journal of Laser Applications*. Vol. 10, no. 1, pp. 18-28.

Schaffer, C.B., Jamison, A.O. and Mazur, E. (2001). “Morphology of femtosecond laser-induced structural changes in bulk transparent materials”. *Applied Physics Letters*. Vol. 84, no. 9, pp 1441-1443.

Schaffer, C.B. (2001). “Interaction of femtosecond laser pulses with transparent materials”. *PHD thesis*.

See, L.C., Petit, S., Borne, F. and Miyazaki, K. (1999). “The white light supercontinuum is indeed an ultrafast white light laser”. *Japanese Journal of Applied Physics, Part 2 (Letters)*. Vol. 38, no. 2A, pp. L126-8.

Seifret, G., Kaempfe, M., Syrowatka, F., Harnagea, C., Hesse, D. and Graener, H. (2005). “Self-organized structure formation on the bottom of femtosecond laser ablation craters in glass”. *Applied Physics A (Materials Science Processing)*. Vol. A81, no. 4, pp.

Shen, Y.R. (1984). “The Principles of Nonlinear Optics”. *Wiley, Hoboken*, NJ.

Siegel, J., Puerto, D., Gawelda, W., Bachelier, G., Solis, J., Ehrentraut, L. and Bonse, J. (2007). “Plasma formation and structural modification below the visible ablation threshold in fused silica upon femtosecond laser irradiation”. *Applied Physics Letters*. Vol. 91, no. 8, pp. 082902-1-3.

Singh, A.P., Kapoor, A. and Tripathi, K.N. (2003). “Recrystallization of germanium surfaces by femtosecond laser pulses”. *Optics and Laser Technology*. Vol. 35, no. 2, pp. 87-97.

Singh, A.P., Kapoor, A., Tripathi, K.N., and Ravindra, K.G. (2002). “Laser damage studies of silicon surfaces using ultra-short laser pulses”. *Optics and Laser Technology*. Vol. 34, no. 1, pp. 37-43.

Sohn, I.B., Lee, M.S., Lee, S.M., Woo, J.S., and Jung, J.Y. (2004). “Fabrication of three-dimensional photonic devices using femtosecond laser pulses”. *Proceedings of the SPIE - The International Society for Optical Engineering*. Vol. 5715, no. 1, pp. 92-100.

Staudt, W., Borneis, S. and Pippert, K.D. (1998). “TFT annealing with excimer laser. Technology and market outlook”. *Physica Status Solidi (A) Applied Research*. Vol. 166, no. 2, pp. 743-749.

Strickland, D. and Mourou, G. (1985). “Compression of amplified chirped optical pulses”. *Optics Communication*. Vol. 56, pp. 219-221.

Stuart, B.C., Feit, M.D., Herman, S., Rubenchik, A.M., Shore, B.W. and Perry, M.D. (1996). “Nanosecond-to-femtosecond laser-induced breakdown in dielectrics”. *Physical Review B (Condensed Matter)*. Vol. 53, no. 4, pp. 1749-61.

Stuart, B.C., Perry, M.D., Feit, M.D., Da Silva, L.B., Rubenchik, A.M., Neev, J., Herman, S., Nguyen, H. and Armstrong, P. (1997). “Femtosecond laser materials processing”. *Conference Proceedings - Lasers and Electro-Optics Society Annual Meeting-LEO*. Vol. 11, p 159-160.

Sung, H.K., Ik, B.S. and Sohn, S.J. (2001). “Parallel ripple formation during femtosecond laser grooving of ceramic”. *Applied Physics A: Materials Science & Processing*. Vol. 103, no. 4, pp. 1053-7.

Tan, B. and Venkatakrishnan, K. (2006). “Femtosecond laser-induced periodical surface structure on crystalline silicon”. *Journal of Micromechanics and Microengineering*. Vol. 16, no. 5, pp. 1080-5.

Tao, S., Wu, B. and Lei, S. (2011). “Study of laser beam propagation in microholes and the effect on femtosecond laser micromachining”. *Journal of Applied Physics*. Vol. 109, no. 12, pp. 123506-123512.

Theppakuttai, S. and Chen, S. (2003). “Nanoscale surface modification of glass using a 1064 nm pulsed laser”. *Applied Physics Letters*. Vol. 83, no. 4, pp. 758-760.

Theppakuttai, S. and Chen, S. (2004). “Submicron ripples formation on glass surface upon laser-nanosphere interaction”. *Journal of Applied Physics*. Vol. 95, no. 9, pp. 5049-5052.

Thibaut, D.R., Jean-Paul, C.L., Michel, B., Emilien, L. and Laurent B. (2010). “Wave Propagation in materials for modern applications”. *Book edited by: Andrey Petrin*, ISBN 978-953-7619-65-7, pp. 526

Tnshoff, H.K., Ostendorf, A. and Wagner, T. (2001). “Structuring silicon with femtosecond lasers”. *Proceedings of the SPIE - The International Society for Optical Engineering*. Vol. 4274, pp. 88-97.

Tomita, T., Kinoshita, K., Matsuo, S. and Hashimoto, S. (2007). “Effect of surface roughening on femtosecond laser-induced ripple structures”. *Applied Physics Letters*. Vol. 90, no. 15, pp. 153115-1-3.

Tomita, T., Kumai, R., Kinoshita, K., Matsuo, S., Hashimto, S., Nagase, H., Nakajima, M. and Suemoto, T. (2009). “Femtosecond laser-induced surface patterning on 4H-SiC”. *Materials Science Forum*. Vol. 600-603, pt.2, pp. 879-82.

Treacy, E.B. (1969) "Optical pulse compression with diffraction gratings". *IEEE Journal of Quantum Electron*. QE-5, pp. 454-458.

Trebino, R. and Kane, D.J. (1993). “Using phase retrieval to measure the intensity and phase of ultrashort pulses: frequency-resolved optical gating”. *Journal of the Optical Society of America A (Optics and Image Science)*. Vol. 10, no. 5, pp. 1101-1111.

Tsai, C.H. and Chen, H.W. (2003). “Laser cutting of thick ceramic substrates by controlled fracture technique”. *Journal of Materials Processing Technology*. Vol. 136, pp. 166-73.

Tunna, L., Khan, A., O'Neill, W. and Sutcliffe, C.J. (2006). “The effect of processing wavelength and fluence on the microdrilling of 316 L stainless steel with a diode pumped solid state laser”. *Journal of Laser Applications*. Vol. 18, no. 3, pp. 205-209.

Vadillo, J.M., Fernández Romero, J.M., Rodríguez, C. and Laserna, J.J. (1999). “Effect of plasma shielding on laser ablation rate of pure metals at reduced pressure”. *Surface and Interface Analysis*. Vol. 27, no.11, pp. 1009-1015.

Vajpayee, S., Khare, K., Yang, S., Hui, C.Y. and Jagota, A. (2011). “Adhesion selectivity using rippled surfaces”. *Advanced Functional Materials*. Vol. 21, no. 3, pp. 547-555.

Valette, S., Audouard, E., Le Harzic, R., Huot, N., Laporte, P. and Fortunier, R. (2005). “Heat affected zone in aluminum single crystals submitted to femtosecond laser irradiations”. *Applied Surface Science*. Vol. 239, no. 3-4, pp. 381-386.

Van Vechten, J.A. (1981). “Experimental tests for boson condensation and superconductivity in semiconductors during pulsed beam annealing”. *Solid State Communications*. Vol. 39, no. 12, pp. 1285-91.

Vanagas, E., Kawai, J., Tuzhilin, D., Kudryashov, I., Mizuyama, A., Nakamura, K.G., Kondo, K., Shin-ya Koshihara, Takesada, M., Matsuda, K., Juodkazis, S., Jarutis, V., Matsuo, S. and Misawa, H. (2004). **“**Glass cutting by femtosecond pulsed irradiation”. *Journal of Microlithography, Microfabrication, and Microsystems*. Vol. 3, no. 2, pp. 358-63.

Varlamova, O., Costache, F., Reif, J. and Bestehorn, M. (2006). “Self-organized pattern formation upon femtosecond laser ablation by circularly polarized light”. *Applied Surface Science*. Vol. 252, no. 13, p 4702-4706.

Varlamova, O., Costache, F., Ratzke, M. and Reif, J. (2007). “Control parameters in pattern formation upon femtosecond laser ablation”. *Applied Surface Science*. Vol. 253, no. 19, pp. 7932-6.

Vazquez, R.M., Osellame, R., Cerullo, G., Laporta, P., Ramponi, R., Chiodini, N., Paleari, A. and Spinolo, G. (2005). “Fabrication of guiding structures in nanostructured tin–silicate glass ceramic by a focused femtosecond laser”. *Journal of Non-Crystalline Solids*. Vol. 351, no. 21-23, pp. 1855-9.

Venkatakrishnan, K., Tan, B., Stanley, P. and Sivakumar, N.R. (2002). “The effect of polarization on ultrashort pulsed laser ablation of thin metal films”. *Journal of Applied Physics*. Vol. 92, no. 3, pp. 1604-1607.

Venkatakrishnan, K and Tan, B. (2007). “Thin silicon wafer dicing with a dual-focused laser beam”. *Journal of Micromechanics and Microengineering*. Vol. 17, no. 12, pp. 2505-2515.

Von der Linde, D., Engers, T., Jenke, G., Agostini, P., Grillon, G., Nibbering, E., Mysyrowicz, A. and Antonetti, A. (1995). “Generation of high-order harmonics from solid surfaces by intense femtosecond laser pulses”. *Physical Review A - Atomic, Molecular, and Optical Physics*. Vol. 52, no. 1, pp. R25-R27.

Wachtman, J.B. (1969). “Mechanical and Thermal Properties of Ceramics: Proceedings”. *Goggle E-book*. Issue 303.

Wagner, R. and Gottmann, J. (2007). “Sub-wavelength ripple formation on various materials induced by tightly focused femtosecond laser radiation”. *Journal of Physics: Conference Series*. Vol. 59, no. 1, pp. 333-7.

Wagner, R., Gottmann, J., Horn, A. and Kreutz, E.K. (2006). “Subwavelength ripple formation induced by tightly focused femtosecond laser radiation”. *Applied Surface Science*. Vol. 252, no. 24, pp. 8576-9.

Wai, L.C, Averback, R.S, Cahill, D.G and Lagoutchev, A. (2008). “Dynamics of femtosecond laser-induced melting of silver”. *Physical Review B (Condensed Matter and Materials Physics)*. Vol. 78, no. 21, pp. 214107-15.

Wang, X.C., Lim, G.C., Ng, F.L, Liu, W. and Chua, S.J. (2005). “Subwavelength periodic ripple formation on GaN surface by femtosecond laser pulses”**.** *Surface Review and Letters*. Vol. 12, no. 4, pp. 651-657.

Wang, X.C., Zheng, H.Y., Chu, P.L., Tan, J.L., Teh, K.M., Liu, T., Ang, B.C.Y. and Tay, G.H. (2010). “Femtosecond laser drilling of alumina ceramic substrates”. *Applied Physics A: Materials Science & Processing*. Vol. 101, no. 2, pp. 271-8.

Wang, Z.B., Hong, M.H., Yin, L. and Chong, T.C. (2004). “Ultrafast laser processing of transparent materials”. *Proceedings of the SPIE - The International Society for Optical Engineering*. Vol. 5662, no. 1, pp. 215-20.

Watanabe, W., Onda, S., Tamaki, T. and Itoh, K. (2007). “Direct joining of glass substrates by 1 kHz femtosecond laser pulses”. *Applied Physics B (Lasers and Optics)*. Vol. B87, no. 1, pp. 85-9.

Weizman, M., Nickel, N.H., Sieber, I. and Yan, B. (2008). "Laser-induced self-organization in silicon-germanium thin films". *Journal of Applied Physics*. Vol. 103, no. 9, pp. 093536 (10 pp).

White, Y.V., Parrish, M., Li, X., Davis, L.M. and Hofmeister, W. (2008). "Femtosecond micro- and nano-machining of materials for microfluidic applications". *Proceedings of the SPIE - The International Society for Optical Engineering*. Vol. 7039, pp. 70390J (10 pp.).

Willis, L.J., and Emmony, D.C. (1975). "Laser damage in germanium". *Optics and Laser Technology*. Vol. 7, no. 5, pp. 222-228.

Witte, R., Moser, T., Liebers, R. and Holtz, R. (2007). "Laser micro-drilling with nanoseconds: Parametrical influences and results". *Proceedings of SPIE - The International Society for Optical Engineering*. Vol. 7022, pp. 702208-1-13.

Wong, K., Sascha, V. and Kresin, V.V. (2003). "Work functions, ionization potentials, and in between: scaling relations based on the image-charge model". *Physical Review B (Condensed Matter and Materials Physics)*. Vol. 67, no. 3, pp. 35406-1-9.

Wu, Z., Jiang, H., Zhang, Z., Sun, Q., Yang, H and Gong, Q. (2002). "Morphological investigation at the front and rear surfaces of fused silica processed with femtosecond laser pulses in air". *Optics Express*. Vol. 10, no. 22, pp. 1244-1249.

Xu, L., Spielmann, C., Krausz, F. and Szipocs, R. (1996). "Ultrabroad band ring oscillator for sub-10-fs pulse generation". *Optics Letters*. Vol. 21, no. 16, pp. 1259-1261.

Yakar, A., Byer, R.L., Harkin, A., Ashmore, J., Stone, H.A., Mengyan Shen and Mazur, E. (2003). "Morphology of femtosecond-laser-ablated borosilicate glass surfaces". *Applied Physics Letters*. Vol. 83, no. 15, pp. 3030-3032.

Yan, L., Itoh, K. and Watanabe, W. (2001). "Hole drilling of silica glass with infrared femtosecond laser pulses". *Technical Digest. CLEO/Pacific Rim 2001. 4th Pacific Rim Conference on Lasers and Electro-Optics (Cat. No.01TH8557)*. Vol. 1, pp. 304-305.

Yang, G. and Shen, Y.R. (1984). "Spectral broadening of ultrashort pulses in a nonlinear medium". *Optics Letters*. Vol. 9, no. 11, pp. 510-512.

Yang, W., Li, L., Yang, L., Liu, B. and Wang, Z. (2008). "Simulation and experimental research on water-jet guided laser cutting silicon wafer". *International Conference on Electronic Packaging Technology & High Density Packaging (ICEPT-HDP)*. Pp. 6.

Yang, X., Dai, N., Long, H., Lu, P., Li, W. and Jiang, F. (2010). "Experimental femtosecond laser photodisruption of rabbit sclera for minimally invasive laser sclerostomy: An in vitro study." *Optics and Lasers in Engineering*. Vol. 48, no. 7-8, pp. 806-810.

Yang, Y., Yang, J., Xue, L. and Guo, Y. (2010). "Surface patterning on periodicity of femtosecond laser-induced ripples". *Applied Physics Letters*. Vol. 97, no. 14, pp. 141101-141103.

Yang, H.F, Liu, L., Wang, Y.Q., Fang, L. and Ge, S.R. (2011). "Fabrication and mechanical measurements of micro- and nano-textured surfaces induced by laser processing". *Lasers in Engineering*. Vol. 22, no. 3-4, pp. 235-245.

Yasui, M., Aoki, H. and Miyamoto, I. (2003). "Machining of micro-through-holes on glass plate by femtosecond laser pulses". *Proceedings of the SPIE - The International Society for Optical Engineering*. Vol. 4830, pp. 585-589.

Yasumaru, N., Miyazaki, K. and Kiuchi, J. (2005). "Fluence dependence of femtosecond-laser-induced nanostructure formed on TiN and CrN". *Applied Physics A: Materials Science and Processing*. Vol. 81, no. 5, pp. 933-937.

Yokotani, A., Kurogi, Y., Matsuo, N., Sawada, H., Ninomiya, T., Kawahara, K. and Kurosawa, K. (2004). "Development of dicing technique for thin semiconductor substrate using temporally shaped femtosecond laser". *Electrical Engineering in Japan*. Vol. 149, no. 3, pp. 43-8.

Yoshida, H., Fujita, H., Nakatsuka, M., Yoshimura, M., Sasaki, T., Kamimura, T. and Yoshida, K. (2006). **“**Dependences of laser-induced bulk damage threshold and crack patterns in several nonlinear crystals on irradiation direction”. *Japanese Journal of Applied Physics, Part 1 (Regular Papers, Short Notes & Review Papers)*. Vol. 45, no. 2A, pp. 766-9.

Young, J.F., Sipe, J.E. and van Driel, H.M. (1984). “Laser-induced periodic surface structure. III. Fluence regimes, the role of feedback, and details of the induced topography in germanium”. *Physical Review B (Condensed Matter)*. Vol. 30, no. 4, pp. 2001-2005.

Yu, J.J. and Lu, Y.F. (1999). “Laser-induced ripple structures on Ni-P substrates”. *Applied Surface Science*. Vol. 148, no. 3-4, pp. 248-52.

Yuan, X., Zhu, C., Zhu,X., Zhu, G., Liu,L. and Lu, P. (2005). “Practical applications of femtosecond laser micromachining and fabrication”. *Proceedings of the SPIE - The International Society for Optical Engineering*. Vol. 5629, no. 1, pp 284-290.

Yuan, Y., Jiang, L., Li, X., Wang, C., Xiao, H., Lu, Y., and Tsai, H. (2012). “Formation mechanisms of sub-wavelength ripples during femtosecond laser pulse train processing of dielectrics”**.** *Journal of Physics D: Applied Physics*. Vol. 45, no. 17, pp. 175301 (6 pp).

Zhang, G., Gu, D., Gan, F., Jiang, X. and Chen, Q. (2005). “Femtosecond laser-induced crystallization in amorphous $Ge_2Sb_2Te_5$ films”. *Thin Solid Films*. Vol. 474, no. 1-2, pp. 169-172.

Zhao, M., Yin, G., Zhu, J.T. and Zhao, L. (2003). “Picosecond pulse laser microstructuring of silicon”. *Chinese Physics Letters*. Vol. 20, no. 10, pp. 1789-91.

Zhao, Q.Z., Malzer, S. and Wang, L.J. (2007). “Self-organized tungsten nanospikes grown on subwavelength ripples induced by femtosecond laser pulses”. *Optics Express*. Vol. 15, no. 24, pp. 15741-15746.

Zheng, H.Y., Zhou, W., Qian, H.X., Tan, T.T. and Lim, G.C. (2004). "Polarisation-independence of femtosecond laser machining of fused silica". *Applied Surface Science*. Vol.236, no. 1-4, pp. 114-19.

Zheng, H.Y., Liu, H., Wan, S., Lim, G.C., Nikumb, S. and Chen, Q. (2006). "Ultrashort pulse laser micromachined microchannels and their application in an optical switch". *International Journal of Advanced Manufacturing Technology*. Vol. 27, no. 9-10, pp. 925-929.

Zhigilei, L.V., Lin, Z.B. and Ivanov, D.S. (2009). "Atomistic modeling of short pulse laser ablation of metals: Connections between melting, spallation, and phase explosion". *Journal of Physical Chemistry C*. Vol. 113, no. 27, pp. 11892-906.

Zimmer, K., Bohme, R. and Rauschenbach, B. (2007). "Using IR laser radiation for backside etching of fused silica". *Applied Physics A (Materials Science Processing)*. Vol. A86, no. 3, pp. 409-414.

Zoubir, A., Richardson, M., Canioni, L., Brocas, A. and Sarger, L. (2005). "Optical properties of infrared femtosecond laser-modified fused silica and application to waveguide fabrication". *Journal of the Optical Society of America B: Optical Physics*. Vol. 22, no. 10, pp. 2138-2143.

Zoubir, A., Shah, L., Richardson, K. and Richardson, M. (2003). "Practical uses of femtosecond laser micro-materials processing". *Applied Physics A: Materials Science and Processing*. Vol. 77, no. 2, pp. 311-315.

Appendix

Appendix A

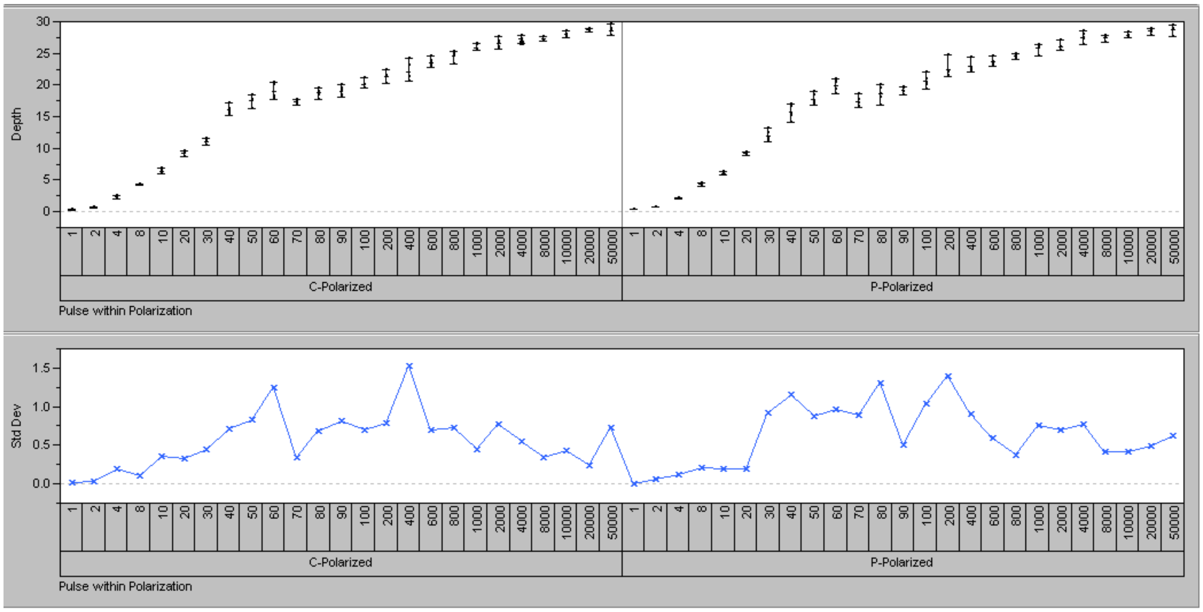

Femtosecond laser drilling depth as a function of the number of pulses at different polarization.

Appendix B

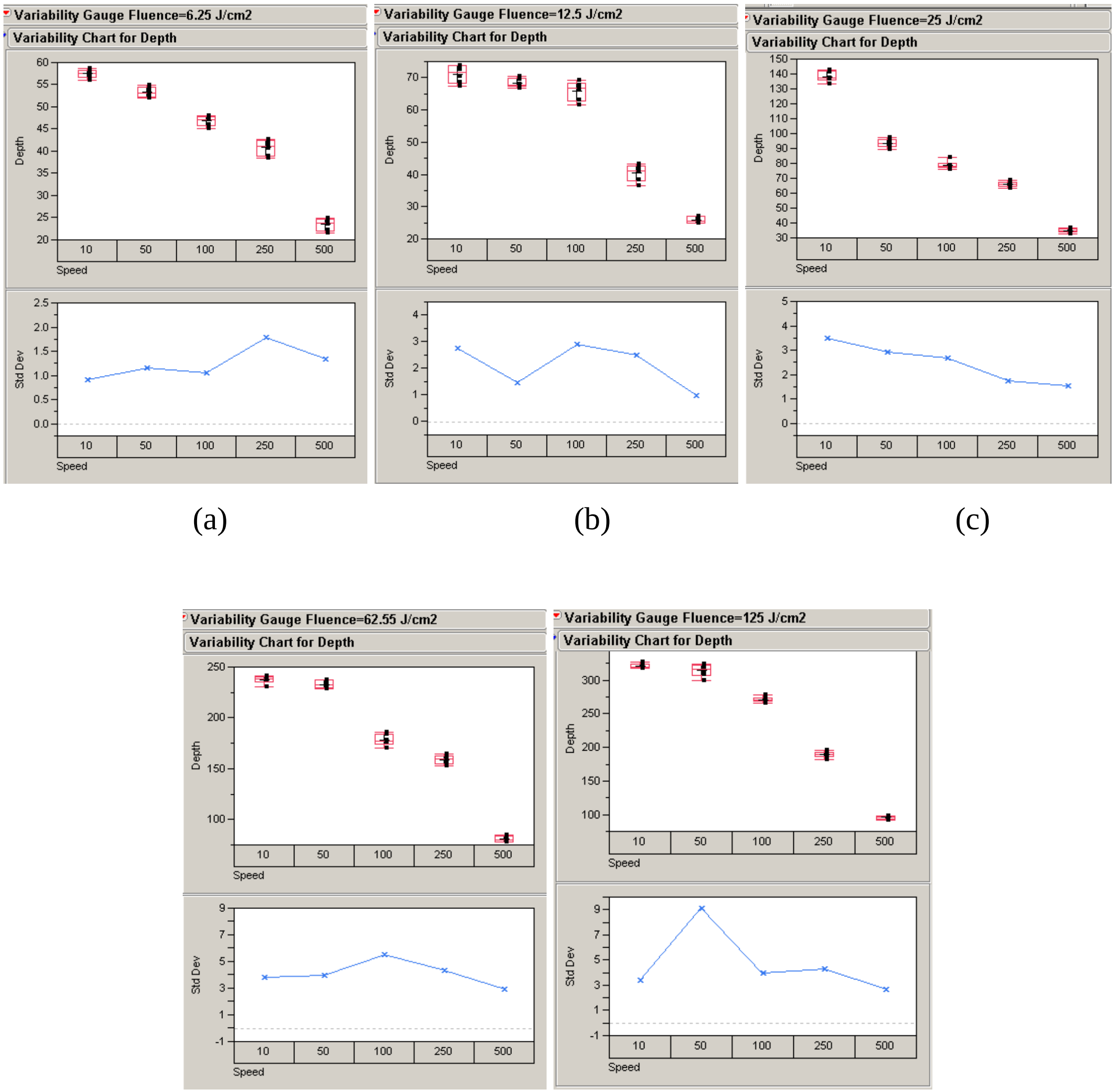

(a) (b) (c)

(d) (e)

Influence of laser fluence on the depth of cut at speed ranging from 10µm/sec to 500µm/sec. (a) 6.25 J/cm^2, (b) 12.5 J/cm^2, (c) 25 J/cm^2, (d) 62.55 J/cm^2 and (e) 125 J/cm^2.

Appendix C

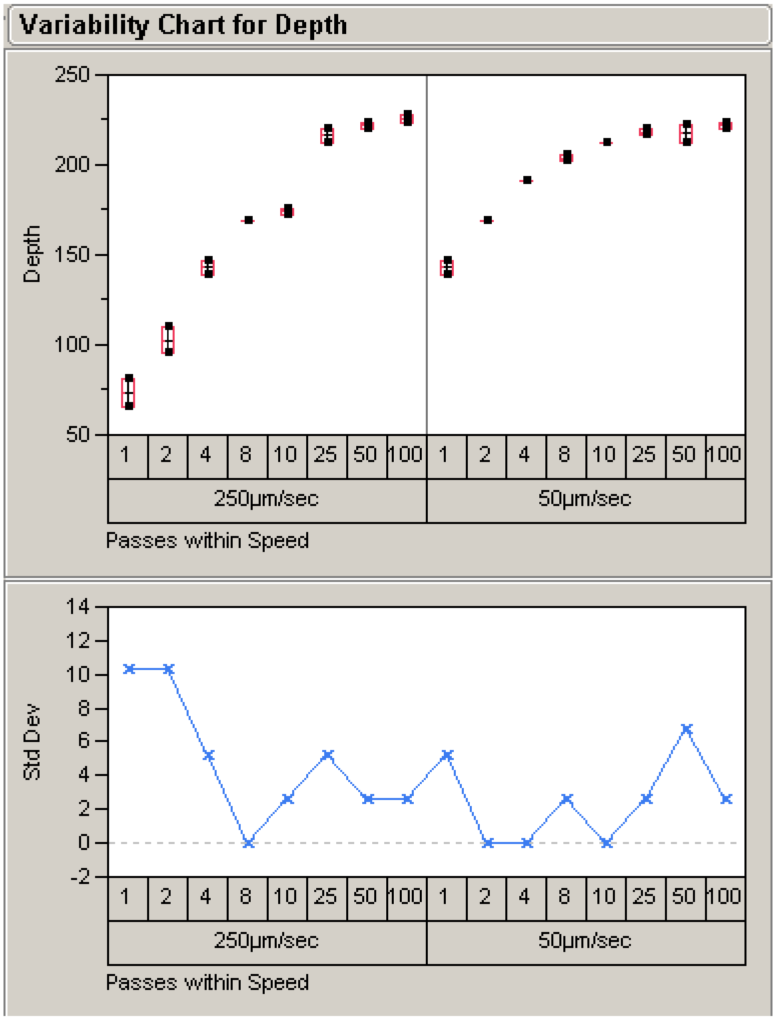

Groove depths as a function of the number of consecutive passes for a fluence of 12.5 J/cm^2.